EXAMINATION OF THE ADVERSE EFFECTS OF GASEOUS AND PARTICULATE OXIDANT AIR POLLUTANTS IN HUMAN AIRWAY EPITHELIAL CELLS

Eugene A. Gibbs II - Flournoy

A dissertation submitted to the faculty of the University of North Carolina at Chapel Hill in partial fulfillment of the requirements for the degree of Doctor of Philosophy in the Curriculum in Toxicology.

Chapel Hill
2012

Approved By:

James M. Samet, PhD

Lee M. Graves, PhD

Marila Cordeiro-Stone, PhD

Miroslav Styblo, PhD

Michael Chua, PhD

Abstract

EUGENE A. GIBBS-FLOURNOY: Examination of the Adverse Effects of Exposure to Gaseous and Particulate Oxidant Air Pollutants in Human Airway Epithelial Cells (Under the direction of Dr. James M. Samet)

Human exposure to ambient air pollution is a pervasive global public health problem. Ambient levels of air pollutants, such as particulate matter and ozone, are associated with multiple adverse health effects, including increases in the incidence of morbidity and mortality. The underlying mechanism(s) responsible for the adverse effects of most air pollutants is not well understood. However, oxidative stress has been implicated as being a major contributor to the mechanism of toxic action of numerous gaseous and particulate air pollutants. The lungs serve as the primary route of exposure for air pollutants, making cells of the respiratory epithelia principal targets for many of the toxicological outcomes of air pollution exposure. The concentrations of gaseous and particulate matter (PM) air pollutants are primary determinants of the pulmonary toxicity resultant from air pollutant exposure. The study of oxidative responses to air pollutant exposure requires that a number of methodological challenges be overcome. The studies of this dissertation purposely address these challenges in the following manner: 1) Development and implementation of imaging methodologies for the investigation of effects resulting from particulate and

gaseous air pollutant exposure to Human Airway Epithelial Cells (HAEC); 2) Examination of the cellular mechanisms that underlie oxidative stress responses to air pollution exposures in HAEC using live cell imaging methodologies; and 3) Examination of factors that mediate air pollution-induced changes in intracellular redox status. The major features of this body of work were able to validate and establish significant methodologies for examining the interaction of nano-scaled particulates with cellular environments, and observe oxidative alterations in the intracellular redox environment of oxidant-exposed cells in real-time. Moreover, these findings reveal that exposure to oxidative air pollutants, such as ozone, induces a profound increase in the intracellular glutathione redox potential of human airway epithelial cells that is indicative of an oxidant-dependent impairment of redox homeostasis in the cell. Cumulatively, this work advances current toxicological knowledge regarding the spatiotemporal interaction of gaseous and particulate air pollutants with cellular environments, while producing effective methodologies for the assessment of implications resulting from air pollutant exposure. Furthermore, the methodologies described herein can be used in broader toxicological applications assessing similar endpoints from other types of xenobiotic exposures.

Acknowledgments

First and foremost, all that I do in life is only achievable through the grace of GOD, and the completion of this dissertation is merely one example of many, for which I am truly thankful. Additionally, the support of my family throughout my personal and professional endeavors has been vital to all of the successes that I have achieved. I would like to thank my wonderful wife, Katoria Gibbs, for her encouragement and companionship as both my friend and my colleague. Similarly, I must thank my parents, Carolyn P. Flournoy and Eugene A. Gibbs, for providing me with the fundamental tools needed to overcome life's challenges as well as instilling the importance of education.

I would truly like to express my deepest appreciation for my mentor, Dr. James M. Samet, as he has provided me with outstanding leadership, guidance, encouragement, and support throughout my tenure in his lab. Without hesitation, I can truly say that he is a great mentor to all students that train in his lab, as well as a life-long friend to me. Also, I am thankful to my doctoral committee members, Dr. Lee Graves, Dr. Marila Codeiro-Stone, Dr. Miroslav Styblo, and Dr. Michael Chua, for their time, commitment, active participation, expertise, and constructive criticism provided during my training as a graduate student in the Curriculum in Toxicology. Likewise, I am

appreciative of my clinical co-mentor, Dr. Philip Bromberg, for his participation in my graduate project as well as our personal interactions.

Lastly, the work that I have accomplished at the US EPA Human Studies Facility was certainly not completed without the aid of others. I would like to thank all of my friends and colleagues that have helped and encouraged me throughout my time at UNC. The success of a graduate student is often aided by the support network which enables his/her accomplishments, and I have certainly been blessed with an awesome group of individuals over the years. While the names of all the people that have helped me are too numerous to exhaustively enumerate, I would like to specifically thank Lisa Dailey, Rob Silbajoris, Wan-Yun Cheng, Samantha Snow, Phillip Wages, Missy Brighton, Steve Simmons, Joleen Soukup, Andy Ghio, Weidong Wu, Ashalla Freeman, and Patrick Brandt for their camaraderie and professional input. Also, I thank all of my friends in the 2008 cohort of toxicology graduate students, and my IMSD extended family.

Table of Contents

List of Figures

List of Abbreviations

2-AAPA	2-acetylamino-3-[4-(2-acetylamino-2- carboxyethyl sulfanylthiocarbonylamino)phenylthiocarbamoylsulfanyl] propionic acid
AH2	Ascorbic Acid
ALI	Air-Liquid Interface
AP-1	Activator Protein-1
AQI	Air Quality Index
ARE	Antioxidant Response Element
BSO	Buthionine Sulfoximine
CAA	Clean Air Act
CLSM	Confocal Laser Scanning Microscopy
CMB	Cell Mask Blue
CO	Carbon Monoxide
COPD	Chronic Obstructive Pulmonary Disease
cpYFP	circularly permuted Yellow Fluorescence Protein
DAPI	4',6-diamidino-2-phenylindole
DEP	Diesel Exhaust Particles
DF	Darkfield
dH_2O	Deioninzed Water
DTT	Dithiothreitol
eGFP	enhanced Green Fluorescence Protein

EGFR	Epidermal Growth Factor Receptor
E_{GSH}	Glutathione Redox Potential
ELF	Epithelial Lining Fluid
EM	Electron Microscopy
EPA	Environmental Protection Agency
EpRE	Electrophile Response Element
FEV1	Forced Expiratory Volume in 1 second
FVC	Forced Vital Capacity
G6PD	Glucose-6-Phosphate Dehydrogenase
γ-GCL	gamma-Glutamyl Cysteine Ligase
γ-GCS	gamma-Glutamyl Cysteine Synthetase
GFP	Green Fluorescence Protein
GPx	Glutathione Peroxidase
GR	Glutathione Reductase
Grx	Glutaredoxin
GSH	Reduced Glutathione
GSSG	Oxidized Glutathione
GST	Glutathione-S-Transferase
HAEC	Human Airway Epithelial Cells
HO-1	Hemeoxygenase-1
Hr	Hour
IL-6	Interleukin-6
IL-8	Interleukin-8

Keap-1	Kelch-like ECH Associating Protein-1
KGM	Keratinocyte Growth Medium
LOOH	Lipid Peroxides
LOPs	Lipid Ozonation Products
LS+G	Locke Solution with Glucose
LS-G	Locke Solution without Glucose
MAPK	Mitogen-Activate Protein Kinases
MOI	Multiplicity of Infection
NAAQS	National Ambient Air Quality Standards
NADH	Nicotinamide Adenine Dinucleotide
NADPH	Nicotinamide Adenine Dinucleotide Phosphate
NF-kB	Nuclear Factor-kappa B
NHBE	Normal Human Bronchial Epithelial Cells
NO_2	Nitrogen dioxide
NO_X	Nitrogen oxides
NP	Nanoparticles
NQO1	Nicotinamide Adenine Dinucleotide Phosphate:Quinone Oxidoreductase-1
Nrf2	Nuclear Factor Erythroid 2-Related Factor 2
O_3	Ozone
pCat	pegylated Catalase
PF	Paraformaldehyde
PG-1	Peroxy Green-1

PM	Particulate Matter
PMT	Photomultiplier Tube
PPP	Pentose Phosphate Pathway
PSSG	Protein mixed disulfides
QA	Quality Assurance
RD	Regulatory Domain
RNS	Reactive Nitrogen Species
roGFP	redox-sensitive Green Fluorescence Protein
roGFP-cyto	Cytosolically-targeted Redox Sensitive Green Fluorescence Protein
roGFP-mito	Mitochondrially-targeted Redox Sensitive Green Fluorescence Protein
ROI	Region of Interest
ROS	Reactive Oxygen Species
Sec	Seconds
SO_2	Sulfur dioxide
α-T	alpha-Tocopherol
TD	Transmission Detector
TNF-α	Tumor Necrosis Factor-alpha
TRPA1	Transient Receptor Potential Ankyrin 1
UA	Uric Acid
UFP	Ultrafine Particles
UV	Ultraviolet

VOC	Volatile Organic Compound
wtGFP	wild-type Green Fluorescence Protein
YFP	Yellow Fluorescence Protein

Chapter 1

Introduction

1.1 Air Pollution and Human Health

Ambient air pollution is a common problem that afflicts human populations in the industrialized world, which persists despite active local, regional, national, and global regulatory efforts. In the United States, as of 2010, it has been estimated that approximately 124 million Americans live in areas that exceed current standards both established and regulated by the Environmental Protection Agency (EPA) (EPA 2012). While this statistic has decreased by ~22% since the previous 2007 estimate of 158.5 million, these values indicate that a large portion of the population remains exposed to unhealthy levels of air pollution. Moreover, towards the end of the 20th century, air pollution became recognized as a global public health problem with other countries reporting similar estimations of exposure (Ciencewicki et al. 2008; Maynard and Howard, 1999; WHO, 2006).

As stated, exposure to air pollution has been observed to be detrimental to human health. Numerous epidemiological studies over the years have positively associated air pollution exposure with increased incidence of morbidity and mortality (Stanek et al., 2011). Some of the earliest observations correlating acute instances of air pollution with adverse effects on human health include the 1930 Muese Valley

Fog in Belgium, the 1948 Smog of Donora Pennsylvania, and the 1952 “Great Fog” of London (Stanek et al., 2011; Simkhovich et al., 2008; Nemery et al., 2001; Helfand et al. 2001; and Scott, 1953). In each situation, stagnant atmospheric conditions made it favorable for combustion emissions to become trapped, causing marked increases in the localized concentration of air pollutants in and around these urban environments (Stanek et al., 2011). Furthermore, several statistical analyses have revealed direct temporal correlations between the incidence of such acute elevations in air pollution and the number of local hospitalizations and deaths (Simkhovich et al., 2008; Yang and Omaye, 2009; and Stanek et al., 2011). All these findings, combined with ongoing research, have prompted efforts to increase public awareness of the harmful effects of air pollutant exposure.

There are multiple types of adverse health effects that have been correlated with acute and chronic exposure to air pollution. As expected, the respiratory system is the primary target for many of the injurious effects induced by ambient air pollution. These effects range broadly from mild exasperations to death depending on the susceptibility of individuals within the population being exposed (Laumbach 2010). In general, components of air pollution have been demonstrated to cause airway irritation, decreases in lung function, increases in airway hyperactivity, increases in pulmonary inflammation, and exacerbation of pulmonary diseases, such as asthma and chronic obstructive pulmonary disease (COPD), as well as cardiovascular system dysfunctions including myocardial infarction, stroke, and atherosclerosis (Stanek et al., 2011; Laumbach 2010; Yang and Omaye 2009). In addition, several risk factors have been associated with individuals most vulnerable

to the effects of air pollution; these include age (children and older adults), underlying disease burden of the pulmonary and cardiovascular systems, diabetes, pregnancy, and genetic polymorphism (American Lung Association, 2012; Bolton et al., 2012; Ciencewicki et al., 2008; Kampa and Castana, 2007; Shannahan et al., 2010; Curtis et al., 2006; Laumbach 2010). These factors, combined with the known health implications resultant from exposure to air pollution, have emphasized the need for environmental quality standards used to limit the amount of common air pollutants released to the environment.

Air pollution is a complex mixture largely comprised of two main components, gases and particulate matter (PM), both of which are derived from natural and anthropogenic sources. Currently, the U.S. EPA regulates six of these components known as “criteria” air pollutants. They include: ozone, particulate matter, lead, nitrogen dioxide (NO_2), carbon monoxide (CO), and sulfur dioxide (SO_2). Through the mandates of the federal Clean Air Act (CAA), the EPA sets evolving regulations for each criteria air pollutant known as the National Ambient Air Quality Standard (NAAQS). These standards are set at levels meant to protect susceptible portions of the population. Furthermore, NAAQS are the basis of the scale used in the location-specific Air Quality Index (AQI). The AQI incorporate daily forecasts of air quality for NAAQS pollutants, and are used by the public to proactively limit exposure to unhealthy levels of ambient air pollution. Of the 6 criteria air pollutants regulated by the EPA, ozone and PM are both the most common types of pollution experienced in urban environments and they most frequently exceed the established values set to protect public health (Laumbach 2010; Pryor 1992).

1.2 Particulate Matter (PM)

By definition, PM is the suspension of solid particles or liquid droplets in the ambient air (Ciencewicki et al., 2008). PM varies broadly in its size and composition with organic and inorganic materials contributing to its overall make-up. Examples of PM range from natural dusts to mold spores to combustion and industrially-derived particulates of anthropogenic origin. Currently, PM is separated into 3 categories by size based on the aerodynamic diameter of its particles: 1) "coarse" particles, PM_{10}, 2.5 – 10 μm in diameter; 2) "fine" particles, $PM_{2.5}$, ≤ 2.5 μm in diameter; and 3) "ultrafine" particles (UFP), $PM_{0.1}$, particles with diameters ≤ 0.1 μm. Of these 3 categories, the EPA regulates ambient $PM_{2.5}$ and PM_{10} at 35 $\mu g/m^3$ and 150 $\mu g/m^3$, respectively, not to be exceeded within a 24 hr averaged basis (EPA 2012).

Ambient PM is generated from multiple processes via numerous sources, both natural and man-made. Generally speaking, large particulates, ≥ 10 μm, are created by more natural processes such as wind erosion, unsettling of loose soils and dusts via air turbulence, release of plant pollen, and the evaporation of sea spray (Mossman et al., 2007; WHO, 2003; Ogunseitan and Robbins, 2011). In contrast, the ultrafine fraction of PM is largely produced by nucleation, which is a physiochemical process that creates minute particles (nuclei) via condensation of low vapor-pressure materials formed either by high-temperature vaporization (i.e. combustion) or chemical reaction of gases/vapors in the atmosphere (WHO, 2003). Compounds capable of generating particulate nuclei include: vaporized transition

and heavy metals, combustion-derived elemental and organic carbon, nitrates, and sulfates. The resulting particles expand in size by: 1) coagulating with other nuclei to form a larger aggregated particle, and/or 2) having gas or vapors of organic molecules condensed onto their surface, which increases their overall diameter (WHO, 2003). It is important to note that combinations of these components and events often drive the creation of particles, thus contributing to the broad array of ambient PM in relation to size, number, and composition. This process generates particles capable of absorbing and transferring many materials that are toxicologically relevant, such as metals, organic hydrocarbons, reactive gases, and ions, which are all often packaged around a stable carbon core (Mossman et al., 2007; Kampa and Castana, 2007). Ultimately, the overall composition, size, number, and surface reactivity of these particles play a role in the adverse health effects caused by PM.

Respiration of the smaller size fractions of PM, namely fine and ultrafine particles, is believed to pose the greatest threat to human health as particle size is known to correspond to the respirability of particulates to deeper, more vascular, areas of the lung (Valavanidis et al., 2008; Yang and Omaye, 2009; Kampa and Castanas 2008; Stanek et al., 2011). More specifically, deposition of coarse PM is largely confined to the upper extrathoracic portion of the respiratory tract and is largely cleared via physiological mechanisms such as mucociliary clearance; while fine and ultrafine PM are capable of reaching deeper tracheobronchial and alveolar regions of the lung where they often remain for longer periods of time due to less efficient clearance mechanisms (Kampa and Castanas 2008; Olivieri and Scoditti,

2005; Stanek et al., 2011). The latter is of particular concern since particles reaching vascular alveolar regions may be capable of releasing soluble components which can easily access blood vessels for systemic circulation (Yang and Omaye, 2009). Furthermore, depending on the particle size, as well as other physiochemical properties, it is believed that nano-scaled particles are capable of transcending cellular membranes, gaining access to intracellular compartments and even continuing on to extrapulmonary cells, tissues, and organs (Geiser et al., 2005; Oberdorster et al., 2005; Oberdorster and Utell; 2002; Terzano et al., 2010; Nakane, 2012). While most air pollution research regarding the health effects of PM exposure has focused on the larger PM_{10} and $PM_{2.5}$ size fractions, a less exhaustive portfolio of studies has actually examined the toxicological implications of ultrafine PM exposure.

Health concerns over the effects of human exposure to UFP combined with the booming field of nanotechnology have created a need for information on the toxicology of nanomaterials. Current knowledge surrounding the impact of nanomaterials on human health is limited. Furthermore, early work has made it apparent that the effects of nanomaterials cannot be safely extrapolated from the toxicologic properties of larger-scaled materials of the same composition (Biswas and Wu, 2005). Researchers are quickly learning that the minute size and correspondingly large surface to mass ratio of nanomaterials adds additional variables, typically in conjunction with shape and chemical make-up, which can drastically alter their interactions with cells and tissues (Maynard and Howard, 1999; Tetley, 2007). Both incidental and intentional sources of nanomaterials contribute to

direct and indirect routes of human exposure in ambient and occupational settings. Recent estimates of ambient mineral PM place the global burden at greater than 14 megatons, with nano-scaled particles accounting for more than 90% of the PM abundance while contributing minimally to the overall mass (Murr and Garza, 2009; Stanek et al., 2011). Additionally, the global proliferation of nanotechnology has produced more than 600 products that annually require metric tons of raw nanomaterials, which likely get released into the environment via pre- and post-consumer utilization (Jones and Grainger, 2009; Xia et al., 2009). As a matter of practice, ambient PM in the "nano" range is classified as UFP while nanomaterials that are intentionally engineered and synthesized by industry are more commonly known as nanoparticles. In either situation, the term "nano" is applied to particles with at least one dimension at or below 100 nm. For the purpose of this dissertation, the term nanoparticle (NP) will be used to describe all nano-scaled materials regardless of origin.

1.3 Ozone

Triatomic oxygen, more generally known as ozone (O_3), is one of several gaseous components that commonly contribute to ambient air pollution. When high in the stratosphere, O_3 is essential for protecting the Earth's surface from the harmful effects of ultraviolet (UV) radiation produced by the sun. However, when present at ground level (within the troposphere), respiration of O_3 is detrimental to human health due to its oxidative properties. O_3 is a highly reactive oxidant gas that is

tropospherically produced via an intricate series of photochemical reactions involving volatile organic compounds (VOCs) and nitrogen oxides (NO_x) that are catalytically activated by sunlight at wavelengths between 295 - 430 nm (Mudway and Kelly, 2000; and Ciencewicki et al., 2008). Interestingly, O_3 is not directly produced in significant quantities by any anthropogenic source (Mudway and Kelly, 2000). Although created in insignificant amounts by electrostatic means including lightning strikes and the inadvertent emissions of electronic devices, ground-level ozone is largely derived from precursor products, namely VOCs and NO_x, of mobile and stationary combustion sources (Katsouyanni, 2003; Curtis et al., 2006; and Kampa and Castanas 2007).

Currently, the EPA limits ambient O_3 concentrations to 75 ppb, averaged over an 8 hr exposure period. This was recently lowered from the previous standard of 80 ppb, and remains under evaluation for future changes. It appears as though O_3 has a narrow exposure window in relation to levels of tolerance versus concentrations at which adverse effects have been observed. Estimates put natural baseline concentrations of tropospheric O_3 to vary between 20 – 40 ppb, which is very close to the 60 ppb concentration used during controlled “low dose” exposures that were observed to cause decrement in lung function and increases in pulmonary inflammation in human studies (Kim et al., 2011; Mudway and Kelly, 2000).

The pulmonary effects of O_3 exposure are well established. Moreover, many of the studies performed to devise exposure limits were conducted as controlled human studies, largely reducing the need for cross-species extrapolations (Stanek et

al., 2010). In humans, O_3 has been demonstrated to cause decrements in the forced expiratory volume over 1 second (FEV_1), forced vital capacity (FVC), alteration of breathing patterns, increases in airway responsiveness, allergen sensitization, neutrophillic influx, increases in proinflammatory cytokines and prostaglandins, and direct oxidation of cellular and extracellular biomolecules (Stanek et al., 2010; Mudway and Kelly, 2000). While these outcomes have been directly attributed to O_3 exposure, the underlying mechanism driving these endpoints is not fully understood. Due to its potent oxidative properties, O_3 is capable of easily oxidizing important biomolecules causing generation of secondary oxidants and free radicals as well as extensive damage to cellular components. For this reason, oxidative stress has been often implicated as the primary means by which O_3 causes adverse cellular, tissue, and systemic effects.

1.4 Air Pollution and the Lung

By far, inhalation is the most significant exposure route for air pollutants, making the pulmonary system both the initial point of biological interaction and often the primary target for the toxic effects of many ambient air pollutants. In general, the lungs are comprised of two basic functional units: 1) airways that conduct air to and from terminal areas for gas exchange, and 2) the alveoli that serve as the interface where gas exchange occurs (Yang et al., 2008). Overall, the lungs are capable of withstanding moderate insult by certain environmental air pollutants by virtue of a

system of physiological defenses inherent to that organ (Olivieri and Scoditti, 2005; Newhouse et al., 1976)

There are both chemical and mechanical elements at work in defending against air pollutants. The pulmonary system is lined by an epithelium which acts as a protective barrier to exogenous materials. Moreover, this epithelium is protected by a fluid layer that lines the respiratory tract and serves to both neutralize soluble components and trap insoluble components for their successive degradation and/or removal. This epithelial lining fluid (ELF) consists of 2 component layers: 1) an upper layer comprised of mucous, and 2) a lower aqueous layer containing biologically active small molecules, proteins, and ions (Mudway and Kelly, 2000).

The ELF is a highly important protective barrier that impedes the interaction of xenobiotics with the underlying epithelium. In fact, the ELF is the first and primary barrier encountered by air pollutants as they enter the pulmonary system. The upper, gel-like, mucous layer of the ELF floats above the lower aqueous layer, and is continuously moving in an upward direction within the respiratory tract via the action of epithelial cilia in a mechanism known as mucociliary clearance (Nicod, 2005; Samet and Cheng, 2004). Mucociliary clearance aids in protecting the pulmonary system by removing insoluble and biologically active components, such as PM, bacteria, and molds, that become trapped in the mucous as air is inhaled.

Exogenous compounds that make it past the mucosal layer must then interact with the lower aqueous layer prior to reaching the underlying epithelium. The aqueous layer of the ELF is equipped for detoxification of xenobiotics by the

presence of key “antioxidant” compounds, including relatively high levels of reduced glutathione, urate, ascorbate (vitamin C), and α-tocopherol (vitamin E), which have been demonstrated to be protective against various adverse effects of air pollutants (Mudway and Kelly, 2000; Ciencewicki et al., 2008). The presence of antioxidants is especially helpful since it is believed that oxidative stress is a key feature in the mechanism of action for many inhaled xenobiotics, including O_3.

As an additional defense, the lungs also have a robust immune and inflammatory response to exogenous insult. This is especially critical for the lower airways and alveolar regions since the ELF is generally thickest at the tracheal end and thins progressively toward the alveoli (Nicod, 2005; Patton, 1996). In the alveoli, immune cells, such as macrophages, provide additional protection against inhaled microorganisms and PM (Maynard and Howard, 1999). Upon activation, macrophages act quickly to destroy and/or remove potential pathogens. This is accomplished through several mechanisms including direct oxidative attack, phagocytosis, and cytokine/chemokine-mediated inflammatory response (Lohmann-Matthes et al, 1994). Macrophages that have engulfed particles and microorganisms can be removed by the mucociliary escalator, or by migrating to local lymph nodes for organized immune destruction.

Unlike other vital organs, due to its very nature the lungs must interface directly with the external environment, creating a vulnerable interface that enhances potential for localized cellular damage. Of all the components of the pulmonary system, the lung epithelia are arguably most vulnerable to the adverse effects of air

pollutant exposure. This is especially true since the lung epithelium is the first cellular barrier reached once exogenous materials make it past primary defenses in the ELF, mucociliary clearance, and/or local immune cells. Respiratory epithelial cells are equipped to resist the adverse effects of air pollutants. These cells have been reported to have millimolar concentrations of reduced glutathione (GSH) as well as robust expression of key protective enzymes including glutathione peroxidases, glutathione-s-transferases, glutathione reductase, catalase, superoxide dismutase, hemeoxygenase 1, and γ-glutamyl cysteine synthetase to name a few (Rubio et al., 2010; Kelly 2003). All of which are capable of being upregulated via activation of the Nrf2 pathway and the antioxidant response element (ARE) (Lewis et al, 2010).

Over the course of studying lung epithelial responses to air pollution, several models have been used to elucidate mechanistic pathways. Fully differentiated cultures of primary human airway epithelial cells (HAEC), grown on air-liquid interface (ALI), offer responses that are most similar to those of the respiratory epithelium, and therefore remain the gold standard for *in vitro* assessments. However, these cultures are not always the most practical tools for the following reasons: 1) the scarcity of primary HAEC, 2) the amount of time needed to fully differentiate these cells, 3) the specialized growing conditions needed to maintain these cultures, 4) limitations in the length of time each culture can be passaged, and 5) heterogeneity in the genetic makeup of cell donors that may contribute to experimental variability in situations where cells from the same individual cannot be used throughout a study. Similarly, undifferentiated primary cultures have also

proven to be just as useful, but limitations regarding the number of passages that these cells can be carried can discourage their use. Given these limitations, in 1988, a group at the National Cancer Institute reported the stable transformation of human bronchial epithelial cells using an SV-40 adenoviral transduction (Reddel et al., 1988). The resulting immortalized cell line, BEAS-2B, was characterized and found to have retained common features of the normal human bronchial epithelial cells (NHBE) from which they were created. Since then, BEAS-2B cells have become an accepted model for assessing the responses of normal human bronchial epithelial cells while maintaining the proliferative capacity of an immortalized cell line.

1.5 Air Pollutants, Oxidative Stress, and Inflammation

The lungs undergo continuous exposure to both endogenous and exogenous sources of oxidation. At its simplest, the pulmonary system was designed to unremittingly exchange oxygen and carbon dioxide, a situation that itself could potentially cause an oxidative tension within the lung. Although gaseous and particulate air pollutants each have their individual mechanisms of action, most common pollutants, such as O_3 and combustion derived PM, are themselves potent oxidants and are believed to cause their adverse effects through an oxidative mechanism (Rubio et al., 2010; Brunekreef and Holgate, 2002). Upon inhalation, ozone and PM have each been demonstrated to cause adverse pulmonary and cardiovascular effects, primarily through oxidative damage and/or (pro)inflammatory

mechanisms. For PM, this is largely due to the physicochemical factors mentioned earlier: the overall composition, size, number, and surface properties (Kelly 2003). Moreover, the presence of metals and organic hydrocarbons on the surface of combustion-derived PM, such as diesel exhaust particles (DEP), have been demonstrated to be major contributors to PM-induced oxidative damage via the generation of reactive species (Kampa and Castanas, 2008; Cheng et al., 2012; Curtis et al., 2006; Yang and Omaye, 2009; Samet et al., 1998). Ozone, on the other hand, is a potent oxidizing gas that is capable of causing oxidative damage by directly attacking various biomolecules, or through the indirect generation of secondary and tertiary byproducts (Olivieri and Scoditti, 2005).

According to the most accepted definition, oxidative stress occurs when an imbalance in the production of reactive species and free radicals exceeds the capacity of cellular mechanisms to avoid or correct oxidative damage (adapted from Wamelink et al., 2008). Although reactive nitrogen species (RNS) have also been implicated, non-radical reactive oxygen species (ROS) and free radicals are most frequently cited as direct mediators of air pollutant-induced oxidative stress (Jones 2008). Moreover, air pollutant-induced ROS are believed to cause sustainable damage by overwhelming antioxidant defenses of the lung (Kelly 2003). In the proposed mechanism of action, the ensuing “oxidative stress” then drives reactions in which ROS are able to interact with important biomolecules, including proteins, lipids, and nucleic acids, leading to several pathological outcomes often involving aspects of tissue injury and inflammation (Kelly 2003; Ciencewicki et al., 2008). This leads to the onset or exacerbation of common pulmonary diseases such as acute

lung injury, asthma, COPD, emphysema, and cancer (Yang and Omaye, 2009). In Figure 1.5.1 A and B, Frank Kelly visually depicts oxidative stress as an imbalance between antioxidants and free radicals (A), while Ciencewicki and colleagues highlight several mechanisms leading to the adverse health effects caused by air pollutant-induced oxidative stress (B). (Kelly, 2003; Ciencewicki et al., 2008).

Common ROS and free radicals resultant from air pollutant interaction with lung components include: hydrogen peroxide, superoxide anion, and the hydroxyl radical. Such reactive species interact with antioxidant and non-antioxidants components found in the ELF and underlying epithelium. Under sustained exposure conditions, interaction of ROS with antioxidant components like GSH results in depletion of antioxidant defenses, promoting oxidative damage. In addition, interaction of ROS with non-antioxidant components, such as proteins and lipids, leads to the generation of secondary oxidation products such as protein adducts and lipid peroxides (Kelly 2003). The resulting oxidative damage adversely impacts the lung epithelium and resident immune cells, causing elevations in cytokine/chemokine and adhesion molecule expression, as well as tight junction modification, which all promote influx of inflammatory cells (Kelly 2003). Collectively these events increase lung permeability, which in return enables the onset of pulmonary edema. Importantly, the invasion of activated inflammatory cells likely exacerbates air pollution-induced oxidative stress, since these cells use direct oxidative attack via the generation of ROS, such as superoxide, which contributes to damage of surrounding tissue when not focused on a particular biological pathogen (Ciencewicki et al., 2008; Kelly 2003).

A)

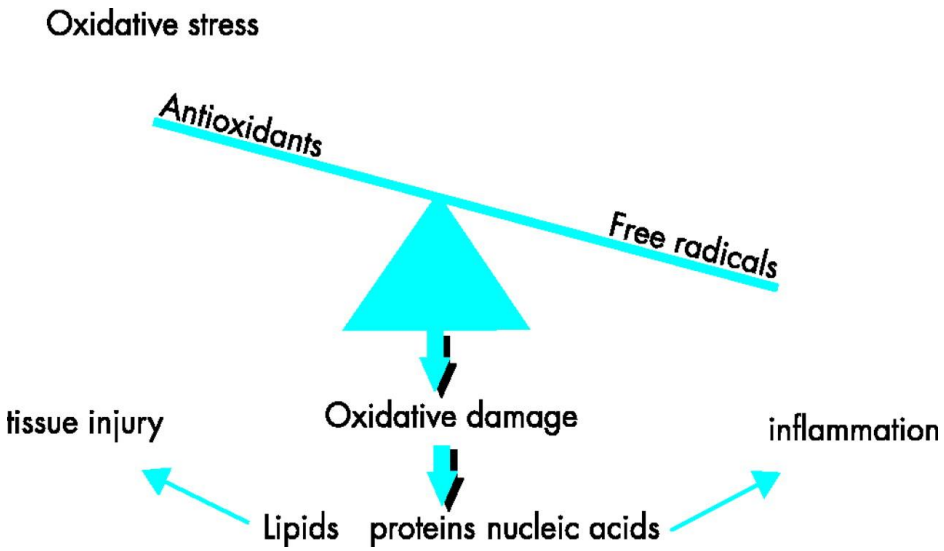

B)

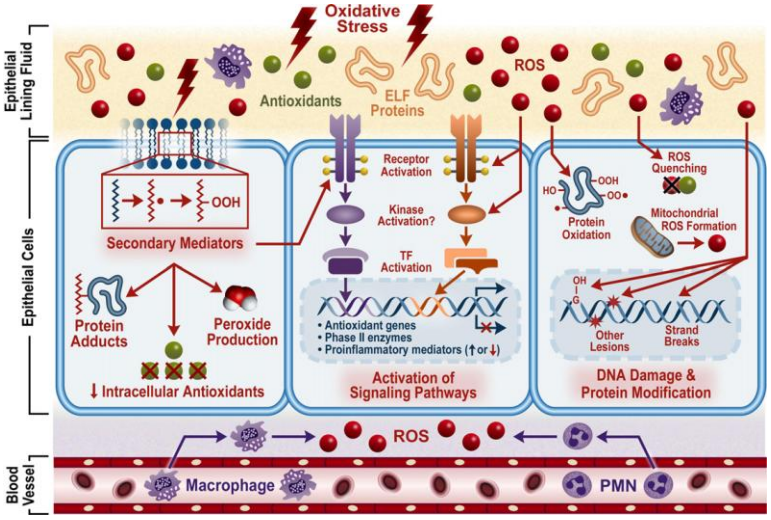

Figure 1.5.1 Oxidative Stress and outcomes related. A) oxidative stress as an imbalance between antioxidants and free radicals (Kelly, 2003). **B)** Mechanisms of air pollutant-induced oxidative stress (Cienciwicki et al, 2008).

In general, the influx of immune cells to a particular area of injury is often associated with inflammation. Both O_3 and PM have been observed to cause increased expression of proinflammatory cytokines including interleukin-6 (IL-6), interleukin-8 (IL-8), and tumor necrosis factor-α (TNF-α) (Devlin et al., 1994; Stone et al., 2007; Ovrevik et al., 2009). Moreover, these pollutants have been demonstrated to increase the expression of proinflammatory proteins through activation of signaling cascades. Inflammatory transcriptional responses to oxidative stress have been demonstrated to involve multiple pathways and transcription factors including: Mitogen-Activated Protein Kinases (MAPK), p53, Nuclear Factor kB (NF-kB), and Activator Protein 1 (AP-1) (Liu and Sun, 2010; Ma 2010; Veranth et al., 2007; Tal et al., 2010). Of these, the transcription factors NF-kB and AP-1 appear to play the most significant roles in mitigating the inflammatory responses induced by air pollution-related oxidative stress (Karin et al., 2001). In brief, NF-kB regulates many genes related to inflammatory response (cytokine/chemokines), cell proliferation/death, immune function and synaptic plasticity, while AP-1 regulates redox sensitive signaling pathways, MAP kinases, and activation of inflammatory mediator gene expression (Stone et al., 2007). More importantly, both of these transcription factors are known to be activated by oxidative stress, and mediators used in their activation appear to be redox-sensitive (Li et al., 2008; Vagaggini et al., 2010; Liu and Sun, 2010; Ma 2010; Xia et al., 2006)

Continued exposure to air pollution-induced oxidative stress is capable of promoting enhanced expression of critical antioxidants and adaptive genes. Activation of AREs (also known as the Electrophile Response Element, EpRE)

through the nuclear factor erythroid 2-related factor 2 (Nrf2) pathway most frequently originates these types of responses. In short, upon oxidant and electrophilic activation, Nrf2 is released from its inhibitory protein, Keap-1 (Kelch ECH Associating Protein-1), freeing it to translocate to the nucleus where it transactivates genes that enhance cell survival. Nrf2 is reported to regulate more than 200 "cytoprotective" genes, making it a robust response mechanism for cellular protection and detoxification of endogenous and exogenous oxidants, electrophilic carcinogens, and oxidatively damaged proteins and organelles (Lewis et al., 2010). Upon oxidant-induced activation, Nrf2 promotes transcription of genes related to: antioxidant molecules, oxidant degrading enzymes, NADPH synthesis, membrane transport, inhibition of cytokine-mediated inflammation, DNA damage recognition, cell cycle/growth-related proteins, and proteome maintenance (Lewis et al., 2010; Cienciwicki et al., 2008; and Kensler et al., 2007). Often critical in counteracting the damage caused by oxidants, classes of "antioxidant" proteins inducible by Nrf2 include ferritin, heme oxygenase-1 (HO-1), metallothionein, peroxiredoxin, sulfiredoxin, and thioredoxin (Lewis et al., 2010). More importantly, of all the transcriptional responses resultant from Nrf2 activation, the most important role of Nrf2 in response to oxidative stress is likely the regulation of glutathione synthesis and maintenance.

1.6 The Importance of Glutathione

Reduced glutathione (GSH) is a biologically-active tripeptide consisting of glutamate, cysteine, and glycine (Kelly 1999). GSH is a critical reducing agent and potent antioxidant molecule found within all eukaryotic cell types in high, millimolar concentrations (Anathy et al., 2012; Meyer and Dick, 2010; Kelly 1999). Most importantly, GSH has been characterized as the major redox buffer of cellular environments, and is physiologically required for cell survival (Anathy et al., 2012). The high concentration of GSH found within cells accounts for ≥ 90% of the total non-protein thiol (sulfur) content, making this compound a major component involved in the overall homeostasis of cellular redox (Anathy et al., 2012; Kelly 1999). Ultimately, maintenance of the intracellular reducing potential by GSH keeps other cellular components in a reduced state, which preserves their biological activity (Meister 1995).

Being a major component of intracellular antioxidant systems, GSH is found in various cellular compartments including the cytosol, mitochondria, and nucleus. *De novo* synthesis of GSH, which is restricted to the cytosol in mammalian cells, consists of two successive steps: 1) glutamate and cysteine residues are conjugated via the action of γ-glutamyl cysteine synthetase (γ-GCS; also known as γ-glutamyl cysteine ligase, γ-GCL) creating the γ-glutamylcysteine intermediate; and 2) glycine is added to γ- glutamylcysteine by glutathione synthetase (Kelly 1999; Meister, 1995; Meyer and Dick, 2010). The synthesis of GSH is tightly regulated by a feedback loop that inhibits γ-GCS activity with increasing concentrations of GSH. The

availability of cysteine combined with γ-GCS activity is considered to be the rate-limiting substrate and step of GSH synthesis, respectively (Meister 1995).

Unlike other tissues and organs, the lung maintains high GSH concentrations both inside and outside cells (Kelly 1999). There are several imperative functions for GSH in relation to intracellular and extracellular environments. These range from direct scavenging of ROS and free radicals; to support of peroxidases as a co-substrate; to enzymatic and non-enzymatic conjugation of xenobiotics (Kelly, 1999). Many of these actions depend on the reactivity of the internal thiol group located within the cysteine residue of GSH. Interaction of GSH with oxidants, electrophiles, and catalytically-dependant enzymes requires oxidation of its thiol, often resulting in the formation of glutathione disulfide (GSSG) and other mixed disulfides (Anathy et al., 2012; Kelly, 1999). In relation to cellular stresses, Dickinson and Forman (2002) best summarized the cascade of events to occur as follows: 1) the cellular thiol content, to which GSH contributes significantly, is consumed in detoxification reactions that protect the cellular environment; 2) barring any overt cytotoxicity, the thiol content is then recovered by either enzymatic reduction of disulfides or *de novo* synthesis; and 3) alterations in thiol content and metabolism will impact signaling pathways like those mentioned earlier. This paradigm makes the participation of GSH, and other thiol-containing constituents, imperative in the mitigation of an ensuing oxidative stress. Cells spend relatively large amount of energy keeping glutathione in its reduced state, suggesting that the reductive maintenance of GSH is key in upholding the intracellular reducing potential (Anathy et al., 2012; Kelly 1999).

The glutathione system consists of a network of accessory proteins that utilize or maintain glutathione. These proteins include: glutathione reductase, glutathione peroxidase, glutaredoxin, and glutathione-S-transferase. Glutathione peroxidases (GPx) oxidize GSH to GSSG during enzymatic reduction of peroxides. To date, eight GPx isoforms have been identified which vary in specificity for substrates as well as cellular and tissue location (Toppo et al., 2008; Burk and Hill, 2010). Of the eight GPx isoforms, five use selenocysteine in lieu of cysteine to reduce peroxides (Lu and Holmgren, 2009). GPx specifically act in response to hydroperoxides, particularly H_2O_2 and lipid peroxides (LOOH), generated during oxidative events. Of relevance to findings to be presented in this dissertation, GPx1 and GPx4, are both selenocysteine peroxidases that largely catalyze the degradation of H_2O_2 and phospholipid hydroperoxides, respectively (Lu and Holmgren, 2008).

As GSH becomes oxidized to GSSG, the action of glutathione reductase (GR) reduces the disulfide back to GSH at the expense of NADPH, which is used as a reducing equivalent. In this regard, GR is a critical component for maintaining the existing GSH pool in its reduced state, especially during periods of oxidative stress, as *de novo* synthesis would likely prove insufficient. This also makes the participation of the pentose phosphate pathway (PPP) vital in mediating the effects of oxidative stress since it is the major mechanism by which NADPH is produced.

Glutaredoxins (Grx) ultimately act as thiol transferases by mediating the reversible reduction of neighboring disulfide bonds to and from the glutathione pool and surrounding thiol-containing proteins (Fernandes and Holmgren, 2004). Grx

largely differ from thioredoxins in that they do not require enzyme-mediated reduction for their regeneration. Under normal conditions, Grx catalyze the reduction of disulfides (de-glutathionylation) in target proteins, which ultimately leads to oxidation of GSH (Fernandes and Holmgren, 2004; Anathy et al., 2012). However, during oxidative stress this mechanism can be reversed resulting in the generation of protein mixed disulfides (PSSG), reflecting the oxidative status of the intracellular glutathione pool (Anathy et al., 2012). Lastly, glutathione-S-transferases (GST) directly conjugate GSH to xenobiotic compounds to facilitate detoxification and elimination. There are at least 7 classes of GSTs, and, most notably, the mu and pi isoforms possess genetic polymorphisms that have been linked to air pollution susceptibility (Wu et al., 2011; Auerbach and Hernandez, Ko and Hui, 2010).

1.7 Assessing Oxidative Stress and Associated Challenges

The internal cellular environment is continuously undergoing physiologically relevant reductive and oxidative (redox) processes, which largely remain in equilibrium outside of externally applied signals (i.e. receptor activation, cellular communication, etc.). When disruption of this equilibrium occurs, such as during xenobiotic-induced generation of ROS, the intracellular redox environment shifts to an oxidative imbalance which, when sustained, leads to oxidative stress and adverse pathophysiological outcomes (Kelly, 2003). An effort to elucidate the causes of pathological outcomes, and to devise appropriate countermeasures,

requires effective assessment of the earliest possible initiating events. Oxidative stress mechanisms range from generation of ROS and other reactive species, to oxidative damage of biomolecules, to impairment of antioxidant defenses. To add to this complexity, the effects of oxidative stress are often reversible, and due to their reactivity, the reactive species generated are typically short-lived. All of these factors make assessment of a specific “oxidative stress” quite challenging since changes in the redox status of cells are not necessarily driven by the impairment of an individual component or the existence of a single oxidative species.

Over the years, various methodologies have been devised to aid in making determinations of specific endpoints related to cellular redox status and oxidative stress. In general, many “oxidative stress” assessments examine one or more of the following types of endpoints: 1) characterization of oxidative damage such as DNA/protein adducts and lipid by-products; 2) examination of reactive species (generation of specific ROS, RNS, or free radicals), and 3) measurement of antioxidant defenses such as glutathione, NADPH, and ascorbic acid. The results of these assessments are generated from a wide range of molecular biology and analytical chemistry techniques including enzymatic assays, gel mobility assays, chromatography, and NMR. While the results of these tests may contain meaning, the assays used are typically flawed due to lack of specificity, lack of sensitivity, disruption of cellular compartments, and/or the unintentional generation of artifacts. For example, a typical assessment of NADPH oxidation via an enzymatic assay would provide reproducible data that gives an indication of the overall effect on the NADPH redox pair. However, such an assay would require disruption of cellular

membranes, which contributes to loss of subcellular compartmental specificity while potentially contributing to the generation of oxidation artifacts. To overcome these limitations, many investigators have moved on to conducting live-cell experiments using fluorescent dyes that report the status of a cellular component or generation of a particular reactive species. While this approach maintains cellular integrity, the limiting factor of these assays is typically the properties of the fluorescent reporter because most conventional dyes lack true specificity for their intended target. For example, 2',7'-dichlorodihydrofluoroscein has been well established for detection of H_2O_2 within cells; however, recent investigations have demonstrated the lack of specificity of this fluorophore as it also reacts to several other ROS/RNS including hydroxyl radicals, peroxynitrite, and nitric oxide (Chen et al., 2010; Gomes et al 2005).

To date there is no single measurement that is accepted to assess "oxidative stress" as a global characteristic. Ideally, the penultimate tool used to determine oxidative stress would be a reporter robust enough to monitor multiple redox pairs/molecules simultaneously, while being sensitive enough to detect small initiating changes and maintain cellular integrity for observation of specific tissues or subcellular compartments that may be responsible for the changes in redox status. While such an ideal sensor does not currently exist, significant progress has been made towards development of more reliable biosensors. Of recent, our collaborators in the lab of Dr. Christopher Chang have developed small molecule probes that are highly specific and sensitive for a particular reactive species, such as H_2O_2 (Miller et al., 2007; Dickinson et al., 2010a). Furthermore, some versions of these dyes are

targetable to subcellular compartments, such as the mitochondria (Dickinson and Chang, 2008; Dickinson et al., 2010b).

1.8 Live-Cell Imaging With Genetically-Encoded Fluorescent Reporters of Cellular Redox

Since the discovery of green fluorescent protein (GFP), efforts have been made to utilize the genetic encoding of this biomolecule to create intracellular redox reporters (biosensors) capable of reporting intracellular conditions in living cells undergoing exogenous manipulation (i.e. live-cell microscopy). There are several characteristics of GFP that make it attractive for usage as a redox reporter. These include: robust resistance to proteolytic activity, tolerance of structural manipulation, and stability in harsh cellular environments (Cannon and Remington, 2008). Wild-type GFP (wtGFP), originally isolated from *Aequorea victoria*, is comprised of 238 amino acids arranged into an 11-stranded β-barrel that shields an internal α-helix (Dooley et al., 2004). The fluorescent chromophore of this protein is located within the internally shielded α-helix, and is the result of spontaneous intramolecular cyclization of three amino acids, Ser65/Tyr66/Gly67 (Meyer and Dick, 2010; Cannon and Remington, 2008). Furthermore, the remarkable stability of this fluorophore is integral to the preservation of its fluorescent properties, as the fluorescence of GFP is extinguished when the protein is unfolded or when its chromophore is improperly shielded (Cannon and Remington, 2008).

More recently, mutagenesis experimentation has led to improvement upon the fluorescent properties of GFP. Most notably, a serine to threonine mutation at position 65 yielded a GFP variant that offers enhanced fluorescent intensity and greater compatibility with commonly used laser excitation wavelengths (Meyer and Dick, 2010). This variant is commonly known as enhanced GFP (eGFP). Importantly, despite genetic manipulation, the spectral properties of wtGFP and eGFP have been largely conserved. Both wtGFP and eGFP have two excitation maxima at ~400 nm and 475-490 nm. Emission of this fluorophore at either excitation wavelength occurs at 510 nm (Meyer and Dick, 2010). Spectral and structural properties of GFP can be further altered via additional site-directed mutagenesis that leads to numerous outcomes, including changes in the emission wavelength (color changes) and even “super-folder” capabilities that further stabilize the protein’s structure (Zhang et al., 2002; Pedelacq et al., 2006)

Currently, several examples of GFP-based, genetically-encoded redox reporters exist which range in their ability to detect changes in specific redox couples, such as GSH/GSSG, or changes in specific ROS, such as H_2O_2 (Meyer and Dick, 2010). These probes have distinct advantages over conventional fluorescent dyes in that they are highly sensitive and specific while being targetable to predetermined subcellular locations. Also, genetically-based probes provide a noninvasive means to monitor redox-related cellular responses to various experimental conditions which can be monitored in real-time using current live-cell imaging techniques (Cannon and Remington, 2008). This greatly improves temporal and spatial resolution related to observation of oxidative stress-induced redox

changes. The following sections describe two examples of protein-based reporters, roGFP and HyPer, both used in experiments described in this dissertation.

1.8.1 roGFP

Redox-sensitive green fluorescent protein (roGFP) is a variant of GFP engineered for monitoring the thiol-disulfide equilibrium, a major determinant of oxidative status. In brief, this biosensor was derived by engineering two surface exposed vicinal cysteines into neighboring strands, 7 and 10, on the β-barrel of GFP. Strands 7 and 10 of the β-barrel are located close to the chromophore responsible for the protein's fluorescent properties. The specific location of the cysteine modifications within the β-barrel depends on the roGFP variant being examined.

Originally, 6 variants of roGFP were developed and tested, with two variants, roGFP1 and roGFP2, being the best characterized. Both roGFP 1 & 2 have cysteine residues inserted at positions 147 and 204, replacing serine and glutamine residues, respectively (Cannon and Remington, 2008; Dooley et al., 2004). Figure 1.8.1.1 demonstrates the structure of roGFP as well as the positioning of the cysteine mutations. The major difference separating roGFP 1 & 2 is the GFP backbone used to make the cysteine modifications. roGFP1 was developed from wtGFP while roGFP2 was created from eGFP. The use of eGFP as the basis for roGFP2 offers several benefits over the wtGFP of roGFP1, including: enhanced fluorescent intensity, increased dynamic range, resistance to photoswitching (redox-independent changes in fluorescent excitation), and greater compatibility with commonly used

laser excitation wavelengths (Schwarzländer et al, 2008; Meyer and Dick, 2010, Hanson et al., 2004).

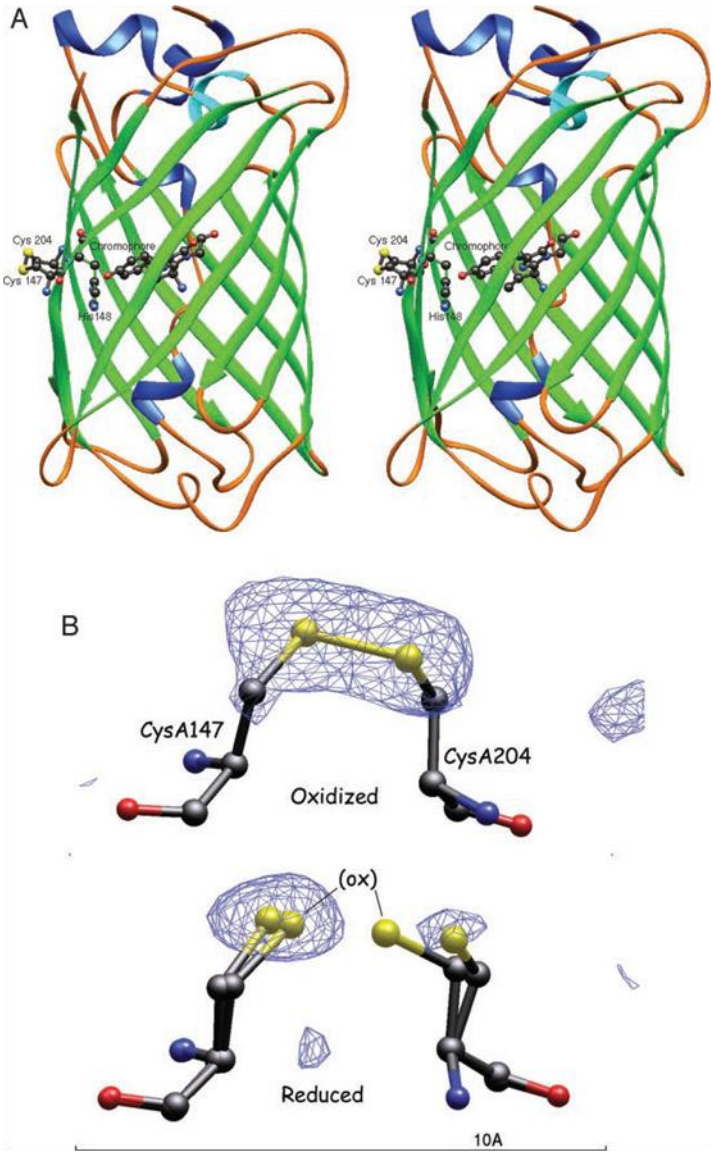

Figure 1.8.1.1 roGFP structure and function. (Hanson et al, 2004) **A)** Key structural alterations within the β-barrel of roGFP2. **B)** roGFP2 engineered cysteine interactions under oxidized (top) and reduced (bottom) conditions

The engineered cysteine residues within roGFP contain thiols that are critical in the function of this redox reporter. Upon oxidizing conditions, a disulfide bridge is formed between the thiol groups of the two engineered cysteines, causing a change in the emission intensity of the fluorophore at each excitation of its two maxima. The dual-excitation/single-emission spectral characteristics of GFP allow for ratiometric measurements by roGFP variants. Ratiometry is an important property of any redox reporter because it reduces or eliminates measurement errors resultant from inconsistencies in fluorophore concentration, illumination intensity, and specimen thickness (Cannon and Remington, 2008). Traditionally, ratiometric measurements are accomplished by independently monitoring the emissions of each excitation wavelength, and then using the emission from one excitation wavelength to normalize the intensity changes observed at the other excitation. During oxidation of roGFP, excitation at 405 nm causes increases the intensity of the emitted fluorescence intensity while the opposite change in intensity occurs during 488 nm excitation. In practice, the final emission intensity is expressed as a ratio of 405/488.

The most important feature of roGFP is that it has been demonstrated to specifically report the redox status of the GSH/GSSG redox pair, which as discussed earlier is the major redox pair in the cell. (Gutscher et al., 2008; Meyer and Dick 2010). The mechanism of this interaction can be described as follows: 1) GPx oxidizes GSH to GSSG in response to peroxides, including H_2O_2 and lipid hydroperoxides (LOOH), thus increasing the glutathione redox potential (E_{GSH}); 2) In response to the increase in GSSG, one of the engineered vicinal cysteines of roGFP2 becomes S-glutathionylated by Grx; 3) Glutathionylation in turn causes

disulfide bond formation and alteration of the spectral properties of the GFP fluorophore (Meyer and Dick, 2010). As with any dynamic reporter of redox conditions, the changes in fluorescence intensity of roGFP are reversible. During recovery, Grx catalyzes the reduction of roGFP disulfide bonds through deglutathionylation as GSSG levels decrease and normal levels of GSH are reestablished by GR, at the expense of NADPH. Thus, the ensuing reduction causes a renormalization of E_{GSH} as GSSG levels decrease, and the baseline ratio of GSH/GSSG is restored (Meyer and Dick 2010).

1.8.2 HyPer

HyPer is a genetically-encoded fluorescent reporter designed for the specific detection of intracellular H_2O_2 (Belousov et al., 2006; Meyer and Dick, 2010). The specificity of this fluorophore comes from incorporation of the OxyR regulatory domain into the structure of yellow fluorescent protein (YFP). As reported by Belousov and colleagues, OxyR is a prokaryotic stress-response transcription factor that specifically responds to the presence of H_2O_2 (2006). Moreover, in *E. coli*, OxyR is reported to control the expression of nearly 40 genes meant to intervene in H_2O_2-mediated toxicity (Chiang and Schellhorn, 2012). Within prokaryotes, OxyR is a 305 amino acid polypeptide comprised of two domains: 1) a regulatory domain (RD) that is responsive to H_2O_2, and 2) a DNA-binding domain used to activate transcription of cytoprotective genes (Belousov et al., 2006; Christman et al., 1989). In the presence of H_2O_2, the active site of the OxyR regulatory domain becomes

hydroxylated to form a cysteine sulfenic acid at position 199. The resulting sulfenic acid then forms an intramolecular disulfide bond with a neighboring cysteine at position 208 which creates a conformational change that activates the protein (Meyer and Dick, 2010).

HyPer was created by inserting circularly permuted YFP (cpYFP) into the regulatory domain of OxyR obtained from *E. coli* at positions 205 and 206 (Belousov et al., 2006; Meyer and Dick, 2010). The resulting chimeric protein is a fluorescent reporter of H_2O_2 via the thiol redox state of the OxyR domain. cpYFP is ultimately a variant of GFP, which makes HyPer a ratiometric sensor with two excitation maxima at 420 nm and 500 nm and a single emission maximum at 516 nm (Belousov et al., 2006). As HyPer detects H_2O_2, a disulfide bond forms in the OxyR region of the protein resulting in a conformational change that directly relates to a ratiometric shift in the two excitation maxima of this reporter (Meyer and Dick, 2010). This leads to an increase in the fluorescence intensity at 500 nm excitation while the intensity at 420 nm decreases as the probe is oxidized by H_2O_2. Once calculated, the final emission intensity is usually expressed as the ratio of values produced by 500/420 excitation.

1.9 Conclusions, Hypothesis, and Specific Aims

Human exposure to gaseous and particulate air pollution is associated with elevated rates of morbidity and mortality. Given that inhalation is the primary route of exposure to air pollutants, the cells of the airway epithelium are a major target for

many of the toxicological effects of air pollution exposure. The composition of air pollution ranges from well-defined gases, to highly complex mixtures of organic and inorganic compounds that comprise PM. Of recent, the recognition of NP as important constituents of PM has added to this complexity, identifying new knowledge gaps concerning the impact of cellular interaction with NP. As is the case with pollutants of other environmental media, oxidative stress has repeatedly been implicated as a critical feature of the mechanism of action of air pollutants. Specifically, oxidative stress has been implicated as an important mechanism by which PM exerts adverse effects. Among the gaseous air pollutants, ozone is a highly reactive oxidant gas that remains a major component of air pollution in many urban areas. While the direct effects of ozone on biological systems have been fairly well characterized, there are significant informational deficits in regards to the specific oxidative effects of ozone. Thus, it is the overall hypothesis of this dissertation that the initiating oxidative events, which influence the downstream adverse pulmonary effects from particulate and gaseous exposures, can be studied in HAEC with high temporal and spatial resolution using live-cell molecular imaging approaches.

Oxidative stress has been demonstrated to be an important component in the toxicity of many air pollutants, including ozone and various types of PM. However, the specific mechanisms involved in air pollutant-induced oxidative stress remain undetermined. Elucidation of key oxidative events/components is critical in understanding the mechanisms involved in air pollutant-induced oxidative stress in HAEC. Moreover, real-time observation of oxidative effects resulting from HAEC

exposure to gaseous and particulate air pollutants in live-cell studies will expand the experimental evidence pertaining to the role of oxidative stress in cellular susceptibility to air pollution. Given the transient nature of oxidative events, direct fluorescence detection of ROS and redox potential via live-cell imaging using dynamic biosensors is an especially effective means of observing these very short-lived molecules/changes. Application of newly devised live-cell imaging methodologies, combined with the use of molecular probes capable of 1) assessing changes in intracellular redox status and 2) monitoring levels of intracellular ROS, should aid in the examination of oxidative stress endpoints with high temporal and spatial resolution. Additionally, these molecular probes are targetable to specific cellular compartments, which will aid in pinpointing intracellular targets for oxidative damage as well as determination of cellular responses to changes in oxidative stress.

The hypothesis of this dissertation is addressed with three specific goals: **1)** Develop and implement imaging methodologies for the investigation of effects resulting from particulate and gaseous air pollutant exposure to HAEC; **2)** Examine the factors driving oxidative stress responses to air pollution exposures in HAEC using live cell imaging methodologies; and **3)** Examine factors affecting air pollution-induced changes in intracellular redox status.

Chapter 2

Darkfield-Confocal Microscopy detection of nanoscale particle internalization by human lung cells[1]

2.1 Introduction

The recent proliferation of nanotechnology combined with concerns over the health effects of human exposure to ambient ultrafine particulate matter (UFP) have created a need for information on the toxicology of nanomaterials. Studies to date have made it apparent that the effects of nanomaterials cannot be safely extrapolated from the toxicological properties of larger-scaled materials of the same composition (Biswas and Wu, 2005; Hallok et al, 2009).

Nano-scaled materials are generally defined as structures possessing at least one dimension that is 100 nm or less (Oberdörster et al, 2005a; Oberdörster et al, 2005b). The small size and correspondingly large surface to mass ratio of nanomaterials are features which may alter their interactions with cells and tissues (Jefferson and Tilley, 1999; Tetley, 2007). Incidental human exposure to environmental nanomaterials most often occurs through the inhalation of ambient ultrafine particulate matter that is primarily produced during the combustion of fossil fuels (Harrison and Yin, 2000). Conversely, nanomaterials that are intentionally

[1] The findings of this chapter were published as follows: Gibbs-Flournoy E, Bromberg P, Hofer T, Samet J, Zucker R. 2011. Darkfield-confocal microscopy detection of nanoscale particle internalization by human lung cells. Particle and Fibre Toxicology 8:2.

engineered are more commonly known as nanoparticles. In this manuscript, the term nanoparticle (NP) will be used to refer to nano-scaled materials without regard to their origin and are considered to be under 100 nm in size.

Relative to ingestion and dermal absorption, inhalation of NP may be the most likely route of human exposure. The small size of NPs not only allows them to become airborne easily, but promotes deposition in the deep lung as well (Biswas and Wu, 2005). Indeed, inhaled UFP have been reported to be more potent in inducing adverse health effects than larger particles (Biswas and Wu 2005; Oberdörster et al, 2005a; Oberdörster et al, 1994; Nurkiewicz et al, 2008). Some studies have suggested that inhaled NP penetrate the respiratory epithelial barrier and are distributed systemically to various organs and tissues, including the brain (Jefferson and Tilley, 1999; Oberdörster et al, 2004; Pui et al, 2008; Rothen-Rutishauser, 2007).

Imaging is a powerful technique for the study of cellular interactions with extracellular substrates, including particles (Geiser and Kreyling, 2010; Marquis et al, 2009). Many critically important toxicological processes, such as the mechanisms through which nanomaterials penetrate into cells, are best addressed using imaging approaches. However, with the exception of fluorescently tagged synthetic particles, the small size of nanoparticles puts them beyond the limit of detection of about 200 nm using conventional bright-field light microscopy techniques. As an alternative, application of electron microscopy (EM) in NP studies has grown considerably in the past few years and remains the “gold standard” for many NP studies as this

technology can easily observe particles below 100 nm in size. Unfortunately, EM is costly, labor intensive, limited to materials with sufficient electron density contrast, and primarily restricted to fixed specimens.

Conventional darkfield (DF) microscopy is an illumination technique used in light microscopy to optimize differences in contrast by selectively capturing light scattered by the specimen. In brief, this is accomplished with the attachment of a specialized light condenser that uses a light stop comprised of an annulus with a narrow aperture to obliquely illuminate the specimen via a hollow cone of light (Murphy, 2001; Spencer M, 1982; Wayne R, 2009). Using a confocal microscope, the light illuminating the specimen is focused by the objective, and detected by a darkfield condenser. Essentially, these instruments use a reverse light path from normal DF applications for DF detection in confocal mode. Consistent with normal DF illumination, the blockage of centralized light results in DF-CLSM, reveals only structures of the specimen that are capable of scattering the oblique rays of light towards the objective are detected via this technique. DF detects light that is refracted, diffracted or reflected. This light scattering allows DF to detect extremely small structures, offering a potential light microscopy tool for the study of nanoparticles associated with cells. If a DF oil condenser with a 1.2-1.4 numerical aperture is used, it allows lenses with a higher numerical aperture to also be used which diminishes resolution losses in the microscope. However, the numerical aperture of the lens must be slightly below that of the numerical aperture of the condenser for DF to work. Previous studies have used DF imaging to observe NP (Craig et al, 2010; Murdock et al, 2008; Skebo et al, 2007; Zucker et al, 2010; Heidi

and Byron, 2009; Xiao et al, 2010). Largely, these studies have been limited by visualizing NP in only a single 2D plane instead of producing a 3D image as presented in this communication.

In the present study, we show that the capability of DF to detect nanoparticles that can be effectively interfaced with a confocal laser scanning microscope (CLSM) to spatially localize nanoparticles along the z-axis of the cell, thereby permitting a determination as to whether nanoparticles are associated with the cell surface or within the cell. This communication reports the novel integration of DF and CLSM microscopy and its utilization in the measurement of nano-particle uptake and localization relative to intracellular organelles and the nucleus in cultured human lung cells.

2.2 Methods

2.2.1 Materials and Reagents

Green fluorescent 6.5 µm, 2.0 µm, 0.5 µm, 140 nm, 100 nm, and 50 nm polystyrene spheres (beads) were acquired from Polysciences Inc. (Warrington, PA) and Bangs Laboratories Inc. (Fishers, IN). Titanium dioxide nanoparticles with an average diameter of 27 nm were obtained from Degussa (Aeroxide TiO_2, Parsippany, NJ). HCS Cell Mask Blue (H32720) and Prolong Gold Antifade Reagent with and without DAPI (P36934 and P36935) were purchased from Invitrogen (Molecular Probes, Eugene, OR). First Contact cleaning polymer was obtained from Photonic Cleaning Technologies (Platteville, WI).

2.2.2 Specimen Preparation

Slide cleaning: A slide cleaning protocol was devised to minimize the presence of unwanted background debris detectable by darkfield microscopy (Bonin and Bonissi, 2009; Waterman-Storer, 2001). New “pre-cleaned” microscope slides (Fisher Scientific, Pittsburgh, PA) were subjected to additional cleaning by wiping them using ammonia based glass cleaner and lens paper. As the slides were wiped, they were placed into a slide rack taking care to provide even spacing between each slide. Next, the slide rack was placed into a lidded vessel large enough to fully submerge the slides and washed successively in the following solutions: 1) 1:5 dilution of ammonia based glass cleaner in deionized water (dH_20), 2) deionized water, and 3) 70% ethanol. Importantly, for each wash step, the lidded vessel containing the slides was placed in a bath sonicator and the entire apparatus was

sonicated for 30 minutes in each wash solution. Washed slides were stored in 70% ethanol until needed. Just prior to coverslip mounting, a slide was removed from the 70% ethanol, briefly rinsed in 100% ethanol and allowed to air dry for approximately five minutes. Lastly, to further aid in the removal of slide debris, the specimen area of the slide was painted with a commercially available cleaning polymer (First Contact), allowed to cure for a minimum of 15 minutes, and peeled off immediately before mounting coverslips. All reagents used to wash slides were filtered using 0.22 µm filters. All steps in which the slides were exposed to air (i.e. removal from the various wash solutions) were carried out in a biological hood to minimize contamination with airborne debris. Use of this slide cleaning procedure produced slides that were relatively free of debris detectable by darkfield microscopy.

Fluorescent Polystyrene Beads: Suspensions of 50 nm, 100 nm, 140 nm 500 nm, 2 µm, and 6.5 µm Fluorescent polystyrene beads (Polysciences, Warrington, PA) were prepared in dH_2O and directly applied to freshly cleaned glass slides. Following a drying time of 15 to 20 minutes, #1.5 coverslips were mounted onto the slides using Prolong Gold Antifade Reagent.

2.2.3 Cell Culture and Exposure

Transformed human airway epithelial cells (BEAS-2B, subclone S6; (Reddel et al, 1988) were cultured as described previously (Tal et al, 2010) and maintained in serum-free KGM (Lonza, Walkersville, MD). The cells were incubated in a humidified incubator at 37◦C in 5% CO_2. For fixed cell studies, cells were sparsely

plated (≤ 1.5 x 10^6 cells/well) on 12 mm, #1.5 coverslips located in 6-well culture dishes and allowed to grow for one day prior to exposure. At the time of exposure, media was removed from the cell cultures and 2 ml of a freshly prepared homogeneous suspension of 27 nm TiO2 was applied immediately. Cells were typically exposed for either 5 minutes or 2 hours (120 minutes) prior to washing and fixation. Pulsed exposures involved continuous exposure for 5 minutes followed by removal of exposure media, a brief wash using KGM, and incubation in fresh, particle free, media for an additional 115 min. After exposure, cells were washed twice in 1X Dulbecco's Phosphate Buffered Saline (PBS, Gibco, Grand Island, NY) and then fixed in 4% paraformaldehyde (PF) made up in PBS and stained.

Titanium dioxide Preparation: For each cell exposure experiment, a fresh stock solution of 27 nm TiO_2 was prepared by resuspending 1 mg of dry particles in 1 ml of sterile dH_2O. This solution was then sonicated for 30 seconds using a temperature-controlled cup-horn sonicator (Fisher Scientific, Pittsburgh, PA). The TiO_2 particles were further diluted to their final concentration of 0.5 or 2.5 µg/ml using Keratinocyte Growth Medium (KGM). Just prior to cell exposure, these particle suspensions were sonicated again for 30 seconds and then immediately applied to 6-well dishes that contained 12 mm cover slips.

2.2.4 Cell Fixation, Staining, and Mounting

Following NP exposure, cells were thoroughly washed in PBS, and fixed for approximately 30-60 minutes using 1 ml of 4% paraformaldehyde per well. After fixation, cells were stained using HCS Cell Mask Blue (CMB) as a cytoplasmic stain

or 4',6-diamidino-2-phenylindole (DAPI) for nuclear staining. Staining using CMB was done as an adaptation of the procedure provided by the manufacturer. Briefly, 1 ml of 0.1 µg/ml CMB in 1X PBS was added to each well and allowed to incubate overnight at room temperature. The next morning, cells were washed in 1X PBS followed by a final rinse in dH_2O. Lastly, the coverslips from each well were mounted on newly cleaned slides using Prolong Gold Antifade Reagent. In experiments where DAPI staining was performed, cells were mounted using Prolong Gold Antifade Reagent with DAPI in lieu of overnight staining.

2.2.5 Confocal Microscopy Quality Assurance (QA)

The confocal microscope, lenses and optical components utilized in this study were evaluated for QA using the procedures described by Zucker and Zucker et al. (Taatjes et al, 2006; Zucker, 2006a-c; Zucker et al, 2007). Briefly, colocalization was examined using PSF beads, and field illumination and laser powers were monitored. In the Nikon confocal system, laser fluorescence colocalization was present between the 488 and 561 lines, while the 404 showed a z axis spectral shift with the other 2 visible wavelengths (488 nm and 561 nm) and was not colocalized. This lack of colocalization of UV and visible laser light with the Nikon C1Si is quite typical of confocal microscopes from all manufacturers.

2.2.6 Simultaneous DF and CLSM

In conventional DF microscopy, light travels through a DF condenser with a numerical aperture that is higher than that of the objective lens. The light illuminates the sample and is detected by an objective with a lower numerical aperture than that

of the condenser. It is useful to have an iris in the lens to accurately and ideally control the numerical aperture of the objective and the amount of scattered light entering it. In the technique described here the conventional DF optical path has been reversed. The light is focused on the sample with a lens containing an iris, and then the scattered light is detected with a transmitted light detector. The numerical aperture of the objective must be below the numerical aperture of the condenser for DF to work (Figure 2.2.6.1).

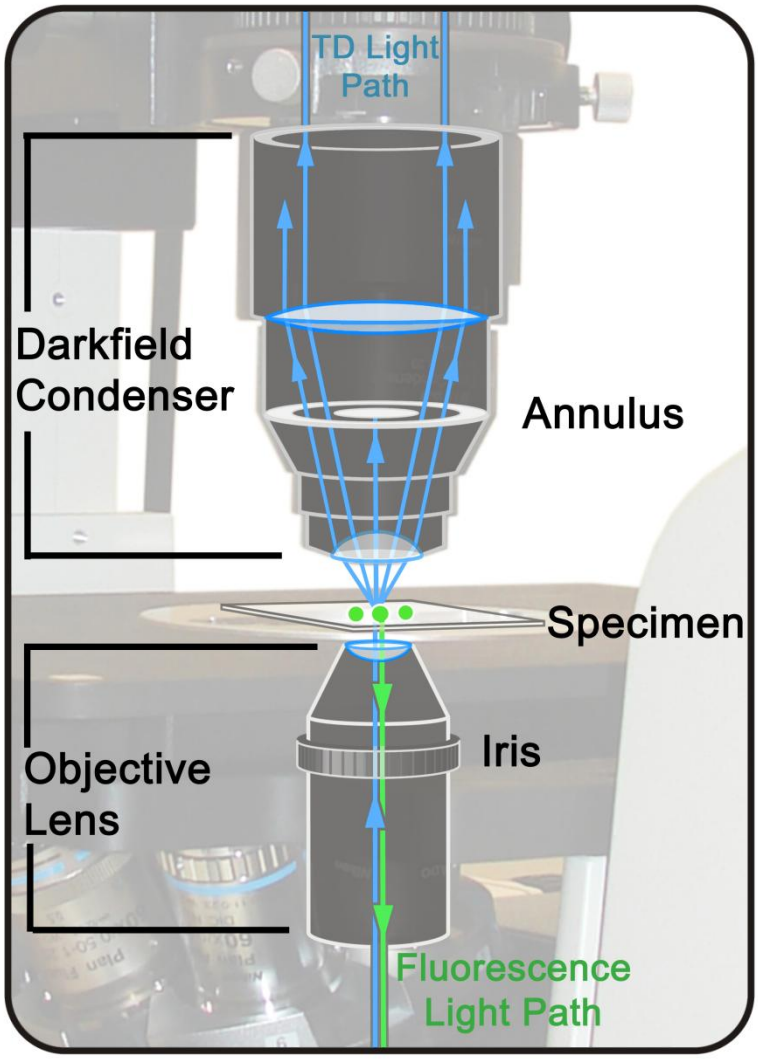

Figure 2.2.6.1 Schematic diagram of an inverted confocal system equipped for simultaneous fluorescence and darkfield imaging. In this example, source laser light (Blue) is focused on the specimen for fluorescence excitation. Fluorescence light emitted by the specimen (Green) is collected by the objective in a conventional CLSM manner. The darkfield condenser collects the scattered light. The numerical aperture of the objective is adjusted using the iris diaphragm to allow only excitation source light that is scattered by the specimen to reach the transmitted light detector (TD).

Imaging was carried out on two different configurations of confocal microscopes from Nikon and Leica. 1) A Nikon Eclipse C1si Spectral Confocal imaging system (Nikon Instruments Corporation, Melville, NY) equipped with an oil immersion Darkfield condenser (numerical aperture = 1.2 − 1.43) and 404 nm, 488 nm, 561 nm, and 633 nm lasers served as the primary means for experimental analysis. Specimens were observed via an Eclipse Ti microscope using either a 60x or 100x Plan Fluor oil immersion objective lens with adjustable iris permitting an numerical aperture ranging from 0.5 to 1.25. DF images were acquired via a transmission detector (TD). For fluorescence excitation, a conventional confocal optical path is maintained in which laser light originating from the objective lens is focused onto the specimen and then collected through the objective lens, Fluorescent light is then passed through an aperture (pinhole), and focused onto a detector consisting of a photomultiplier tube (PMT) tuned to detect specific wavelengths of light. Transmitted light detection of darkfield images begins with illumination by the same laser light originating from the objective lens. An occluding disc built into the darkfield condenser above the specimen blocks incoming light travelling on a direct path from the source but collects light scattered by the specimen and allows it to reach a transmission detector coupled to a PMT capable of monitoring multiple wavelengths of light. It is essential to have the numerical aperture of the condenser to be greater than the numerical aperture of the objective lens. 2) The 2nd configuration was used to show the methodology is applicable on instrument from different manufacturers. A Leica DIRBE microscope with a dark field condenser, 1 mm condenser lens and Plan Apo 63x with an adjustable iris

diaphragm that was variable between 1.32 numerical aperture and 0.6 numerical aperture was employed. This system used a dry condenser, compared with the oil condenser from the Nikon system. The Leica system used a Plan Apo lens with an air condenser while the Nikon system used a Plan Fluor lens with an oil condenser. A higher numerical aperture with better resolution was achievable with the Nikon system due to the oil condenser. However this oil condenser is not applicable on all manufacturers' inverted microscopes.

DF-CLSM images of fluorescent polystyrene beads observed in the absence of cells were acquired under 404 nm and 488 nm laser illumination/excitation while images of TiO_2 exposed cells were obtained primarily using 404 nm laser light for better resolution. Cellular and organelle-specific fluorescent stains were used to image the space in which the NP were localized. Simultaneous fluorescent (Confocal) and transmission (Darkfield) imaging were performed for all two- and three-dimensional images acquired using this technique. All images were collected using Nikon EZ-C1 software, and post-acquisitional processing was performed using the Nikon NIS-Elements AR software package. The confocal slice number corresponding to maximal light scatter intensity was taken as the location of the nanoparticle. Similarly, the slice at which maximal fluorescence intensity was observed was used to identify the location of the nucleus. For statistical comparison, normalization of particle position relative to the nuclei of multiple cells was accomplished by subtracting the nuclear slice number from the particle slice number, dividing by the total number of slices, and multiplying by a factor of 100 to obtain the closest whole-number.

2.2.7 Statistical Analyses

Pairwise comparisons were analyzed by the Wilcoxon's signed rank test using GraphPad Prism statistical software (San Diego, CA); $p<0.05$ was considered significant.

2.3 Results

2.3.1 DF-CLSM detection of nanoscale particles

In order to validate the DF-CLSM approach to nanoparticle detection, we imaged various intrinsically fluorescent polystyrene spheres of known size, ranging from 50 nm to 6.5 µm in diameter. As demonstrated in Figure 2.3.1.1A, the DF and CLSM images of polystyrene spheres colocalized in the XY plane with discrete particles down to 100 nm in diameter using the 488 nm laser line for optimal fluorescence excitation. Preparations of 50 nm fluorescent particles showed weak fluorescence with 488 nm excitation, but could still be resolved as monomeric units by DF detection (Figure 2.3.1.1A). Figure 2.3.1.1B confirms colocalization of DF particle image with fluorescence image in all three spatial axes. These results demonstrated the feasibility of the DF-CLSM combination in detecting particles in the nano size range using transmitted light detector and correlating these transmitted light images (DF) to a specific fluorescence signal which was derived from the same laser source. Experiments using 3 laser lines revealed that colocalization of the 404 nm, 488 nm and 561 nm excitation wavelengths was not attainable in the DF-CLSM optical path (Figure 2.3.1.1C). There was a z-axis distortion between 404 nm and remaining visible laser lines, as well as a lateral shift between the 561 nm and 488 nm excitation lines. The co-localization problems were greater with NP than it was with micron and submicron particles.

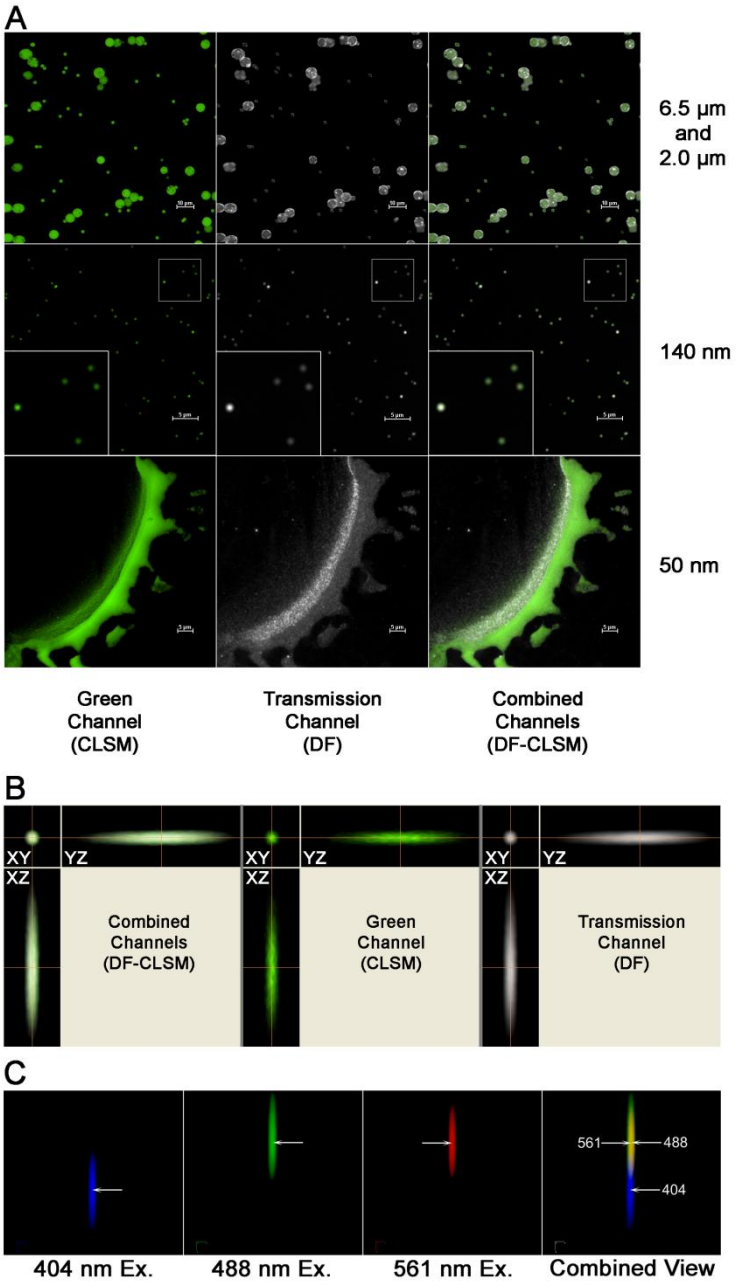

Figure 2.3.1.1 Detection of fluorescent polystyrene spheres by co-localized confocal and darkfield microscopy. A. Fluorescent polystyrene beads of the indicated sizes were illuminated with 488 nm laser light. Emitted particle fluorescence was detected using the confocal microscope in the green channel while scattered incident light collected by the darkfield condenser was simultaneously observed via the transmitted light detector. For the 140 nm spheres, insets in the

lower left-hand corner show an enlarged area for clarity. **B.** Three dimensional colocalization analysis of a 500 nm fluorescent polystyrene sphere imaged by DF-CLSM. The sphere shown was excited by 488 nm laser light while simultaneous monitoring for fluorescence and scattered light occurred via the green and transmitted light channels. Each set of images shows the XY, XZ, and YZ orientation for the combined, green (CLSM), and transmission (DF) channels, respectively. The large crosshairs represent the same point in space across all the axial views. **C.** Variability in spatial localization of DF images obtained with multiple wavelengths of light. Shown are 10x pseudo-colored images of the same 27 nm TiO2 particle illuminated by 404 (Blue), 488 (Green), and 561 (Red) laser light. Each set of images depicts the X, Y, and Z orientation for the transmission (DF) channel. For the combined view, areas of overlap in the 488 and 561 excitations are observed in yellow. The arrows represent the midpoint of the same particle illuminated at each wavelength, showing a small x,y lateral distortion between the 488 and 561 nm excitation lines, while both the 488 and 561 have a much larger axial (z) dispersions from the 404 excitation line. Note the large separation between the blue excitation and the visible laser excitation lines. 60x Plan Fluor, Magnification 600x + 1, 5, or 10x zoom as designated.

The use of multiline lasers including the 404 nm laser will yield significant axial distortion in the cellular localization of the particle. For these reasons, subsequent measurements made with DF-CLSM were restricted to single-line excitation or sequential multi-line acquisitions in the visible range with only one laser line being used to excite the DF signal. As expected the shortest wavelength (404 nm) was found to provide the best resolution and was used for high resolution work. However the 488 laser provides more functionality as it is compatible with a greater number of cellular probes.

We next evaluated the utility of the DF-CLSM approach in detecting nanoparticles associated with cells. BEAS 2B cells were exposed to 27 nm TiO_2 for 2 hrs, fixed and imaged using DF-CLSM. Three-dimensional analysis of these cells stained with Cell Mask Blue (CMB) revealed the expected cellular morphology (Figure 2.3.1.2). Due to the lack of confocality, and the scattering of light in the DF light path, three-dimensional reconstruction depicts nanoparticles as elongated rod-like structures whose longitudinal spread extends symmetrically through the slices of the z-stack. A typical fluorescent PSF (Point Spread Function) is not obtained in darkfield with the DF-CLSM method. When superimposed on the confocal image of the cell, the TiO_2 nanoparticle rods appeared to localize through the body of the cell, suggesting that they are within the cells. The center of the nanoparticle can be determined by the position of maximum intensity in the cigar type image of the NP.

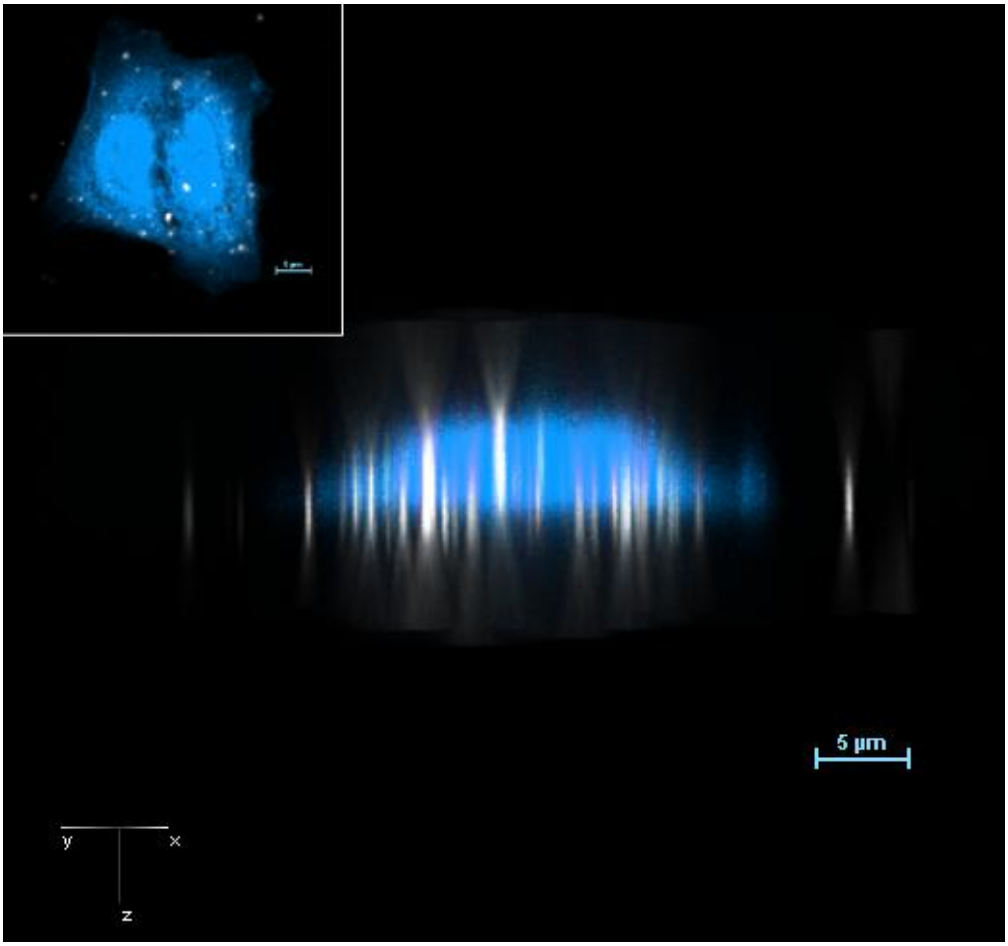

Figure 2.3.1.2 Darkfield(DF)/Confocal(CLSM) imaging of TiO2 nano particles internalized by human bronchial epithelial cells. BEAS 2B cells were exposed to 27 nm TiO_2 for 2 hours followed by fixation and staining with HCS Cell Mask-Blue to visualize the cytoplasm. Shown is a pseudo-colored side view taken along the Z-axis of these cells. Particles appear as elongated structures due to the lack of confocality in the darkfield optical path. The inset displays a top (XY) view of the same cells. Cells were excited using only the 404 laser line while fluorescence was monitored using the blue channel. Magnification 1800x with a 3x zoom. 60x plan fluor objective

2.3.2 Examination of in vitro particle internalization using DF-CLSM

We next undertook a series of experiments designed to measure particle internalization using DF-CLSM by exploiting the expectation that particle internalization is a time-dependent process. Figure 4 shows abridged galleries corresponding to representative slices from z-stack images for BEAS 2B cells exposed to 27 nm TiO_2 for 5 or 120 min. After incubation, the cells were washed in PBS and fixed in a medium containing DAPI to stain the cell nucleus. Relative to the 5 min time point, nanoparticles in cells exposed to TiO_2 particles for 120 min were detected at slice numbers corresponding to deeper locations within the cell (Figure 2.3.2.1), consistent with a time-dependent penetration of particles into the cell. The actual position of the particle can be determined by the confocal slice that has the maximum intensity in the DF image.

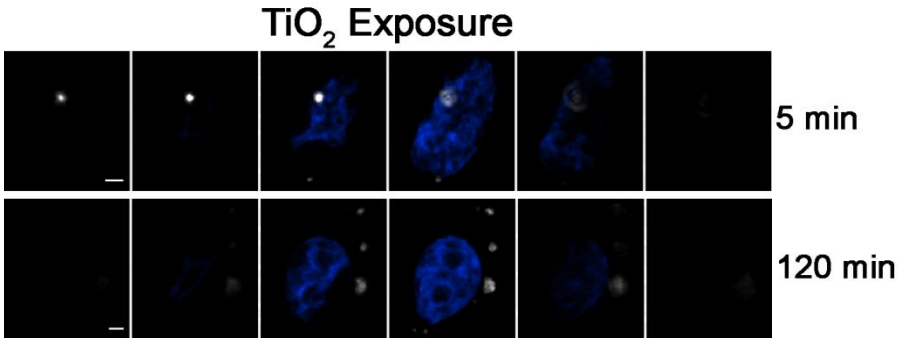

Figure 2.3.2.1 Image galleries of BEAS cells exposed to nanoparticles for 5 and 120 min. Shown are optical sections taken from a confocal z-stack of nuclear fluorescence with darkfield detection of NP. Results show time-dependent internalization of nanoparticle uptake by human bronchial epithelial cells imaged by Darkfield (DF) / Confocal (CLSM) microscopy. BEAS-2B cells were exposed to 27 nm TiO_2 particles for 5 min (top gallery) or 120 min (bottom gallery), fixed and stained with DAPI. The nanoparticles (depicted as white) were located in slices above the blue nucleus at 5 min but were on the same sections as the nuclei at 120 min. Cells were excited using the 404 laser line while fluorescence was monitored using the blue channel. Scale bar represents 2 µm. Magnification 3000x with a 5x zoom.

In order to provide an empirical expression of nanoparticle penetration in the cell, scattered light and DAPI fluorescence intensities were plotted as a function of z-stack slice number for BEAS cells exposed to TiO_2 for 5 or 120 min (Figure 2.3.2.2). Following 5 min of exposure, the peak scatter intensity of a representative particle was found at a slice number located above the slice that corresponded with the peak fluorescence of the nucleus (Figure 2.3.2.2, panels A and B). In contrast, by 120 min of TiO_2 nanoparticle exposure, the peak scatter intensity of a representative particle was found at a slice number that coincided with the location of the center of the nucleus (Figure 2.3.2.2, panels C and D). This shows that this technique can be used to measure the transport of particles though the cell.

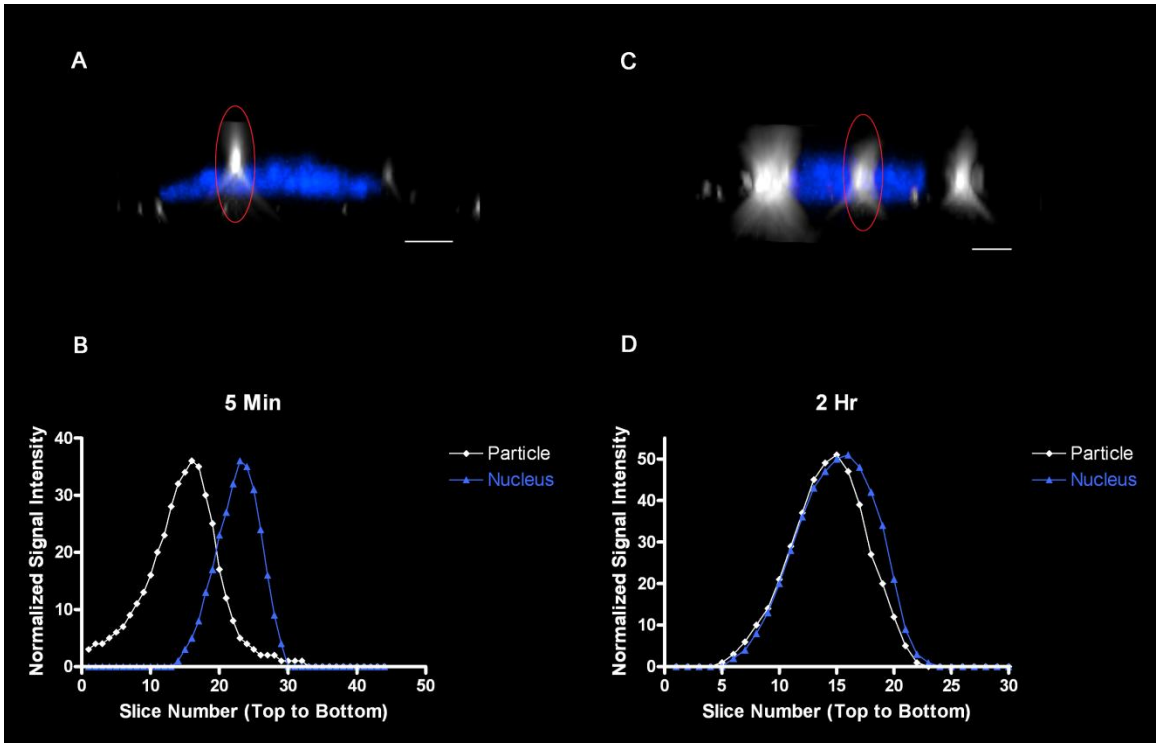

Figure 2.3.2.2 Determination of nanoparticle location using the maximum intensity technique. Scatter and fluorescence intensity plots through the z-axis of the entire cell volume are plotted for cells incubated with TiO_2 for 5 min and 2 hr time points for both a selected particle of interest (circled in red) and the corresponding nucleus, respectively. Fluorescent and scatter light intensity values have been normalized to the same peak height for clarity. Scale bar represents 10 µm. Magnification 3000x with a 5x zoom.

To further test this approach in a practical application, we compared the location of maximal particle scatter intensity relative to the nucleus in the z-axis for BEAS cells exposed to 27 nm TiO_2 continuously for either 5 min, or “pulsed” for 5 min followed by washing and an additional 115 min incubation in particle-free media prior to fixation (120 min-pulsed). The data were normalized for slice number and the slice in which the nucleus was centered was designated as zero. Similar to the results in Figure 2.3.2.2, a clear shift in the mean particle location inferred from maximal light scatter was observed between cells exposed to particles for the 5 and the 120 min-pulsed groups. Specifically, there was a time-dependent change in the location of the particle maximum intensity and presumed center away from the cell surface towards the nucleus and slide surface (Figure 2.3.2.3). Interestingly, the 120 min-pulse cells showed particles clustered above, coincident with and below the nucleus center. This may reflect distinct intracellular paths established by the presence of the nucleus within a large fraction of the cell volume or may be due to in part to the variation in intracellular “z” volumes. These findings demonstrate that DF-CLSM is useful to observe time-dependent NP transit within the cell.

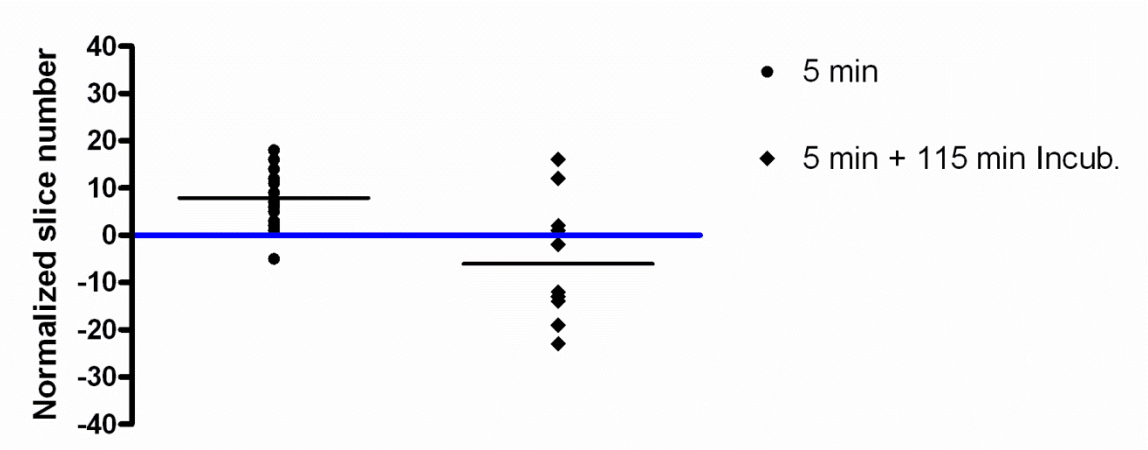

Figure 2.3.2.3 Statistical analysis of mean particle location in cells exposed to 27 nm TiO_2 for varying lengths of time. Particle localization within the z-axis was taken as the optical section containing maximal intensity in the dark field channel, and is plotted relative to the section in which DAPI fluorescence was most intense (center of nucleus normalized to zero, depicted as horizontal blue bar). Within each group of particles, the black line illustrates an averaged (mean) particle location for the center of each particle, as detected using DF-CLSM. Note that at 120 min incubation the particles are located above, below and at the midpoint of the nucleus, suggesting variations in cell morphology and distinct transit paths.

2.4 Discussion

While the use of NP in consumer products, industrial processes, and pharmaceutical applications continues to grow, knowledge of the impact of nanomaterials on human health remains limited (Yang et al, 2008). Compounding the challenge presented by the paucity of toxicological information on nanomaterials, investigators studying the biological effects of nanomaterials are faced with a number of unique challenges. Fundamental questions pertinent to the interaction between nanoparticles and the cell are best addressed with imaging studies. However, NP are usually not detectable by conventional light microscopy methods. In some instances, fluorescent nano materials (i.e., Q-dots) can be used with fluorescent microscopy. Darkfield microscopy can detect the presence of nanoparticles, but their location within the cell or on the surface of the cell cannot be determined with accuracy using a wide field microscope. The combination of darkfield and confocal microscopy described in this manuscript was developed in an effort to address some of these imaging challenges by bringing the strengths of two distinct light microscopy techniques (DF and CLSM) to study the interactions of cells with environmentally relevant NP.

While confocal and wide-field fluorescence microscopy are commonly used to image synthetic nanoparticles tagged with fluorophores (e.g., Q-dots) evidence that particle surface chemistry plays a critical role in toxicity raises questions about the relevance of these materials as surrogates for “real world” nanoparticles (Meng et al, 2009; Nel et al, 2009). Electron microscopy (EM) is usually thought of as the “gold

standard" for investigation of the biological impacts of nanomaterials. Unfortunately, EM can be quite laborious and costly to employ. Darkfield microscopy is essentially an illumination-based imaging technique used to enhance the contrast of specimens for increased visibility (Murphy, 2001; Spencer M, 1982; Wayne R, 2009; Chandler and Roberson, 2009). Confocal microscopy is a multifaceted light microscopy technique that contributes increased resolution and optical sectioning of specimens for three dimensional analyses, as well as the precise application of excitation wavelengths (Mills et al, 1994; Hibbs, 2004; Smith, 2001). The utility of DF-CLSM in detecting NP was established by experiments in which we show that the DF scatter signal colocalizes with the fluorescence of polystyrene particles with sizes as low as 50 nm in diameter. In fact, the DF signal appeared to provide superior discrimination of monomeric units relative to fluorescence for 50 nm particles. In this study, the location of maximal scatter intensity in the z-axis was presumed to be the physical center of the particle. Using this approach, it was possible to determine the depth of penetration of the particle within the cell relative to an organelle or the nucleus. In separate experiments, similar measurements of particle penetration were made using DF-CLSM with the cell membrane as a reference. Thus, the combination of DF optics with the power of a confocal microscope yields an image in which NP can be visualized within a narrow and precise focal plane for the spatial determination of NP within the cell in the z-axis. With the application of currently available and novel deconvolution processing algorithms, it may be possible to better localize the NP within the volume of the cell in three dimensions. Importantly, the DF-CLSM technique allows the visualization of non-fluorescent particles, making it suitable to

the study of environmentally relevant NP. An additional advantage of DF-CLSM is its potential to be used in experiments involving live-cell imaging, which is impossible with conventional EM.

Detection of NP using DF-CLSM relies heavily on the intrinsic light scattering properties of the material being observed. In the validation of this technique, DF-CLSM proved to be sufficiently robust to detect several types of NP comprised of different materials ranging from polymers to nanodiamonds and metal oxides (Gibbs et al, unpublished). Interestingly, even materials with relatively smooth surfaces, like the polymers of polystyrene beads, have sufficient light scattering properties to be detected by this technique. The associated signal from larger polystyrene beads is less than that produced by smaller TiO_2 nanoparticles.

The DF-CLSM imaging approach holds considerable promise for future applications in the study of the biological interactions of NP. While in the present study we chose to use a simple nuclear stain in the assessment of particle internalization, other biological processes and interactions could be examined by DF-CLSM using the numerous biosensors and staining reagents available. For laboratories with existing CLSM imaging equipment, implementation of DF-CLSM requires only the acquisition of a relatively inexpensive darkfield condenser and objective lenses with a suitable variable iris to adjust the numerical aperture, or objectives lenses with low fixed numerical aperture values. We have been able to successfully adapt both Leica and Nikon inverted confocal microscopes with condensers costing between $70 and $700, respectively.

As with any technique, DF-CLSM has limitations. In this regard, it is important to bear in mind that this application of DF is a detection method, not a technique that permits direct observation or exact size of the NP. Thus, this method does not produce an accurate size representation of nanoparticles. Likewise, agglomerates of nanoparticles may be represented as a single point with a larger size and increased light scatter. Therefore, inferences regarding size, shape, and number (i.e., agglomeration) of the structures being examined are limited, as other factors such as surface irregularity and reflectivity contribute significantly to the signal strength in DF detection. Furthermore, although they are less expensive than their high numerical aperture counterparts, it should also be noted that low numerical aperture objectives required for DF present disadvantages as well. Low numerical aperture objectives impose limits on optical resolution and may introduce chromatic aberration into the image. In our characterization of this technique, we have found that choosing a single excitation wavelength is the best way to avoid chromatic aberration and colocalization errors. Similarly, the DF and confocal fluorescence signals should ideally be acquired using the same excitation wavelength in order to avoid possible colocalization errors between different wavelengths of lights, as shown in Figure 2.3.1.1C. In cases where multiple excitation wavelengths are needed, they should be used sequentially rather than simultaneously and the 404 nm line should not be used with the visible wavelengths. The shortest wavelength should be used for the acquisition of the DF signals, but it is important to use a wavelength in which the NP is being localized with the fluorescence structure. Notably, appropriate use of the excitation wavelengths used during image

acquisition must be taken into account because data acquired with sequential excitation of multiple wavelengths may introduce chromatic aberration errors in the sample between the nanoparticles derived from one wavelength and the fluorescent signals derived from the other laser lines. This is not necessarily a limitation unique to this application, but more likely a limitation resulting from the UV and visible colocalization issues in CLSM and the quality and alignment of the optical components used in the CLSM equipment. It appears that the nanoparticles accentuate these colocalization problems relative to submicron and micron particles. It is recommended that characterization of issues regarding chromatic aberration and colocalization of various wavelengths should be made for each imaging system and each lens used.

2.5 Conclusions

Even with the acknowledged limitations, the DF-CLSM methodology represents a novel and workable option for many investigators searching for a light microscopy technique that can be used to study the interactions between cells and NP in the environment. By interfacing the ability of darkfield microscopy to use light scatter to detect very small structures with the power of confocal microscopy to render specimens in three dimensions, DF-CSLM provides a solution to the unique challenges of conducting toxicological studies in the nano-scale. The DF-CLSM technique is superior to widefield DF as it uses the power of the confocal microscope to produce 3D images of nanoparticles within cells.

Chapter 3

Monitoring Intracellular Redox Changes in Airway Epithelial Cells Exposed to Ozone[1]

3.1 Introduction

The intracellular redox environment is a highly dynamic setting governed by the formation and degradation of various reactive species of oxygen and nitrogen. Under normal physiological conditions, the cytosol, nucleus, and mitochondrial matrix space maintain homeostatic conditions in favor of a highly reducing environment (Cannon and Remington 2009). Intracellular reducing conditions are largely maintained by millimolar concentrations of reduced glutathione and its accessory enzymes that together comprise the glutathione system (Anderson 1998). Ultimately, maintenance of the intracellular glutathione redox potential (E_{GSH}) comes from the metabolism of glucose, as glutathione is reduced by glutathione reductase using NADPH produced by the pentose phosphate pathway (Wamelink et al. 2008).

A number of pathophysiological states are associated with changes in the intracellular glutathione redox potential (Dubinina and Dadali 2010; Ma 2010; Yang and Omaye 2009). Such "oxidative stress" is commonly cited as a mechanistic

[1] The findings of this chapter have been accepted for publication as follows: Eugene A. Gibbs-Flournoy, Steven O. Simmons, Philip A. Bromberg, Tobias P. Dick, and James M. Samet. "Monitoring Intracellular Redox Changes in Ozone-Exposed Airway Epithelial Cells" Environmental Health Perspectives, epub ahead of print *2012*

feature of the toxicity of numerous xenobiotic compounds linked to adverse health outcomes (Bargagli et al. 2009; Ciencewicki et al. 2008; Kohen and Nyska 2002). For instance, the health effects of the potent ambient air pollutant ozone (O_3) are understood to be mediated through an oxidative stress mechanism involving the oxidation of cellular biomolecules (Ballatori et al. 2009; Kelly et al. 1995; Mudway and Kelly 2000). In the lung, ozone exposure causes decrements in pulmonary function and induces inflammatory responses derived from the bronchial epithelium, a major target of ozone exposure (Ballinger et al. 2005; Kelly et al. 1995; Mudway and Kelly 2000; Pryor 1992; Pryor et al. 1995; Song et al. 2010). Due to its high reactivity, O_3 interacts with cellular and extracellular biomolecules, resulting in multiple types of oxidative damage to lipids, proteins, and nucleic acids (Kelly et al. 1995; Laumbach ; Mudway and Kelly 2000; Srebot et al. 2009; Van der Vliet et al. 1995; Yang and Omaye 2009). While numerous studies have established oxidant damage of biomolecules as a result of O_3 exposure, direct measures of ozone-mediated 'oxidative stress' have been difficult to achieve, yet alteration of a defined intracellular redox couple like glutathione would represent an important early indicator of the oxidative effects of O_3 exposure.

Recent methodological advances have made it possible to focus studies of pro-oxidative changes to specific redox couples within defined subcellular compartments (Meyer and Dick 2010), potentially affording greater specificity in mechanistic investigations of the oxidative effects of xenobiotic exposures. A new generation of genetically-encoded fluorophores permits direct assessment of the oxidative effects of xenobiotic compounds in relation to the glutathione redox pair

(GSSG/GSH) with unprecedented spatial and temporal resolution (Cheng et al. 2012; Meyer and Dick 2010). roGFP2 acts as a reporter of intracellular glutathione redox potential by equilibrating with the GSH/GSSG redox pair (Cannon and Remington 2006, 2008; Dooley et al. 2004; Meyer and Dick 2010; Morgan et al. 2011). In short, in a reaction that depends on catalysis by glutaredoxins, roGFP2 responds to oxidation of reduced glutathione (GSH) to its oxidized form, GSSG, via the internal formation of a disulfide bond (Gutscher et al. 2008; Meyer 2008; Meyer and Dick 2010) (Figure 3.1.1). The formation of the disulfide bond alters the spectral characteristics of the GFP fluorophore, causing the intensity of the emitted green fluorescence (~520 nm) induced by excitation at 488 nm to decrease, while causing the emitted fluorescence after excitation at 405 nm to increase, thus making this sensor a ratiometric probe.

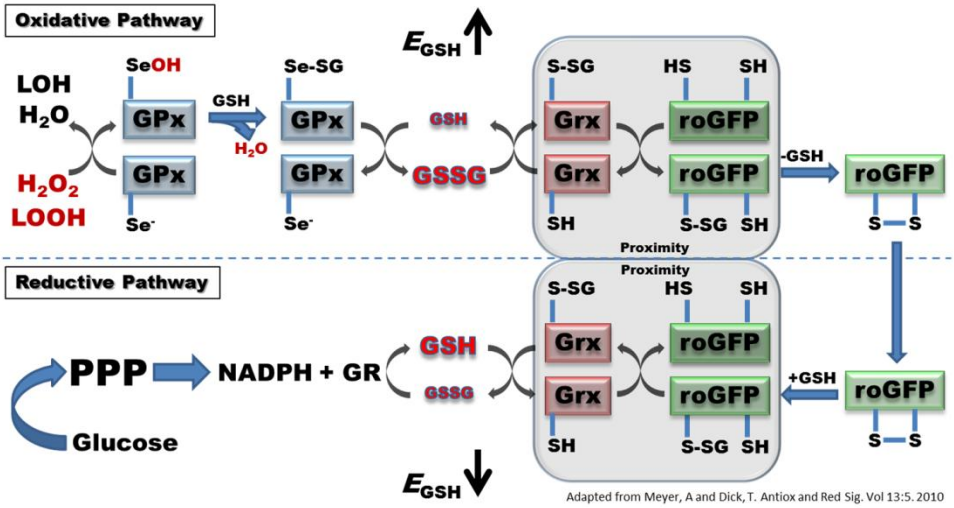

Figure 3.1.1 roGFP2 interactions with the glutathione system. (adapted from Meyer and Dick, 2010). Glutathione peroxidases (GPx) oxidize GSH to GSSG in response to peroxides, including H_2O_2 and lipid hydroperoxides (LOOH), thus increasing the glutathione redox potential (E_{GSH}). In response to the increase in GSSG, one of the engineered vicinal cysteines of roGFP2 becomes S-glutathionylated by glutaredoxin (Grx). Glutathionylation in turn causes disulfide bond formation and alteration of the spectral properties of the GFP fluorophore. In the reductive pathway, Grx catalyzes the reduction of roGFP2 disulfide bonds through deglutathionylation as GSSG levels decrease and normal levels of GSH are reestablished by glutathione reductase (GR), at the expense of NADPH, causing a renormalization of E_{GSH}. Glucose and the pentose-phosphate pathway (PPP) create NADPH, which is used by GR to reduce GSSG to GSH.

Further efforts to improve the responsiveness of roGFP2 have led to the conjugation of pathway-specific enzymes to create a chimeric fusion of proteins operating as redox relays. In particular, the conjugation of glutaredoxin 1 (Grx1) to roGFP2 has been shown to enhance the kinetics of the roGFP2 response to the oxidation of glutathione (Gutscher et al. 2008).

In the present study, we used live-cell microscopy to monitor the cytosolic E_{GSH} of airway epithelial cells undergoing exposure to ozone in real-time. Here, we report an approach to validate the use of roGFP2-based redox sensors in toxicological studies of xenobiotics with strong oxidizing properties.

3.2 Methods

3.2.1 Materials and Reagents

Tissue culture media and supplements were purchased from Lonza (Walkersville, MD). Wilco Wells glass-bottom culture dishes were obtained from Ted Pella (Redding, CA) and Warner Instruments (Hamden, CT). Fugene 6 transfection reagent was acquired from Roche Applied Science (Indianapolis, IN). Kits to measure intracellular glutathione and NADPH were bought from Promega (Madison, WI) and AbCam (Cambridge, MA), respectively. Laboratory reagents and chemicals including Hydrogen peroxide, Dithiothreitol (DTT), 2-acetylamino-3-[4-(2-acetylamino-2-carboxyethylsulfanylthiocarbonylamino)phenylthiocarbamoylsulfanyl]propionic acid (2-AAPA), Buthionine sulfoximine (BSO), and Sodium selenite were obtained from Sigma-Aldrich (St. Louis, MO). Basic laboratory supplies were purchased from Fisher Scientific (Raleigh, NC).

3.2.2 Cell Culture

Transformed human airway epithelial cells (BEAS-2B, subclone S6; (Reddel et al. 1988)) were cultured as previously described (Tal et al. 2010) and maintained in serum-free keratinocyte growth medium, KGM (Lonza, Walkersville, MD). The cells were incubated in a humidified incubator at 37°C in 5% CO_2. For most live-cell

exposures, BEAS-2B cells were plated in 35mm Wilco Wells glass-bottom dishes with a 12 mm #1.5 glass aperture (Ted Pella, Redding, CA).

3.2.3 Genetically Encoded Redox Sensors

Plasmid for the redox-sensitive green fluorescent protein 2, roGFP2, was the generous gift of Dr. S. J. Remington (University of Oregon, Eugene, OR). Plasmid for the hydrogen peroxide sensor, HyPer, was purchased from Evrogen (Axxora, Farmingdale, NY). Cytosolic and mitochondrially targeted versions of roGFP2 and HyPer were placed in lentiviral vectors as described previously (Cheng et al. 2012).

3.2.4 Plasmid Transfection and Lentiviral Transduction

One to two days prior to exposure, BEAS-2B cells were transiently transfected with 1 – 2 ug of plasmid DNA encoding Grx1-roGFP2, HyPer, or roGFP2 using 3 – 5 ul of Fugene 6 transfection reagent for each 35mm culture dish. Stable expression of a specific genetically encoded fluorescent reporter was performed via lentiviral transduction. In short, a lentivirus encoding roGFP2 or HyPer (specifically targeted to the cytosol or mitochondria) was incubated for 4 hrs (37°C / 5% CO_2) with wild-type BEAS-2B cells using a multiplicity of infection (MOI) of 5 – 10 in a single well of a 6-well dish. The viral particles were then removed and fresh KGM was placed on the cells, and the BEAS-2B cells were then allowed to grow to confluency. Upon confluency, the cells were expanded to T75 dishes where they

were propagated for multiple passages. For some experiments, stably transduced cells were sorted for optimal fluorescence expression at the UNC Core Flow Cytometry Facility

3.2.5 Exposure Conditions

Newly transfected or stably transduced BEAS-2B cells expressing the fluorescent reporter of interest were cultured as described above. Prior to exposure, subconfluent cells were equilibrated in Locke solution (Taylor-Clark and Undem 2010) for 2 hrs. at 37°C in 5% CO_2. For the studies herein, two versions of Locke Solution were derived by adding or excluding 1 mg/ml dl-glucose. Irrespective of the type of Locke solution used to equilibrate cells, all live-cell O_3 exposures were performed using 0.5 ml of Locke solution without glucose. For all imaging experiments, cells were exposed in a custom-built stage-top exposure system maintained at 37°C with 1.5 L/min of 5% CO_2/balance air at a relative humidity ≥ 95% (Figure 3.2.5). In some experiments, cells were pretreated with 100 µM 2-AAPA, a dithiocarbamate inhibitor of glutaredoxins, during the 2 hr buffer equilibration period. Similarly, pretreatment of cells with 1 µM sodium selenite for 24 – 48 hrs prior to O_3 exposure was carried out to induce the overexpression of glutathione peroxidases (GPx).

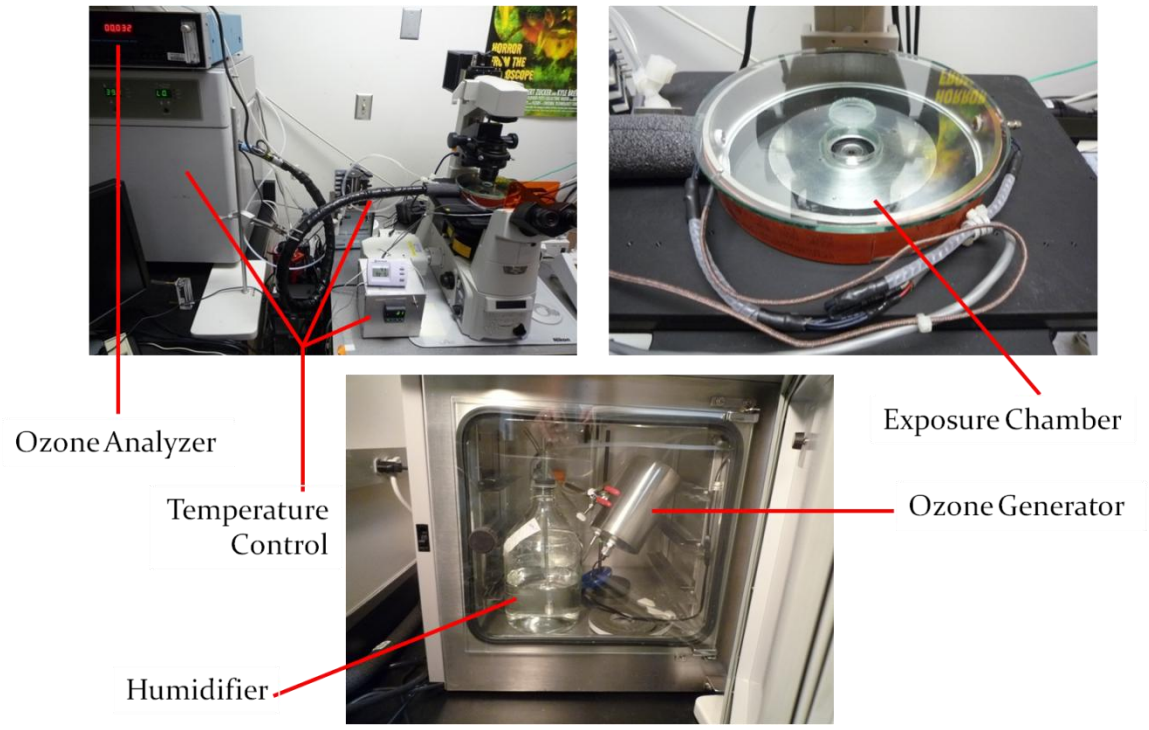

Figure 3.2.5 Stage-top ozone exposure system. Displayed are components of the stage-top ozone exposure system used for all real-time assessments of living cells undergoing O_3 exposure. 5% CO_2/Balance Air entering the system is first humidified by bubbling it through autoclaved dH_2O housed in a 37°C incubator. The gas is then passed through an O_3 generator where O_3 is created by using a UV pen lamp. Concentrations of O_3 are controlled by a voltage regulator which adjusts lamp intensity. The newly generated O_3 then flows to a temperature-controlled, stage-top exposure chamber via a heated line. All gas entering the exposure chamber is sampled by a Dasibi ozone analyzer at a T-fitting placed at the end of the heated line, just before the entrance to the chamber. The humidity of gas diverted to the O_3 analyzer is removed using a Perma Pure gas drier. All heated components are maintained at or above 37°C to maintain ≥90% humidity of the flowing gas.

For each experiment, cells were exposed to control air (5% CO_2/Balance air) or ozone concentrations ranging from 0.15 – 1.0 ppm. The entire exposure period typically consisted of 3 component intervals collectively lasting up to an hour in length. They included: 1) an initial untreated baseline period of 5 min; 2) an exposure period of up to 45 min; and 3) a 10 min control exposure period in which cells were oxidized by 0.1 to 1.0 mM hydrogen peroxide for 5 min and then reduced by 10 mM DTT for an additional 5 min. During these exposures, the ozone concentration in the exposure chamber was monitored in real-time using a Dasibi Model 1003-AH Ozone Analyzer sampling at a flow of 2.0 L/min. Ozone exposures for non-imaging assays were performed using exposure chambers operated by the U.S. Environmental Protection Agency's (EPA) Environmental Public Health Division.

3.2.6 Imaging Analysis

All live-cell experiments done in real-time were conducted using a Nikon Eclipse C1si spectral confocal imaging system equipped with an Eclipse Ti microscope, Perfect Focus System, and 404 nm, 488 nm, 561 nm, and 633 nm primary laser lines (Nikon Instruments Corporation, Melville, NY). Images were acquired using a 60X Plan Apo lens. For experiments involving the genetically encoded fluorescent reporters, roGFP2 and HyPer, green fluorescence was observed via the use of independent excitations at 404 and 488 nm while emitted light was collected for each using a 525/30 nm band-pass filter (Chroma, Bellows

Falls, VT). Results were calculated as ratios of the emissions excited by the 488 nm and 404 nm lasers scanned sequentially at a frequency of 1 min. All imaging data were acquired using the Nikon EZ-C1 software.

3.2.7 Measurement of Intracellular NADPH

After cells were equilibrated in fresh KGM or Locke solution (+/- glucose) for 2 hrs, the intracellular levels of total NADPH were assessed using an AbCam NADP/NADPH assay kit. The manufacturer's instructions provided with the kit were used to carry out this assay. Following the equilibration period, cells were immediately placed on ice and washed with cold 1X PBS just prior to the initial lysis step. Absorbance was read at 450 nm using a PolarStar Optima microplate reader (BMG Labtech, Durham, NC).

3.2.8 Statistical Analysis

All imaging data were quantified using NIS-Elements AR software (Nikon, Melville, NY). For each experiment, the responses of 5–10 cells were collected as regions of interest (ROI) and then averaged to derive an overall response. Data are expressed as the mean of at least three repeated experiments. Pairwise comparisons of control and treatment groups were performed using ANOVA and linear regression with $p < 0.05$ taken as being statistically significant.

3.3 Results

3.3.1 Ozone exposure induces an increase in the cytosolic glutathione redox potential

The presence of glucose in the exposure media is known to shorten the half-life of O_3 (Taylor-Clark and Undem 2010). Therefore, in these experiments, cells were first equilibrated in Locke solution containing glucose (LS+G) for 2 hrs prior, and then switched to Locke solution without glucose (LS-G) for the exposure. Exposure of BEAS-2B cells expressing cytosolic roGFP2 to 0.15 - 0.50 ppm O_3 resulted in a dose- and time- dependent probe response, reflecting an increase in the cytosolic glutathione redox potential (Figure 3.3.1). Increasing O_3 concentration hastened the onset while elevating the magnitude of the oxidative response reported by roGFP2 (Figure 3.3.1). Addition of 0.1 mM H_2O_2 at the end of each O_3 exposure produced a maximal response which was fully reversible with the addition of 10 mM DTT.

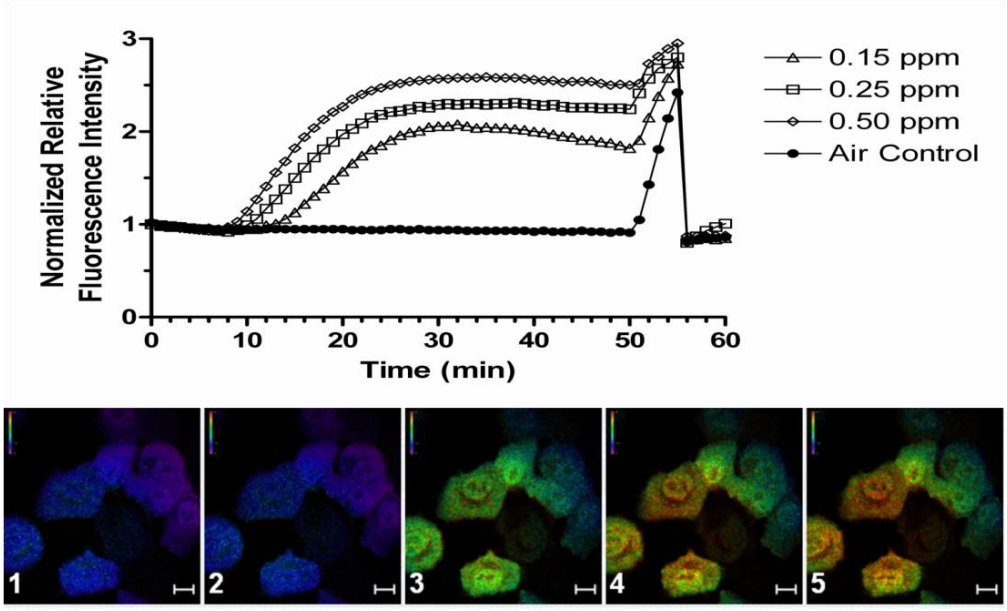

Figure 3.3.1 Exposure to O_3 induces a dose- and time-dependent increase in the cytosolic glutathione redox potential in airway epithelial cells. BEAS-2B cells expressing cytosolic roGFP2 were exposed to clean air for 5 min followed by a 0 (Air Control), 0.15, 0.25 or 0.50 ppm O_3 exposure for 35 min in a stage-top exposure system maintained at 37 °C, >90% relative humidity, and 5 % CO_2. Shown are the ratiometric values (404/488) calculated from the fluorescence intensity emitted at 510 nm induced by sequential excitation at 404 and 488 nm, and plotted relative to the 5 min baseline. Addition of 0.1 mM H_2O_2 at the end of the O_3 exposure produced a maximal response which was fully reversible with the addition of 10 mM DTT. The pseudo-colored images displayed below the plotted data represent ratiometric changes in fluorescence of cells being exposed to 0.5 ppm O_3. Increases in the ratiometric fluorescence intensity are represented by changes in color from Violet/Blue to Red as indicated by the scale bar in the upper left hand corner of each image. Each panel was taken in series at 10 min intervals starting at T=0 min for panel 1 and ending with T=40 min for panel 5. The scale bar in the bottom right corner of each panel is 10 µm in length. The data shown were derived from 3 or more separate experiments monitoring 7 or more cells in real-time throughout the exposure period.

3.3.2 Glucose deprivation potentiates the elevation of E_{GSH} induced by ozone exposure

On an individual basis, BEAS 2B cells equilibrated in the presence of glucose (LS+G) were observed to respond variably to a given concentration of O_3, suggesting substantial heterogeneity of redox homeostasis within the cellular population under the given conditions. Figure 3.3.2.1A shows the individual responses of seven BEAS-2B cells in the same field of view being exposed to 0.5 ppm O_3, with some cells responding with strongly increasing E_{GSH}, while others responded only minimally. Furthermore, some cells exhibited an intermediate response followed by a recovery of E_{GSH} despite continued O_3 exposure. Given the importance of pentose phosphate pathway (PPP)-generated NADPH in maintaining intracellular reduced glutathione levels, we hypothesized that glucose deprivation would sensitize the cells to a subsequent O_3 exposure. As shown in Figure 3.3.2.1B, depriving the cells of glucose for 2 hr prior to exposure homogenized the magnitude, time of onset, and rate of response of the cells to O_3. Glucose status did not affect the probe response to addition of H_2O_2 and DTT (Figures 3.3.2.1 A and B). As expected, glucose deprivation led to decreased cellular NADPH levels (Figure 3.3.2.2).

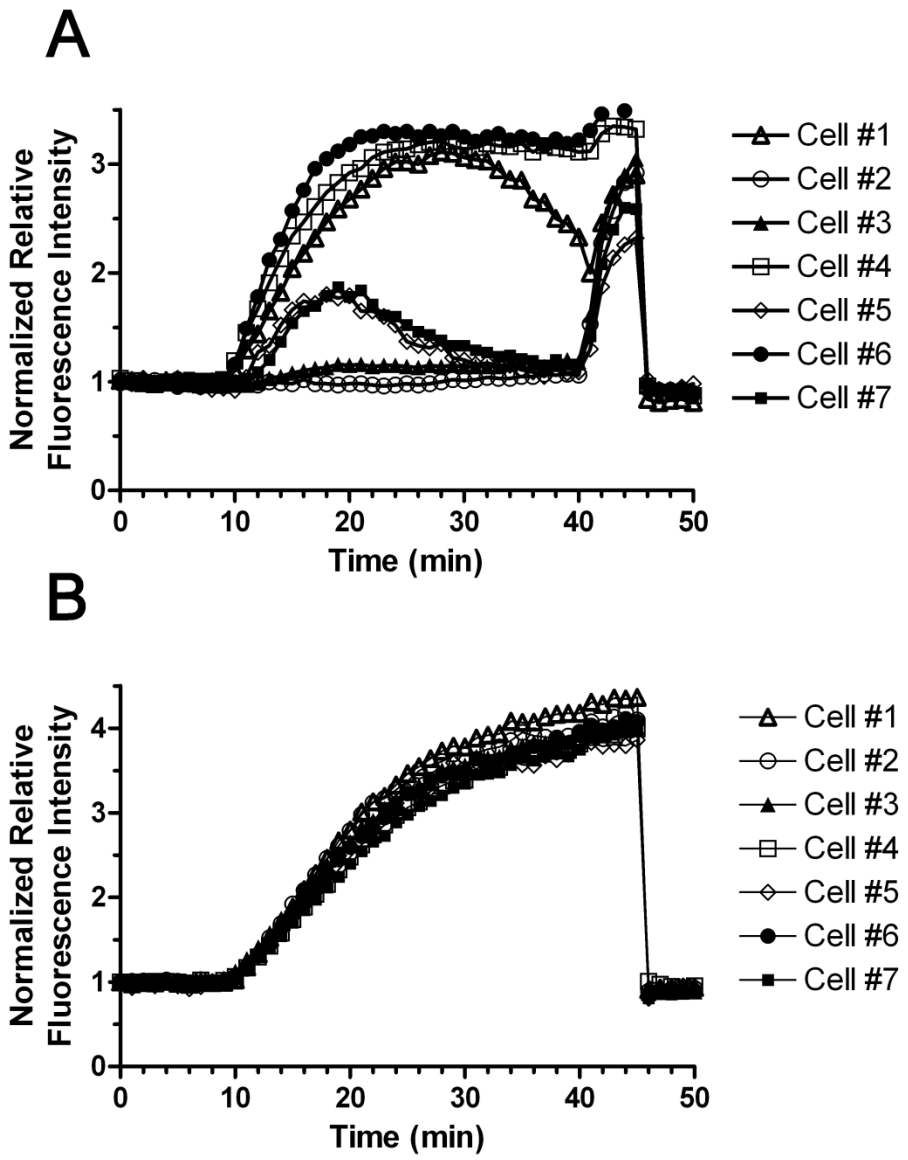

Figure 3.3.2.1 Glucose deprivation sensitizes cells to O_3-induced roGFP2 oxidation. Shown are the responses of 7 BEAS-2B cells equilibrated in Locke Solution containing 1 mg/ml glucose (A), or 0 mg/ml (B). Cells were exposed to 0.5 ppm O_3. Addition of 0.1 mM H_2O_2 at the end of the O_3 exposure produced a maximal response which was fully reversible with the addition of 10 mM DTT.

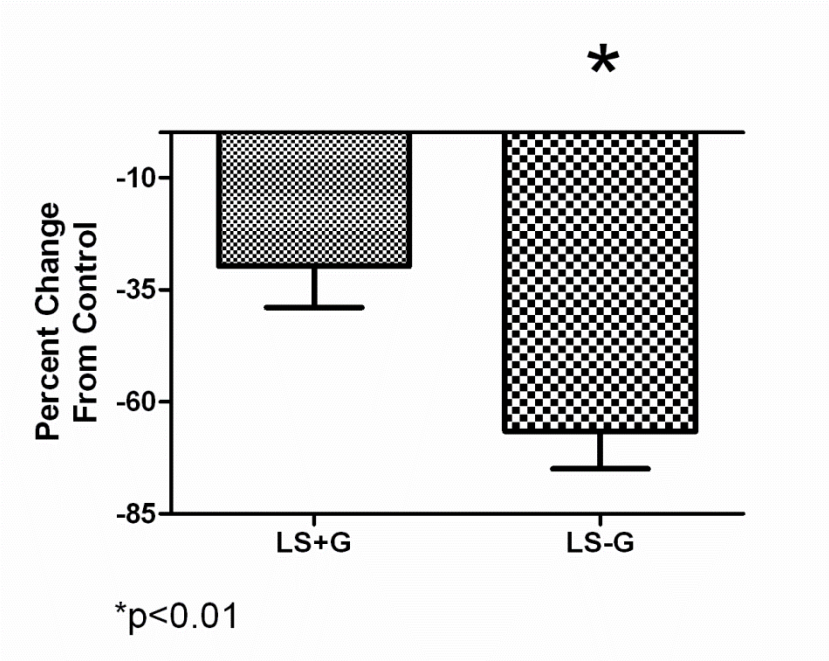

Figure 3.3.2.2 Determination of NADPH levels. The effect of glucose deprivation on NADPH was assessed following a 2 hr equilibration in either Locke Solution with glucose (LS+G) or Locke Solution without glucose (LS-G), and expressed as percent change from the mean NADPH concentration measured from cells maintained in growth media (KGM). *$p<0.01$, $n \geq 3$ experiments.

3.3.3 Validation of glutathione-dependent roGFP2 responses to ozone exposure

Given the extreme reactivity of O_3 with biomolecules, we considered the possibility that the spectral changes of the probe interpreted as changes in E_{GSH} are the result of a direct oxidation of roGFP2 by O_3 itself or by an O_3-generated secondary oxidant. We therefore undertook a series of experiments to determine whether O_3-induced changes in the roGFP2 fluorescence intensity ratio involve components of the glutathione system through which roGFP2 has been demonstrated to respond (Figure 3.1.1). We first aimed to confirm that O_3 exposure leads to increased levels of GSSG. To this end we assessed the extent of intracellular glutathione oxidation in control and ozone treated cells. We observed up to 3-fold increases in GSSG following 1 ppm O_3 exposure in LS-G as compared to air controls (Figure 3.3.3.1), which agrees with previous reports of the effect of O_3 exposure on intracellular glutathione (Chalfant and Bernd 2011; Todokoro et al. 2004).

A

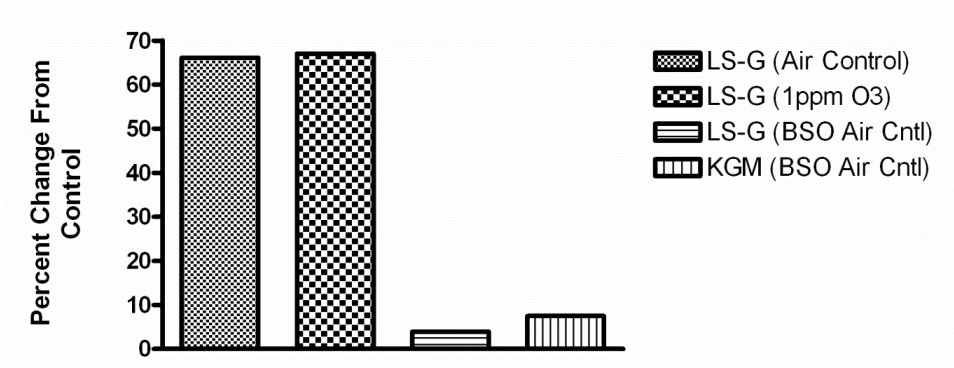

B

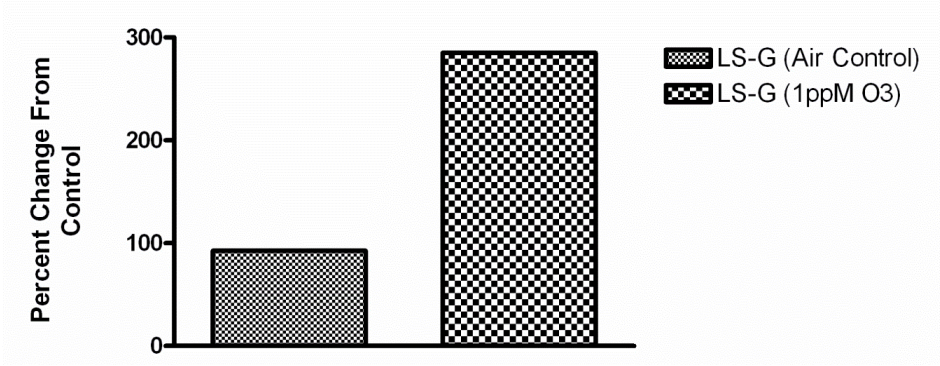

Figure 3.3.3.1 Determination of intracellular glutathione. A) The total glutathione content (GSH + GSSG) of cells exposed to either 0 (air control) or 1 ppm O_3 in Locke solution without glucose (LS-G) for 50 min. To ensure the total glutathione content could be modulated, cells were exposed to an air control in either LS-G or growth medium (KGM) following pretreatment with buthionine sulfoximine (BSO), a γ-glutamylcysteine synthetase inhibitor used to decrease glutathione levels. The responses are plotted as percent change from the KGM air control. B) The oxidized glutathione content (GSSG) of cells exposed either 0 (air control) or 1 ppm O_3 for 50 min in LS-G. Cells exposed to 0 ppm O_3 in growth media (KGM) serve as the control, and responses are plotted as percent change from the control.

Next, we asked whether the roGFP2 response to O_3 is influenced by glutaredoxin (Grx) activity. Grx is essential to mediate roGFP2 oxidation by GSSG (Figure 3.1.1), but should play no role if roGFP2 is directly oxidized by O_3. On the one hand, we compared the response of roGFP2 (which interacts with endogenous Grx) with that of Grx1-roGFP2, a translational fusion of glutaredoxin-1 and roGFP2. The fusion of these components is known to kinetically improve the equilibration between roGFP2 and GSSG in a highly specific manner (Gutscher et al. 2008; Meyer and Dick 2010). We found that the O_3-induced increase of E_{GSH} in BEAS cells expressing Grx1-roGFP2 occurred earlier and at a faster rate relative to that reported by cells expressing unlinked roGFP2, thus indicating a GSSG/Grx-specific response (Figure 3.3.3.2A). In contrast, we investigated the effect of glutaredoxin inhibition by pretreating cells with the dithiocarbamate derivative 2-AAPA (Sadhu et al. 2012). The inhibitor completely ablated roGFP2 responses to ozone, as well as to H_2O_2 and DTT (which also act indirectly through glutathione oxidation and reduction, respectively) (Figure 3.3.3.2B), thus confirming the role of glutaredoxin as the catalyst necessary for roGFP2 responsiveness to O_3. Together these observations confirm that O_3 is not simply sensed by the probe through direct oxidation, but rather by its specific effects on the glutathione redox couple.

Having confirmed that O_3 induces formation of GSSG, which is then detected by the roGFP2 probe, we asked whether glutathione peroxidases (GPx), major generators of GSSG, are involved in the ozone response. Here we investigated the role of glutathione peroxidase activity in O_3-induced roGFP2 redox changes by pretreating BEAS cells with 1 µM sodium selenite for up to 48 hrs prior to O_3

exposure. Previous studies have used selenium supplementation as an effective means of increasing glutathione peroxidase expression (Helmy et al. 2000; Holben and Smith 1999; Leist et al. 1996), a finding that we also observed in preliminary studies with BEAS cells (Figure 3.3.3.3). Se-induced overexpression of GPx was found to accelerate roGFP2 oxidation during a 0.5 ppm O_3 exposure (Figure 3.3.3.2C), thus suggesting that O_3 gives rise to peroxides, which are then converted by GPx to GSSG, which is in turn reported by roGFP2 through the intervention of Grx.

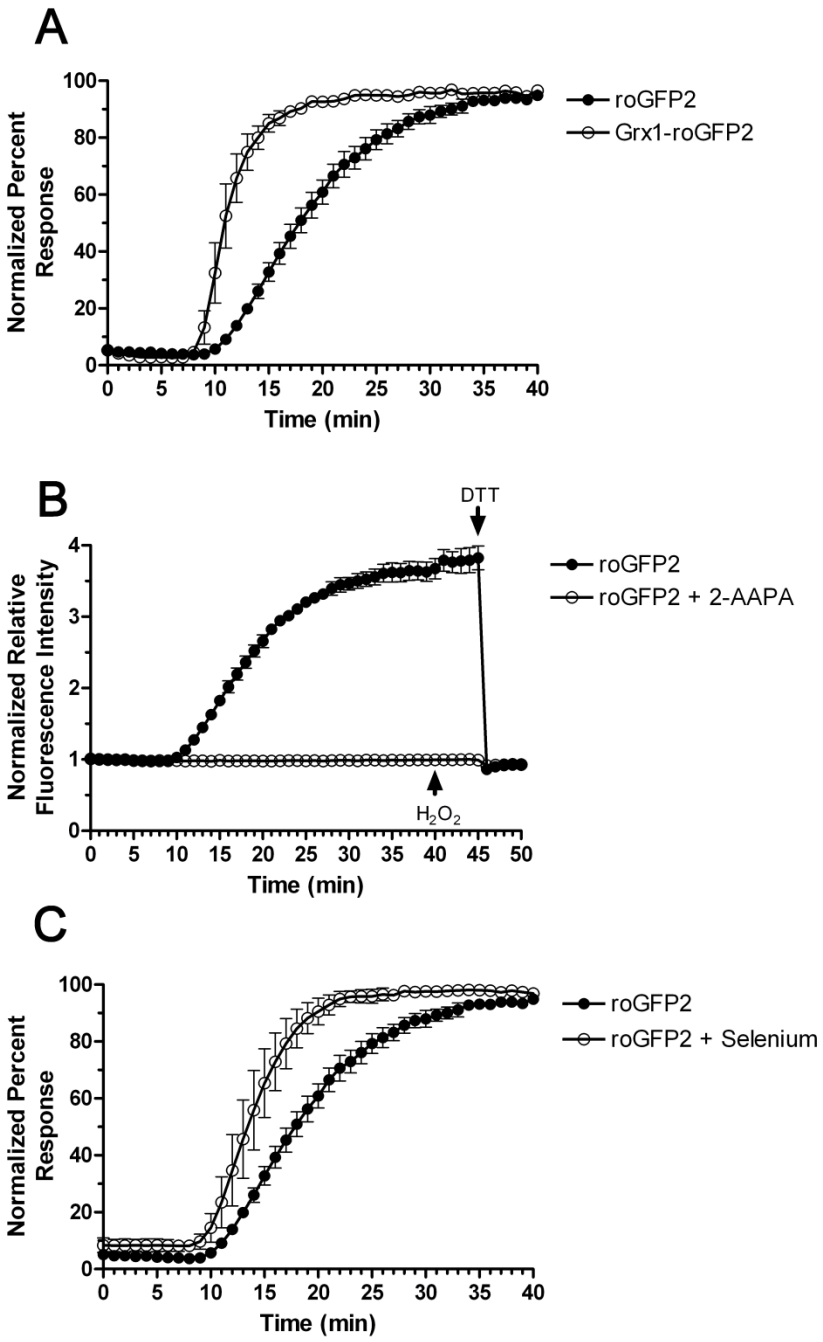

Figure 3.3.3.2 Manipulation of the glutathione system modulates roGFP2 responses to ozone. A. Changes in cytosolic glutathione redox potential induced by 0.5 ppm O_3 exposure as reported by BEAS-2B cells expressing either roGFP2 or Grx1-roGFP2. B. BEAS-2B cells were pretreated with 100 µM 2-AAPA, a glutaredoxin inhibitor, prior to exposure to 0.5 ppm O_3. The responses shown are the normalized 404/488 ratios plotted relative to their established baseline. C. BEAS-

2B cells were pretreated with 1 µM sodium selenite for 48 hrs prior to 0.5 ppm O_3 exposure. To facilitate comparison of the responses in A and C, the normalized ratios were plotted as a percentage of the signals obtained at maximal oxidizing and reducing conditions achieved using 1 mM H_2O_2 and 10 mM DTT, respectively. Other experimental conditions were as described for Figure 3.3.1. Values shown are mean ± SE (n ≥ 3).

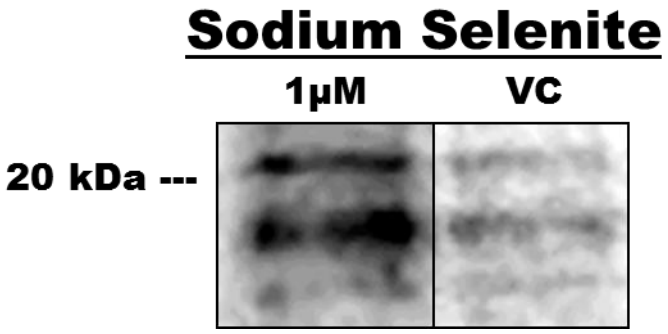

Figure 3.3.3.3 Selenium-induced GPx1 overexpression. Detection of GPx1 expression following a 48 hr pretreatment with either 0 (vehicle control, VC) or 1 uM sodium selenite; cell lysates were separated by SDS-PAGE and immunoblotted with anti-GPx1. The expected size of GPx1 is approximately 22 kDa.

3.3.4 Investigating the role of secondary products in ozone-induced redox changes

Since the data shown in Figure 3.3.3.2-C suggested the involvement of peroxides in the O_3 response, we asked whether there is a specific role for hydrogen peroxide. For these experiments we examined generation of H_2O_2 as a consequence of O_3 exposure using the cytosolic-targeted H_2O_2-sensor, HyPer. O_3 caused a relatively modest increase in the HyPer response during the exposure period (Figure 3.3.4.1). However, the observed HyPer response did not precede nor match the magnitude of the roGFP2 response, making it unlikely that the observed increase in E_{GSH} is primarily caused by H_2O_2 generation.

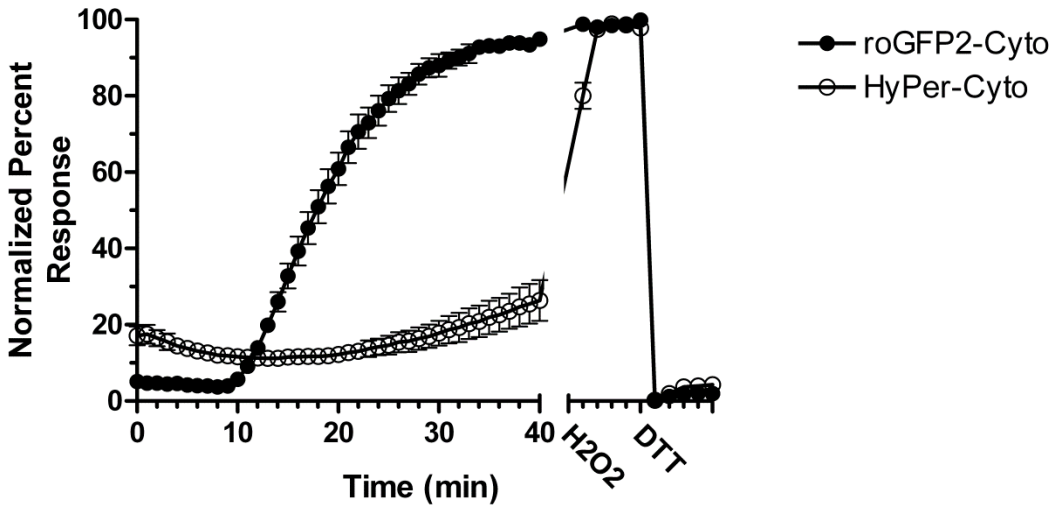

Figure 3.3.4.1 Comparison between roGFP2 and HyPer responses to O_3. BEAS-2B cells expressing either roGFP2 or the H_2O_2 sensor HyPer, were exposed to 0.5 ppm O_3 as described for Figure 3.3.1. To facilitate comparison, the normalized ratios were plotted as a percentage of the signals at maximal oxidation and reduction achieved using 1 mM H_2O_2 and 10 mM DTT, respectively. Values shown are mean ± SE ($n \geq 3$).

Mitochondrial oxidant production, frequently associated with increased oxidation of mitochondrial glutathione, has been implicated as a contributing factor in the cellular response to xenobiotics (Cheng et al. 2010; Cheng et al. 2012; Hanson et al. 2004). Therefore, we next used mitochondrially-targeted roGFP2 (roGFP2-m) to assess the impact of ozone exposure on the mitochondrial glutathione redox potential of BEAS-2B cells. As shown in Figure 3.3.4.2, exposure to 1 ppm ozone, twice the amount used for cytosolic assessments, induced an increase in mitochondrial E_{GSH}. However, relative to the cytosolic roGFP2 response, the

increase in mitochondrial E_{GSH} occurred at a slower rate and achieved a lower magnitude. This suggests that mitochondrial oxidants are not the primary source of the oxidants that lead to increased cytosolic E_{GSH}.

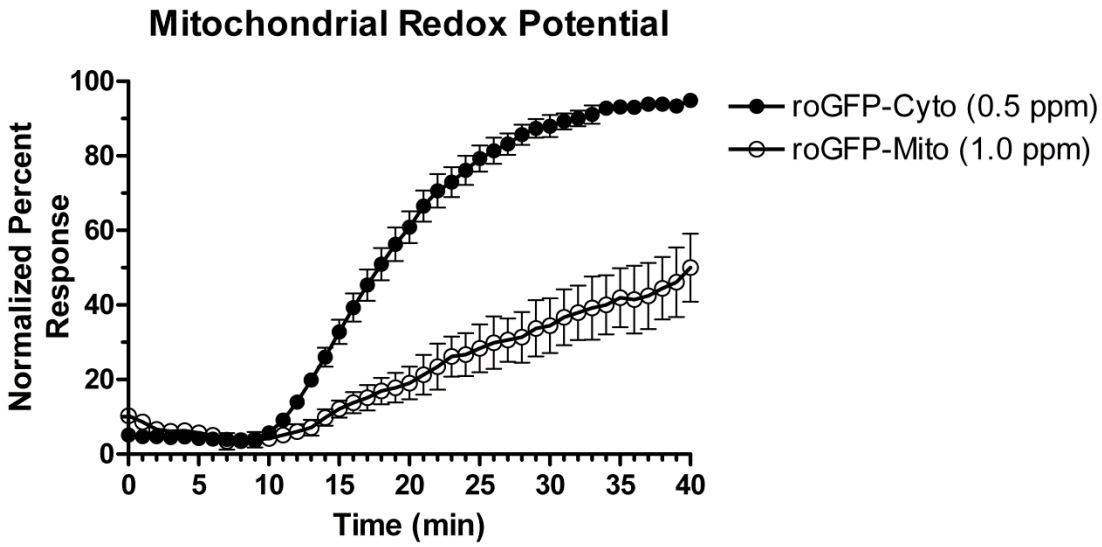

Figure 3.3.4.2. O_3-induced EGSH changes affects the cytosol more rapidly than the mitochondrial matrix. BEAS-2B cells expressing roGFP2 targeted to either the cytosol or mitochondria were exposed to either 0.5 ppm (roGFP2-Cyto) or 1.0 ppm (roGFP2-Mito). For direct comparison, the normalized ratios were plotted as a percentage of the maximal oxidation achieved using 1 mM H_2O_2 and 10 mM DTT. Other experimental conditions were as described in Figure 2. Values shown are mean ± SE ($n \geq 3$).

3.4 Discussion

"Oxidative stress" is a frequently cited mechanistic component of the adverse health effects induced by numerous xenobiotic compounds (Bargagli et al. 2009; Chung and Marwick 2010; Jones 2008; Kohen and Nyska 2002; MacNee 2001; Ward 2010; Yang and Omaye 2009). However, the term "oxidative stress" is a very broad concept and the detection of early and specific indices of oxidant stress has proven to be methodologically difficult. The advent of genetically-encoded fluorescent reporters that are sensitive to their redox environment has enabled real-time imaging-based assessments of oxidant outcomes in living cells with unprecedented spatial and temporal resolution. In this study, we validated the use of one such reporter, roGFP2, for the specific assessment of xenobiotic-induced changes in the glutathione redox potential using ozone as a model toxicant and BEAS-2B cells as a model of the human bronchial epithelium.

The pro-oxidative change in E_{GSH} observed in this study represents an early event in the oxidant injury caused by O_3. Ozone is a potent oxidant gas that has the potential to interact directly with virtually any cellular component, potentially including fluorescent reporter molecules such as roGFP2. Thus, in interpreting the probe response observed in O_3-exposed BEAS-2B cells, we had to consider the possibility that O_3 could be bypassing the glutathione system through which roGFP2 sensors normally respond (Gutscher et al. 2008; Meyer and Dick 2010).

Our findings strongly suggest that even in the presence of a strong oxidant like O_3, roGFP2 is oxidized only indirectly through its known coupling to the

glutathione system. This conclusion is supported by several observations: First, glucose deprivation increased O_3-mediated roGFP2 oxidation, consistent with the requirement for NADPH in robustly maintaining E_{GSH}, the lack of glucose preventing regeneration of reducing equivalents throughout the exposure period. NADPH levels were approximately 70% lower in cells equilibrated in the absence of glucose, which appears to be sufficient to sensitize cells uniformly. In addition, it is important to bear in mind that there are other cellular processes that draw on the NADPH pool, and the continued lack of glucose largely prevents active regeneration of reducing equivalents throughout the exposure period.

Second, we confirmed the role of glutaredoxin in mediating the roGFP2 response to O_3. Grx1 is required to transfer oxidative equivalents from the glutathione pool to roGFP2. In previous studies using Grx1-roGFP2, the chimeric linkage of glutaredoxin-1 to roGFP2 enhanced responses to physiological oxidants such as H_2O_2 (Gutscher et al. 2008; Meyer and Dick 2010). Importantly, Grx1-roGFP2 also accelerated the roGFP2 response to O_3, where as inhibition of endogenous Grx with 2-AAPA prevented roGFP2 oxidation in the presence of O_3. While early reports describe 2-AAPA as being an inhibitor of glutathione reductase, a more recent study reports that this dithiocarbamate derivative acts as a direct inhibitor of glutaredoxins as well (Sadhu et al. 2012). Thus, the finding that 2-AAPA-treated cells failed to respond to O_3 supports the involvement of Grx and is consistent with the claim that 2-AAPA is an inhibitor of glutaredoxins. Importantly, the fact that use of this inhibitor was effective at disconnecting the glutathione pool

from the redox reporter argues against a non-specific interaction between O_3, or a secondary oxidant, and the roGFP2 sensor.

Lastly, findings from experiments examining the effect of overexpression of glutathione peroxidases (GPx) using prolonged selenite supplementations are consistent with an upstream role of GPx in the oxidative pathway leading to O_3-induced roGFP2 oxidation. GPx couple the reduction of (hydro)peroxides to the generation of GSSG (Arthur 2000; Mates and Sanchez-Jimenez 1999; Meyer and Dick 2010). In our system, the increased expression of GPx enhanced roGFP2 oxidation, suggesting that O_3 exposure generates (hydro)peroxides, which then drive the formation of GSSG. In fact, ozone has been shown to produce many types of lipid hydroperoxides upon exposure (Mudway and Kelly 2000; Yang and Omaye 2009). Moreover, cells exposed to O_3 may have an increased H_2O_2 burden as well. Overall, the results from GPx overexpressing cells suggest that the increased activity of these enzymes leads to an enhanced catalytic destruction of peroxides with concomitant GSH oxidation, leading to the roGFP2 response to ozone.

Using the H_2O_2 probe HyPer, our initial assessments suggested slightly elevated H_2O_2 production following ozone exposure of BEAS cells. The quantitative interpretation of HyPer responses is however difficult. It is not clear to what extent the OxyR domain of HyPer may be outcompeted by endogenous peroxidases. In addition, HyPer is highly pH sensitive, as much as the cpYFP module on which it is based (Schwarzlander et al. 2012). Thus, an O_3–induced intracellular acidification could dampen the HyPer response to H_2O_2. Nevertheless, following O_3 exposure,

HyPer responded to exogenously applied H_2O_2 and DTT as expected, which demonstrates the general functionality of the probe. Taken together, the delayed time of onset, slow rates of response, and the relatively low magnitude of the HyPer responses, may suggest that H_2O_2 production is not a major factor in the total O_3-induced E_{GSH} effects. Furthermore, preliminary experiments using mitochondrially-targeted HyPer also show that the mitochondrial E_{GSH} change induced by O_3 is unlikely to be the result of H_2O_2 production by mitochondria. Similarly, there is minimal alteration of the roGFP2 response upon O_3 exposure of cells overexpressing catalase (Gibbs-Flournoy et al., unpublished). Likewise, the measurements in mitochondrially-targeted roGFP do not support a mitochondrial source for the O_3-induced increase in cytosolic E_{GSH}. These results suggest that the relevant oxidant species, potentially a hydroperoxide, is primarily generated in the cytosol, or within the outer membranes, and the mitochondrial E_{GSH} response would be expected to lag behind that of the cytosol. Additionally, differences in peroxidase composition and activity may contribute to the lag in the O_3-induced mitochondrial E_{GSH} response relative to the cytosol.

The studies presented herein cannot completely exclude a partial contribution of direct interactions between O_3, or its secondary byproducts, with the thiols of the roGFP2 sensor. In addition, because the roGFP2 fluorescence ratio reflects E_{GSH}, which is a function of both the GSSG:GSH ratio and the total glutathione concentration, it is possible that O_3-induced electrophilic attack mediates the changes reported by roGFP2 by consuming reduced GSH. It should, however, be noted that the E_{GSH} in the cytosol or mitochondrial matrix is much more sensitive to

an increase in GSSG than to depletion of GSH. This is because the E_{GSH} in the cytosol (around -320 mV, or even lower, in mitochondria) represents nanomolar GSSG in a millimolar pool of GSH. To deflect the roGFP2 signal from -320 mV to about -260 mV, only requires the concentration of GSSG to increase from 200 nM to 20 uM (in a 10 mM total glutathione pool). To achieve the same magnitude of E_{GSH} response by depleting GSH exclusively would require a loss of 90% of GSH (e.g. from 10 mM to 1 mM) (Meyer and Dick, 2010). Such a massive depletion of GSH by ppm concentrations of ozone (which could generate only limited amounts of electrophiles) seems stochiometrically unlikely. If one also considers the relative kinetics of GSSG generation and consumption (GSSG generation by GPx exhibits second order rate constants in the range of $1x10^8$ $M^{-1}s^{-1}$), it appears reasonable to suggest that the ozone effect reported in our study is primarily due to GSSG generation, and that the contribution of glutathionylated electrophile(s) formation is minor.

Thus, while there may be several different O_3-induced processes that together drive glutathione oxidation, including lipid peroxidation, H_2O_2 generation and others, the available evidence strongly suggests that the cytosolic roGFP2 responses to O_3 exposure are appropriately reporting the glutathione redox potential. Taken together, these results demonstrate that roGFP2-based sensors can be used to monitor shifts in glutathione redox homeostasis in O_3-exposed cells. Furthermore, the experimental approach utilized may be used for the validation of “oxidant stress” induced by other reactive xenobiotics in living cells.

3.5 Conclusion

These studies demonstrate the utility of using genetically-encoded fluorescent reporters in making reliable assessments of cells undergoing exposure to xenobiotics with strong oxidizing properties.

Chapter 4

Examination of Factors Affecting Ozone-Induced Oxidative Stress

4.1 Introduction

Exposure to air pollution remains a public health problem. Specifically, inhalation of ozone (O_3), and other common air pollutants, leads to numerous adverse health effects, largely impacting the pulmonary and cardiovascular systems (Curtis et al, 2006; Krewski and Rainham, 2007; Kampa and Castanas, 2008; Simkhovich et al, 2008). The lung is both an initial point of entry as well as a primary target of the deleterious effects of air pollution exposure, including ozone. To counteract the harmful effects of inhaled toxicants, the lung has several protective defenses, which include its robust epithelia, antioxidant-containing epithelial lining fluid (ELF), mucociliary clearance, and native immune response (Nicod 2005). All of these factors combine to provide protection against gaseous and particulate air pollutants.

The adverse effects of air pollution exposure are likely attributable to oxidative stress, and redundant protective elements serve to mitigate oxidant-induced lung injury (Ciencewicki et al, 2008). Specifically, the ELF, which serves as the first point of contact upon inhalation, contains relatively high levels of small molecules and

proteins dedicated to buffering the extracellular redox environment. Such "antioxidants" include: glutathione, glutathione peroxidases, ascorbate (vitamin C), urate, α-tocopherol (vitamin E), catalase, and superoxide dismutase (Van der Vliet et al, 1999; Sun et al, 2001).

Ozone is a potent oxidizing compound that has been shown to interact with specific ELF components (Kermani et al, 2006; Pryor 1991; Mudway and Kelly, 2000). Moreover, the ELF is suspected to be integral in blunting the adverse effects of O_3-induced oxidation by scavenging the potent oxidant before it is able to reach the underlying epithelium (Mudway and Kelly, 2000; Pryor, 1991). This is thought to occur because: 1) the ELF has a robust oxidant-buffering capacity, 2) the high reactivity of O_3 with various biomolecules, and 3) a relatively low solubility of O_3 in aqueous environments. Most important in mitigating the effects of O_3, extracellular concentrations of glutathione, urate, ascorbate, and α-tocopherol have all been shown to react with O_3 in both in vivo and in vitro studies (Kermani et al., 2006; Mudway et al., 1996; Mudway and Kelly, 2000; Van der Vliet et al., 1995).

Despite their demonstrated protective role, studies have also implicated ELF components in potentiating pulmonary oxidative stress during O_3 exposure (Ciencewicki et al., 2008; Ballinger et al., 2005). Moreover, mounting evidence suggests that ozone is capable of interacting with cellular membranes in the generation of secondary products as well as possibly crossing the plasma membrane into the intracellular environment (Garner et al., 2009; Ballinger et al., 2005; Pryor 1991). This suggests that the buffering capacity of the ELF is not

necessarily sufficient to fully protect the underlying epithelium. Recently, our laboratory has demonstrated potent changes in the intracellular glutathione redox potential (E_{GSH}) of airway epithelial cells undergoing O_3 exposure (Gibbs-Flournoy et al., Chapter 3). In succession to these studies, we have now come to evaluate the driving forces by which the observed E_{GSH} changes occur, and the efficacy of extracellular antioxidants in protecting epithelial cells from such changes. Using a novel ozone-reactive fluorophore, VSL1-162-1 (VSL1), we have assessed the ability of O_3 to cross cellular membranes and reach the cytosol unreacted. In addition, this study examines the protective effects of physiologically relevant concentrations of extracellular glutathione (GSH), uric acid (UA), ascorbic acid (AH_2), and α-tocopherol (α-T) at mitigating the E_{GSH} changes observed in previous studies.

4.2 Methods

4.2.1 Materials and Reagents

Tissue culture media and supplements were purchased from Lonza (Walkersville, MD). Wilco Wells glass-bottom culture dishes were obtained from Ted Pella (Redding, CA) and Warner Instruments (Hamden, CT). Pegylated catalase and laboratory reagents/chemicals, including hydrogen peroxide, dithiothreitol (DTT), uric acid, ascorbic acid, reduced glutathione, and α-tocopherol were obtained from Sigma-Aldrich (St. Louis, MO). Basic laboratory supplies were purchased from Fisher Scientific (Raleigh, NC).

4.2.2 Cell Culture

Transformed human airway epithelial cells (BEAS-2B, subclone S6; (Reddel et al. 1988)) were cultured as previously described (Tal et al. 2010) and maintained in serum-free keratinocyte growth medium, KGM (Lonza, Walkersville, MD). The cells were incubated in a humidified incubator at 37°C in 5% CO_2. For most live-cell exposures, BEAS-2B cells were plated in 35mm Wilco Wells glass-bottom dishes with a 12 mm #1.5 glass aperture (Ted Pella, Redding, CA).

4.2.3 Genetically Encoded Redox Sensors

Plasmid for the redox-sensitive green fluorescent protein 2, roGFP2, was the generous gift of Dr. S. J. Remington (University of Oregon, Eugene, OR). A cytosolically targeted version of roGFP2 was placed in a lentiviral vector as described previously (Cheng et al. 2012).

4.2.4 Lentiviral Transduction

Stable expression of roGFP2 was performed via lentiviral transduction. In short, a lentivirus encoding roGFP2 (specifically targeted to the cytosol) was incubated for 4 hrs (37°C / 5% CO2) with wild-type BEAS-2B cells using a multiplicity of infection (MOI) of 5 – 10 in a single well of a 6-well dish. The viral particles were then removed and fresh KGM was placed on the cells, and the BEAS-2B cells were then allowed to grow to confluency. Upon confluency, the cells were expanded to T75 dishes where they were propagated for multiple passages. For some experiments, stably transduced cells were sorted for optimal fluorescence expression at the UNC Core Flow Cytometry Facility

4.2.5 Fluorescent Detection of Ozone

The ozone-specific fluorescent probe, VSL1-162-1, and the fluorescent H_2O_2 probe, PG-1, were the generous gift of Dr. Christopher Chang (University of California, Berkeley, CA). Both probes are boronated fluorescein derivatives, and

both were used to detect the presence of intracellular O_3. For experiments using PG-1, pegylated catalase was used to limit the contribution of H_2O_2 to any increases in fluorescence intensity. Prior to exposure (15-20 min), BEAS-2B cells were stained with 2.5 or 5.0 uM PG-1 or VSL1, and allowed to incubate at 37°C in 5% CO_2. Both probes were allowed to remain in the Locke solution during the O_3 exposures.

4.2.6 Exposure Conditions

Wild-type or stably transduced BEAS-2B cells expressing roGFP2 were cultured as described above. Prior to exposure, subconfluent cells were equilibrated in Locke solution (Taylor-Clark and Undem 2010) for 2 hrs at 37°C in 5% CO_2. For antioxidant assessments, 65 uM AH_2 + 500 uM UA + 250 uM GSH + 25 uM α-Tocopherol were added to the Locke solution to mimic physiologically-relevant concentrations found in human epithelial lining fluid (Mudway and Kelly, 2000). All live-cell O_3 exposures were performed using 0.5 ml of Locke solution without glucose. For all imaging experiments, cells were exposed in a custom-built stage-top exposure system maintained at 37°C with 1.5 L/min of 5% CO_2/balance air at a relative humidity ≥ 95% (Gibbs-Flournoy et al, Chapter 3).

For each experiment, cells were exposed to control air (5% CO_2/balance air) or 0.5 ppm ozone. The entire exposure period typically consisted of 3 component intervals collectively lasting up to 50 min in length. They included: 1) an initial untreated baseline period of 5 min; 2) an exposure period of up to 35 min; and 3) a 5-10 min control exposure period. For roGFP2 assessments, cells were oxidized by

1.0 mM hydrogen peroxide for 5 min and then reduced by 10 mM DTT for an additional 5 min during the control exposure period. Two concentrations of H_2O_2, 0.1 and 1.0 mM, were added during the control period for PG-1 experiments. For VSL1 assessments, the control period consisted of adding 3.5 ml of warm (~37°C) Locke solution onto the cells following the O_3 exposure, resulting in a 8-fold dilution of the extracellular fluid. During these exposures, the ozone concentration in the exposure chamber was monitored in real-time using a Dasibi Model 1003-AH Ozone Analyzer sampling at a flow of 2.0 L/min.

4.2.7 Imaging Analysis

All live-cell experiments done in real-time were conducted using a Nikon Eclipse C1si spectral confocal imaging system equipped with an Eclipse Ti microscope, Perfect Focus System, and 404 nm, 488 nm, 561 nm, and 633 nm primary laser lines (Nikon Instruments Corporation, Melville, NY). Images were acquired using a 60X Plan Apo lens. For experiments involving roGFP2, green fluorescence was observed via the use of independent excitations at 404 and 488 nm while emitted light was collected for each using a 525/30 nm band-pass filter (Chroma, Bellows Falls, VT). All roGFP2 results were calculated as ratios of the emissions excited by the 488 nm and 404 nm lasers scanned sequentially at a frequency of 1 min. For PG-1 and VSL1 experimentation, green fluorescence was observed using 488 nm excitation, and the emitted light was collected using a

525/30 nm band-pass filter. All imaging data were acquired using the Nikon EZ-C1 software.

4.2.8 Statistical Analysis

All imaging data were quantified using NIS-Elements AR software (Nikon, Melville, NY). For each experiment, the responses of 5–10 cells were collected as regions of interest (ROI) and then averaged to derive an overall response. For experiments using the fluorescent probes PG-1 and VSL1, an ROI was drawn in an area devoid of cells in efforts to assess the extracellular fluorescence. Data are expressed as the mean of at least two repeated experiments. Pairwise comparisons of control and treatment groups were performed using a student's T-test, or ANOVA with a Bonferroni post-hoc test, with $p < 0.05$ taken as being statistically significant.

4.3 Results

4.3.1 PG-1 fluorescence increases during O_3 exposure despite the presence of catalase

Peroxy Green-1 (PG-1) is an H_2O_2-specific fluorescent probe that was specifically designed by the Chang lab for the detection of intracellular H_2O_2 (Miller et al., 2007). Because previous studies suggest H_2O_2 generation may be a by-product of O_3 exposure (Pryor 1991), we used PG-1 to investigate this outcome. During these experiments, we observed a pronounced and sustained increase in the intracellular PG-1 fluorescence in BEAS-2B cells undergoing 0.5 ppm O_3 exposure (Figure 4.3.1). To verify that the PG-1 signal is dependent on the concentration of H_2O_2 present, we conducted a control experiment in which the exposure medium was supplemented with pegylated catalase (pCat). The expectation was that the catalase would ablate or reduce the observed increases in PG-1 fluorescence intensity. However, the O_3-induced increase in fluorescence intensity was unaffected despite the addition of 50 units of pCat, an amount that was sufficient to ablate PG-1 fluorescence in response to concentrations of H_2O_2 up to 1 mM (Figure 4.3.1).

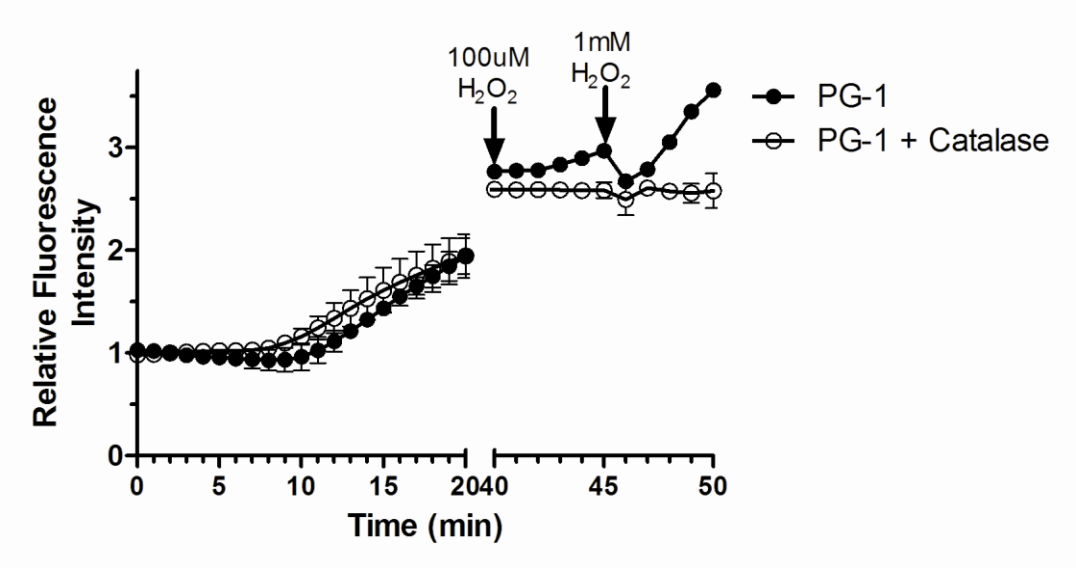

Figure 4.3.1 O_3-induced changes in PG-1 fluorescence intensity. BEAS-2B cells equilibrated with the H_2O_2 probe, PG-1, were exposed in the presence or absence of pegylated catalase to clean air for 5 min followed by 0.50 ppm O_3 exposure for 35 min in a stage-top exposure system maintained at 37°C, >90% relative humidity, and 5 % CO_2. Plotted relative to the 5 min baseline, the data shown are the emitted fluorescence intensity values at 510 nm resultant from 488 nm excitation. Following the O_3 exposures, addition of 0.1 and 1.0 mM H_2O_2 demonstrate the responses of the fluorophore to its intended target. Values shown are mean ± SE (n ≥ 3)

4.3.2 VSL1 detects intracellular ozone

Upon confirmation of our findings, the creators of PG-1 generated a new fluorophore, VSL1-162-1, for the specific detection of ozone within cells. An ideal intracellular O_3 sensor would be a trappable fluorescent probe, meaning that it can be targeted to and contained within a predetermined subcellular compartment(s). While the unreacted VSL1 molecule is not a conventionally trappable fluorophore in that it can diffuse through the membrane and thereby exits the cell, activation of VSL1 with O_3 produces a fluorescent product that is no longer capable of transcending plasma membranes. This is a useful property for examining the presence of intracellular O_3, since any molecule of VSL1 within the intracellular environment that has reacted to O_3 will then become trapped within the confines of the plasma membrane. Conversely, probe molecules that have reacted with O_3 outside of cells will become trapped in the extracellular environment and can therefore be washed away. During characterization studies, VSL1 showed little or no reactivity towards H_2O_2 and other forms of ROS/RNS (Chang, personal communication). Exposure of cells to 0.5 ppm O_3 in the presence of VSL1 caused a marked increase in both the intracellular and extracellular (background) fluorescence of the probe, as assessed by real-time confocal imaging (Figure 4.3.2). Importantly, upon an 8-fold dilution of the exposure medium, the intracellular fluorescence of O_3 exposed cells was observed to be largely retained within the cell while the extracellular fluorescence of VSL1 was substantially reduced (Figure 4.3.2).

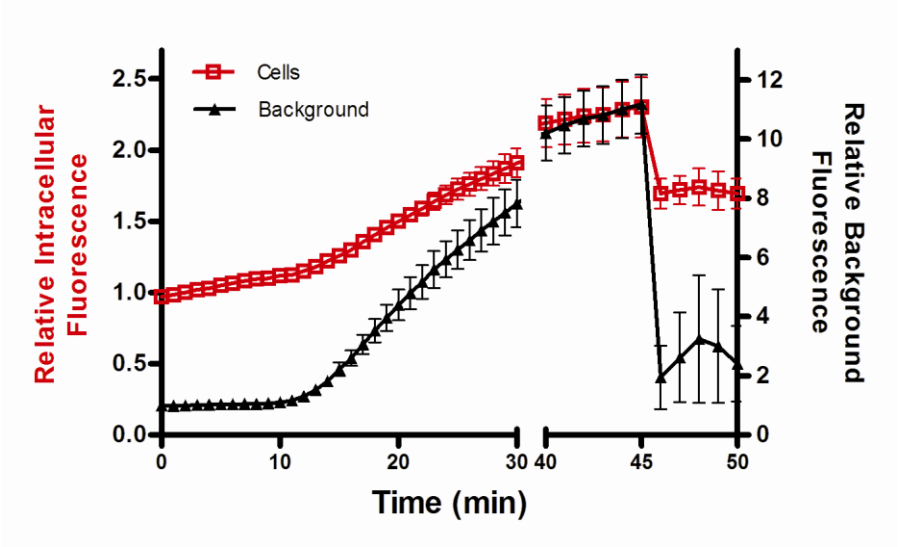

Figure 4.3.2 VSL1 detection of intracellular O_3. BEAS-2B cells equilibrated with the O_3 specific probe, VSL1, were exposed to clean air for 5 min followed by 0.50 ppm O_3 exposure for 35 min in a stage-top exposure system maintained at 37°C, >90% relative humidity, and 5 % CO_2. Plotted relative to the 5 min baseline, the data shown are the emitted fluorescence intensity values at 510 nm resultant from 488 nm excitation. Plotted in red are the intracellular responses of VSL1 for BEAS cells undergoing O_3 exposure. Simultaneously, the extracellular background VSL1 fluorescence is plotted in black. At 45 min, 3.5 ml of pre-warmed Locke solution was added to the exposure dish causing an 8-fold dilution of the existing exposure medium. Any remaining cellular fluorescence following dilution is assumed to be intracellularly trapped O_3-reacted VSL1. Values shown are mean ± SE ($n \geq 3$)

4.3.3 Extracellular antioxidants impair VSL1 responses to O_3

To examine the impact of extracellular antioxidants on the spatial detection of O_3, cells were exposed to 0.5 ppm O_3 in the presence of 65 uM AH_2 + 500 uM UA + 250 uM GSH + 25 uM α-Tocopherol (α-T) supplemented into the exposure medium 2 hrs prior to the beginning of each experiment. During these exposures, the intracellular fluorescence intensity of VSL1 was attenuated in antioxidant-supplemented medium as compared to unsupplemented exposures (Figure 4.3.3A). A similar trend was also observed for the extracellular VSL1 fluorescence, suggesting an impairment of O_3 solubility within the antioxidant-supplemented exposure medium (Figure 4.3.3B). Importantly, for antioxidant supplemented and unsupplemented exposures, the intracellular and extracellular retention of O_3-reacted VSL1 remained unchanged following the 8-fold dilution performed at the end of each exposure period (Figure 4.3.3C).

A

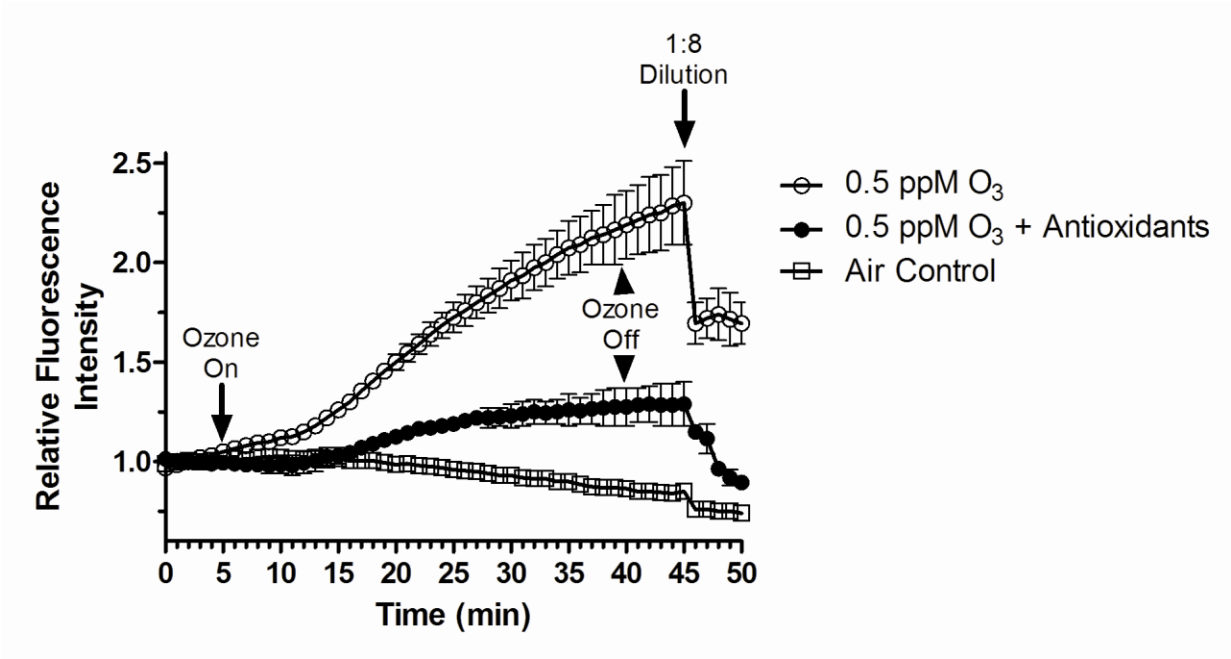
1:8
Dilution
Relative Fluorescence
Intensity
2.5
2.0
1.5
1.0
Ozone
On
Ozone
Off
0
5
10
15
20
25
30
35
40
45
50
Time (min)
0.5 ppM O_3
0.5 ppM O_3 + Antioxidants
Air Control

B

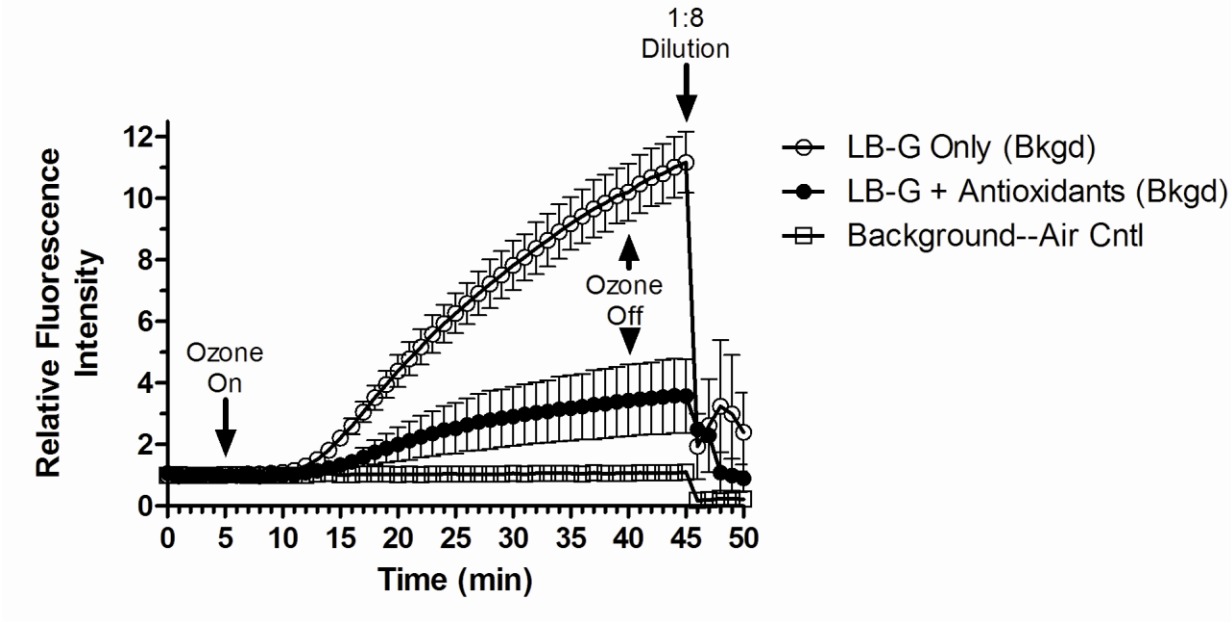
1:8
Dilution
Relative Fluorescence
Intensity
12
10
8
6
4
2
0
Ozone
On
Ozone
Off
0
5
10
15
20
25
30
35
40
45
50
Time (min)
LB-G Only (Bkgd)
LB-G + Antioxidants (Bkgd)
Background--Air Cntl

C

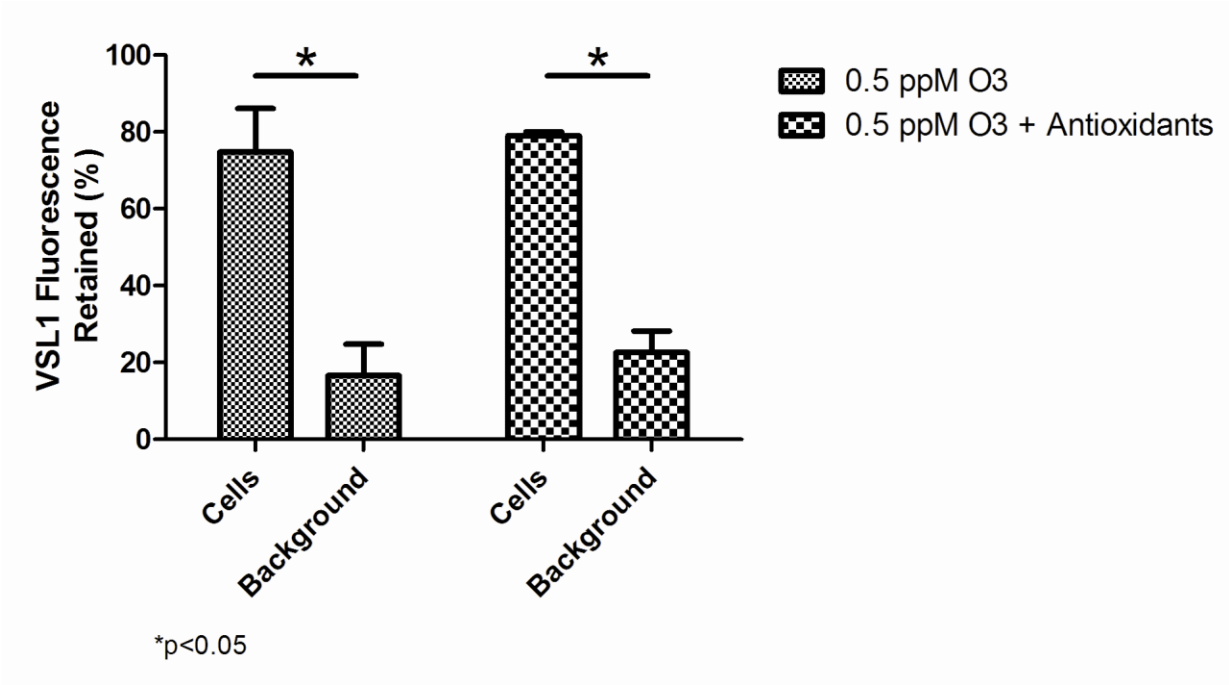

Figure 4.3.3 Extracellular antioxidants impair the intracellular and extracellular detection of O_3 by VSL1. BEAS-2B cells equilibrated with the O_3 specific probe, VSL1, were exposed to clean air for 5 min followed by 0.50 ppm O_3 exposure for 35 min in a stage-top exposure system maintained at 37^{o}C, >90% relative humidity, and 5 % CO_2. Plotted relative to the 5 min baseline, the data shown are the emitted fluorescence intensity values at 510 nm resultant from 488 nm excitation. A) The relative intracellular responses of VSL1 for BEAS cells undergoing O_3 exposure. B) The relative extracellular (background) responses of VSL1 during O_3 exposure. At 45 min, 3.5 ml of pre-warmed Locke solution was added to the exposure dish causing an 8-fold dilution of the existing media. Any remaining fluorescence following dilution is assumed to be O_3-reacted VSL1. C) The percentages of VSL1 fluorescence retained immediately following the 8-fold dilution as compared to the background, for O_3 exposures occurring in the presence and absence of extracellular antioxidants. Values shown are mean ± SE (n ≥ 3)

4.3.4 Extracellular antioxidants decrease O_3-induced changes in the cytosolic glutathione redox potential

Our previous studies using roGFP2 have found potent increases in the E_{GSH} of BEAS-2B cells exposed to various concentrations of O_3 (Gibbs-Flournoy et al., Chapter 3). In order to determine whether antioxidant-mediated scavenging of intracellular O_3 protects against the increased intracellular glutathione redox potential (E_{GSH}), roGFP2-expressing cells were exposed to O_3 in the presence or absence of extracellular antioxidants. In the current study, AH_2, UA, GSH, and α-T were supplemented into the exposure medium of roGFP2 expressing cells. The presence of these antioxidants dramatically attenuated O_3-induced increases in cytosolic E_{GSH} as measured by roGFP2 (Figure 4.3.4).

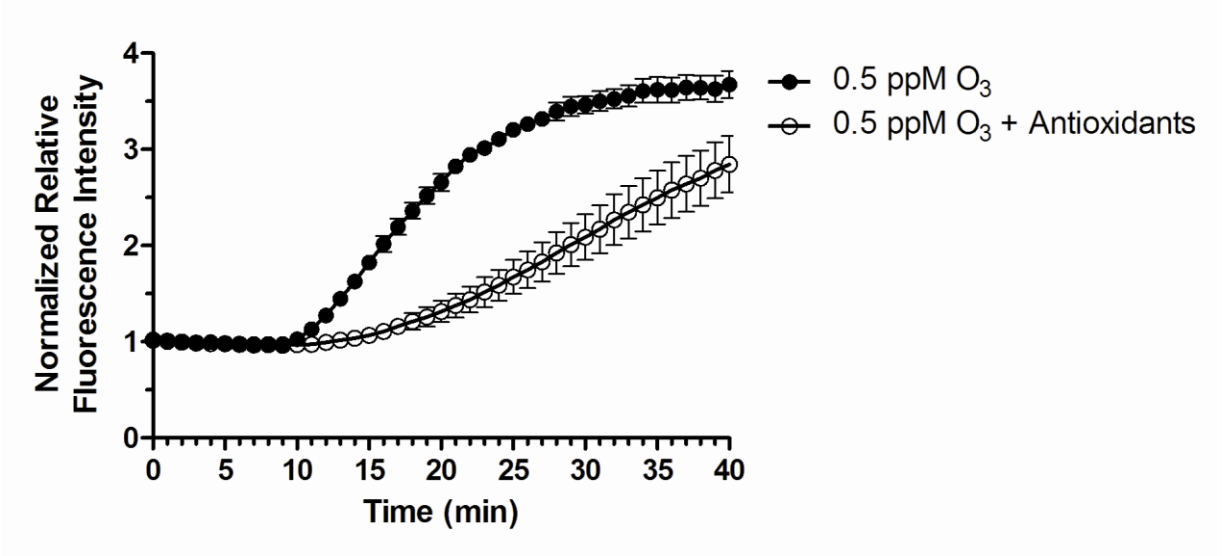

Figure 4.3.4 Extracellular antioxidants blunt O_3-induced increases in cytosolic glutathione redox potential. In the presence or absence of extracellular antioxidants, BEAS-2B cells expressing cytosolic roGFP2 were exposed to clean air for 5 min followed by 0.50 ppm O_3 exposure for 35 min in a stage-top exposure system maintained at 37^{o}C, >90% relative humidity, and 5% CO_2. Shown are the ratiometric values (404/488) calculated from the fluorescence intensity emitted at 510 nm induced by sequential excitation at 404 and 488 nm, and plotted relative to the 5 min baseline. Values shown are mean ± SE ($n \geq 3$)

4.4 Discussion

The reactivity and solubility of O_3 with biomolecules in aqueous conditions have long been thought of as representing factors that limit the ability of this toxicant to reach the underlying respiratory epithelium (Mudway and Kelly, 2000; Pryor 1991). The oxidative changes occurring from O_3 exposure have been largely attributed to the generation of secondary oxidants, such as (hydro)peroxides, lipid aldehydes and other lipid ozonation products, which are more capable of directly interacting with cellular environments (Ciencewicki et al, 2008). In contrast, a recent study by Garner and colleagues demonstrated the feasibility for O_3 to be detected within cells (2009). However, the high concentration of O_3 used in that study, combined with logistical issues regarding the exposure methodology left many unanswered questions about their observations. The present study explores the ability of O_3 to cross cellular membranes into the intracellular environment. In addition, we examined the protective potential of common antioxidants present in human epithelial lining fluid, and their ability to prevent O_3-exposed cells from incurring oxidative injury.

Our initial studies examining H_2O_2 generation during O_3 exposure revealed an unexpected observation. Experiments using the H_2O_2-specific fluorescent reporter, PG-1, demonstrated distinct increases in intracellular fluorescence despite the presence of pegylated catalase (pCat). pCat was chosen for these PG-1 control experiments because of its ability to cross cellular membranes making it available to the intracellular and extracellular environments for the immediate degradation of

H_2O_2 as it is generated. As shown, the 50 units of pCat used for this experiment were enough to prevent PG-1 responses to two doses of H_2O_2 added at the end of each exposure. This finding suggests that the observed PG-1 increases in fluorescence intensity were not induced by H_2O_2, but by O_3.

As a follow up to the PG-1 findings, the O_3-specific fluorophore, VSL1, was used to determine whether unreacted O_3 is capable of crossing cellular membranes into the intracellular environment. As mentioned earlier, upon reaction with O_3, VSL1 becomes intracellularly trapped making any changes in the intensity of the fluorophore shielded from outside manipulation such as dilution of the extracellular media. Indeed, the robust changes in cellular VSL1 fluorescence suggest that O_3 is capable of entering intracellular compartments unreacted. Moreover, this finding is further substantiated by 2 additional observations: 1) the ~4-fold difference in the intracellular and background fluorescence intensities suggests compartmentalization of the fluorophore, and 2) the substantial retention of cellular fluorescence, as compared to the background, suggest that the reacted fluorophore has become trapped within the intracellular environment making it unavailable to be simply diluted away.

Under physiological conditions, the epithelial lining fluid (ELF) is the first line of protection for the respiratory tract against the toxicological effects of inhaled air pollutants. This highly important biological barrier prevents toxicants from directly interacting with the underlying epithelium, which is the first cellular barrier encountered upon entry into the lung. The ELF is comprised of a wide milieu of

biomolecules largely dedicated to trapping and detoxifying respired xenobiotics. In relation to O_3 exposure, four antioxidants have been repeatedly described as being critical for buffering the oxidative effects O_3. They are: uric acid, ascorbic acid, reduced glutathione, and α-Tocopherol (Mudway and Kelly, 2000; Kelly et al., 1995). Hence, in assessing the ability of O_3 to cross cellular membranes, we felt that it was important to take the potential participation of extracellular antioxidants into consideration for possible attenuation or ablation of intracellular O_3 detection.

As evidenced by our studies, the presence of physiologically-relevant concentrations of extracellular antioxidants is sufficient to scavenge extracellular ozone and thus decrease the concentration available to transcend the plasma membrane of exposed BEAS-2B cells. This appears to be a direct antioxidant-mediated limitation of O_3 solubility within the exposure medium since there was a significant attenuation of the background fluorescence during antioxidant-supplemented O_3 exposures. However, it is important to acknowledge that despite the presence of these antioxidants, we still observed increases in the intracellular fluorescence intensity of VSL1 that was largely retained following an 8-fold dilution of the extracellular medium. The concentrations of AH_2, GSH, UA and α-T used in these experiments were based on the upper limits of Mudway and Kelly's estimation of the physiological concentrations of these antioxidants in human airways (2000). Using an exposure volume of 0.5 ml places a conservative estimate of the approximate medium thickness to be ~1.3 mm. At this thickness, our simulated ELF would impose a greater aqueous barrier to O_3 penetration than current estimations of the thickest portions of the ELF located in the upper airways (Mudway and Kelly,

2000). Also, since the cellular and background retention of VSL1 fluorescence was largely conserved across supplemented and unsupplemented antioxidant exposures, it appears that the chemical interaction of O_3 with VSL1 is not directly altered by the presence of extracellular antioxidants. Taken together, these data suggest that although antioxidants in the ELF are capable of scavenging extracellular O_3, the antioxidant defense of our simulated ELF was insufficient in fully protecting cells from direct interaction with O_3 molecules.

To further examine the antioxidant-mediated impairment of intracellular O_3, we tested the effect of these molecules on preventing the alteration of a specific oxidative endpoint. Using cytosolically-targeted roGFP2, we observed profound decreases in oxidative alteration of the intracellular glutathione redox potential (E_{GSH}) induced by O_3 in antioxidant-treated cells. Previously, our lab characterized the impact of O_3 exposure on E_{GSH}, however an ultimate driving force could not be fully attributed to any single initiating event. Taking the times of onset and overall profile of the roGFP2 and VSL1 O_3 responses, the evidence presented here suggests that the interaction of O_3 with intracellular biomolecules could likely be responsible for the oxidative shifts in the E_{GSH} measured by roGFP2.

4.5 Conclusion

Based on preliminary studies, it is tentatively concluded that O_3 is capable of transcending cellular membranes to gain access to the intracellular environment. While our studies simulating the ELF of O_3 exposed cells suggest that pulmonary defenses for buffering O_3-induced oxidation can be overcome, we must acknowledge that these studies are not able to account for the participation of other ELF components in mounting additional protection. However, it is equally fair to speculate that once free radical propagation reactions involving ozone and accessory proteins and lipids are taken into account, the oxidative insult to epithelial cells would likely be potentiated. While the presence of these biomolecules would provide additional targets to further blunt the ability of O_3 to cross cell membranes, the secondary and tertiary byproducts resulting from such interactions would probably create new reactive species capable of promoting additional oxidative damage. All of these events culminate in stimulating cellular oxidative stress, which would likely lead to the detriment of the cells being exposed.

Chapter 5

Overall Conclusions and Significance

Air pollution is a highly complex and variable mixture of gaseous and particulate components. Similarly, the individual mechanisms by which air pollutants induce adverse health effects are numerous, with the pulmonary and cardiovascular systems being most frequently impacted by exposure. Despite the complexity of air pollution and its effects, several common questions remain unresolved regarding the interaction of air pollutants with intra- and extracellular environments, and the initiating events by which these toxicants induce cellular damage. Over years of studying air pollution interactions with human physiology, it has become evident that these mechanistic questions may be answered more clearly through direct observation using imaging-based approaches. The studies described herein use advanced molecular imaging methods to investigate the *in vitro* interaction of common air pollutants with components of the human pulmonary system. Taken together, this body of work yielded useful data towards advancing knowledge of fundamental concepts that have remained elusive due to methodological limitations and shortcomings in the assessment of air pollution interactions with cellular environments. Unlike pollution affecting other environmental media, the implications from exposure to air pollution are particularly challenging since there are currently no means to effectively remediate pollutants in outdoor air. This places a high level of

importance on the study of air pollution since there are no choices in the air we breathe, and no practical intervention, engineered or behavioral, exists which permits full avoidance of ambient air pollutants.

The initial study of this project examines particulate interactions with the intracellular environment of lung epithelial cells. It specifically establishes and utilizes a novel method for determining particle internalization, with a particular focus on environmentally-relevant nanoscaled materials (Chapter 2). Exposure to ambient UFP is estimated to increase since new technologies implemented as a means to limit particulate mass output from internal combustion engines inherently favor the generation of nanoscaled particles as the smaller particles contribute minimally to the total particulate mass emitted (Oberdörster and Utell, 2002). Currently, the US EPA does not regulate the UFP fraction of ambient PM. Moreover, the rapidly expanding field of nanotechnology, combined with increasing levels of ambient UFP, is steadily escalating human exposure to NP while little is known about the health implications of these exposures.

Many NP evade normal pulmonary defenses leaving them free to interact with cellular environments (Oberdörster and Utell, 2002; Oberdörster et al, 2005). Detection of internalization is a specific interest of NP toxicity because assessment of this parameter would aid in answering mechanistic questions regarding particle toxicity and translocation to extrapulmonary tissues. Upon internalization, the intrinsic properties of many toxicologically-active nanomaterials likely induce cellular damage due to direct interaction with intracellular biomolecules. Previous studies

have demonstrated NP depletion of important biomolecules such as glutathione, as well as activation of signaling cascades that lead to expression of proinflammatory cytokines and antioxidant proteins (Xia et al., 2007; Vernanth et al., 2007; Nurkiewicz et al., 2008; Madl and Pinkerton, 2009). However, many of these studies describe these outcomes as global changes with little insight as to how they came about.

For instance, a relatively benign NP, such as carbon black, may be toxicologically inactive in extracellular environments; yet, upon entry, such particles would be free to nonspecifically bind critical proteins and antioxidant molecules, or release surface-bound toxicants such as transition metals, endotoxin, or redox cycling chemicals, which could be detrimental to the host cell (Li et al, 2008; Mühlfeld et al, 2007). Such is likely the case for diesel exhaust particles (DEP), which vary in size and shape, but have an elemental carbon core with numerous organic and inorganic materials, including various transition metals and redox-cycling compounds, adsorbed to their surface (Park et al, 2011). Moreover, DEP has been demonstrated to strongly induce activation of inflammatory signaling cascades often via an oxidation-mediated mechanism (Nemmar et al, 2012; Park et al, 2011; Tal et al, 2010). Discrimination amongst direct and indirect interaction of NP with intracellular targets is often difficult to assess without the aid of fluorescent properties, which is lacking in most environmentally-relevant NP. The method devised in Chapter 2 was specifically designed to permit detection of non-fluorescent ambient particulates.

Interaction of air pollutants with intra- and extracellular environments is critical for the initiation and propagation of mechanistic factors inducing adverse health effects. Hence the importance of the studies performed in Chapters 2 and 4. In Chapter 2, using the nuclei of TiO_2-exposed BEAS-2B cells as points of intracellular reference, we were able to show the time-dependent internalization of an environmentally-relevant NP using the DF-CLSM methodology. These data provide insight into a significant outcome of extracellular NP interaction with lung epithelia. Similarly, in Chapter 4 we were able to examine the impact of extracellular antioxidants on the intracellular detection of O_3, while linking antioxidant-mediated decreases in intracellular O_3 detection to attenuation of O_3-induced changes in intracellular redox status. Detection of air pollutant-induced alterations in cellular redox status is of particular importance because it assesses events directly related to an oxidative stress.

Oxidative stress is a key mechanistic factor driving the adverse health effects caused by gaseous and particulate air pollutants. However, assessment of xenobiotic-induced oxidative stress has been difficult to achieve due to methodological shortcomings for the sensitive, specific, and direct non-disruptive measurement of intracellular redox status. In relation to particulate-induced oxidative stress, ambient UFP and various kinds of engineered NP have been shown to generate numerous types of ROS including H_2O_2, superoxide, and hydroxyl radicals (Figure 5.1) (Li et al, 2008; Xia et al, 2007).

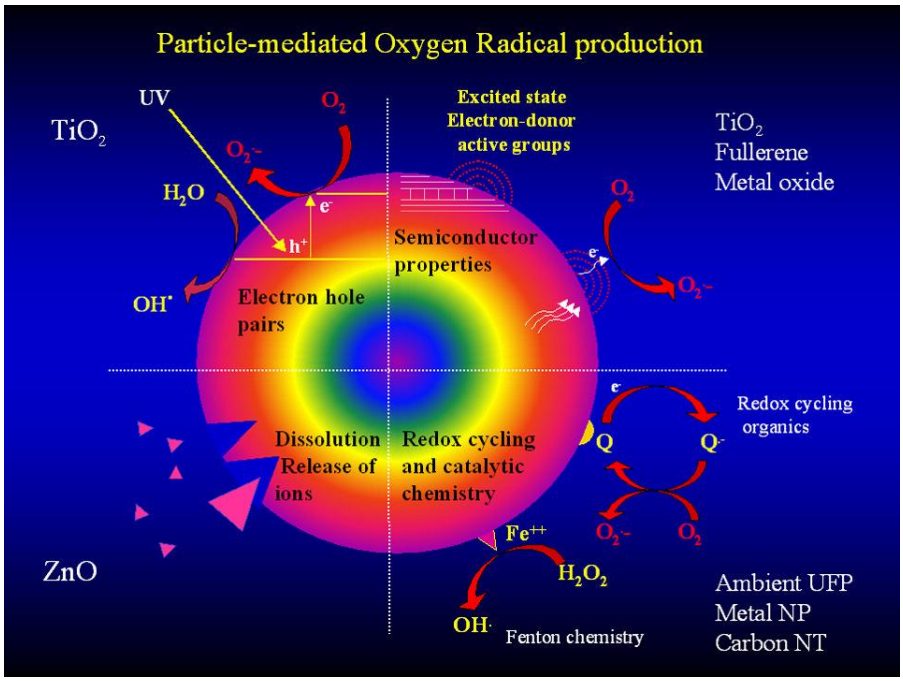

Figure 5.1 Mechanisms of particle-mediated ROS production. (Li et al, 2008)

In efforts to identify changes indicative of oxidative stress, a large portion of this dissertation was dedicated to the observation and validation of an approach for the direct monitoring of endpoints related to intracellular redox status. Chapters 3 and 4 examine the potent oxidative effects of O_3 on intra- and extracellular environments. O_3 is arguably the most potent oxidizing air pollutant, and it was used in these studies as a model to make novel assessments of xenobiotic-induced oxidative stress. Using roGFP2, a genetically-encoded fluorescent reporter of the intracellular glutathione redox potential (E_{GSH}), we observed potent O_3-induced increases in E_{GSH}.

While oxidative stress is a major driving force for many adverse outcomes, the mechanisms by which this cellular state can be triggered are numerous and

often reversible. Within the cellular environment there are multiple redox systems that are not necessarily in equilibrium despite reactions within these systems being thermodynamically favored (Jones, 2006; Meyer and Dick, 2010; Gutscher et al, 2008). Furthermore, it is now clear that cellular "oxidative stress" is not a global characteristic simply inducible by the existence of a particular reactive species or poorly-characterized alterations in an endpoint of the "cellular redox state". However, it is reasonable to use a specific redox pair(s) in assessment of the oxidative status of cells. This is especially relevant when referring to a specific subcellular compartment such as the cytosol.

The non-disruptive monitoring of the intracellular GSH/GSSG redox pair is an advantageous means of assessing the oxidative state of cells undergoing xenobiotic exposure. GSH is a major contributor to the overall maintenance of intracellular redox homeostasis. Moreover, studies show that mice deficient in γ-GCS, the rate-limiting enzyme of glutathione synthesis, readily die of massive apoptosis, demonstrating the critical importance of GSH for cell survival (Dalton et al, 2004). Given the importance of GSH as indicated by its integration into cell survival mechanisms (Circu and Aw, 2010; Anathy et al, 2012), xenobiotic-induced changes in its overall oxidation state likely reflect an important shift in the global redox status of cells. Providing this alteration persists, and is not sufficiently reversed, onset of an oxidative stress is likely to ensue resulting in the aforementioned adverse outcomes ranging from cell death to altered gene expression. Therefore, in reference to the O_3 studies performed in Chapters 3 and 4, the increases in cytosolic E_{GSH} induced by O_3 reflect an oxidative shift in intracellular redox status, which

represents a clear departure from homeostasis, and an unambiguous index of oxidant stress.

Of recent, interest in the oxidation of protein thiol content has steadily gained acceptance as a means of initiating and promoting the adverse effects of xenobiotic exposure. Many of the intracellular redox systems, including glutathione, involve the use of thiol reactivity as the primary means of buffering and/or communicating cellular oxidation. Furthermore, redox-sensitive signaling proteins often employ exposed cysteine(s) in their active sites as oxidative sensors of their surrounding environment. In particular, phosphatases have been demonstrated to have redox-sensitive cysteines whose oxidation causes inactivation of the protein (Samet and Tal, 2010; Sarsour et al, 2009). As a result, the basal level of kinase activity can then prevail causing activation of various signaling pathways leading to outcomes such as inflammatory gene expression (Samet and Tal, 2010). All of these factors make assessment of the thiol/disulfide equilibrium useful in determination of changes in cellular redox status as well as outcomes of sustained oxidative stress.

There are physiological roles for the intra and extracellular generation of ROS that should not be mistaken as a type of oxidative stress. Within cells, ROS have been demonstrated to act as secondary messengers for the specific activation of redox-sensitive signaling pathways (Murphy et al, 2011). Of recent, H_2O_2 has been persuasively argued to be the most likely ROS to act as a secondary messenger (Forman et al, 2010). In relation to pulmonary inflammation, AP-1 and NFkB pathways have been shown to be responsive to oxidative stimulus via DEP and O_3

exposures (Cheng et al, 2012; Cienciwicki et al, 2008). Similarly, ROS such as superoxide and hydroxyl radicals are used by immune cells, including macrophages and neutrophils, in the generation of oxidative bursts used for microbicidal functions (Amulic et al, 2012; Slauch 2011).

While acute, localized increases in physiologically-relevant concentrations of certain ROS, such as H_2O_2, may serve as secondary messengers in cellular communication and activation of signaling cascades, xenobiotic-induced oxidative shifts in cellular redox can potentiate, impede, or otherwise interfere with activation of these physiological pathways that were meant to be transient in nature. By further extrapolating the data presented in Chapters 3 and 4, it appears as though O_3, or its secondary byproducts, would be free to non-specifically attack exposed thiol groups of various proteins upon entry into intracellular compartments. This hypothesis is at least partially substantiated by preliminary experiments in which we were able to observe direct O_3-induced oxidation of GSH to GSSG in acellular experiments (Data not shown). Likewise, O_3 has been reported to selectively activate transient receptor potential ankyrin 1 (TRPA1) cation channels in mouse bronchopulmonary C-fibres (Taylor-Clark and Undem, 2010). In that study, a direct O_3 activation of TRPA1 could not be substantiated nor ruled out; nonetheless, the results of our studies suggest that a direct activation is likely. Moreover, TRPA1 channels are known to be activated via modification of cysteine thiol residues, which is entirely consistent with a direct interaction of O_3 with this ion channel (Song et al, 2011; Bandell et al, 2004). Within humans, airway hyperresponsiveness, decreases in lung function, and other nervous system-mediated pulmonary effects have been demonstrated to

be direct results of O_3 exposure. This suggests that O_3 interactions with membrane-bound ion channels, and other thiol-containing receptors, are capable of inducing activation of pulmonary nerve cells, which in return, underlies these pulmonary responses. Taken together, these data suggest that O_3 have an impact on the direct oxidation of intracellular protein thiols.

A similar series of events is also applicable to the activation of other receptors in airway epithelial cells. For example, both O_3 and PM have been demonstrated to cause activation, and increased expression, of the epidermal growth factor receptor (EGFR) (Afaq et al, 2009; Churg et al, 2005; Leung et al, 2004; Tal et al, 2008). Activation of EGFR leads to transduction of signaling pathways responsible for cellular proliferation and survival (Herbst, 2004). Naturally, a consequence of constituitive activation of EGFR is the initiation and promotion of cancer. In fact, the development of certain types of lung cancer has been attributed to defects in EGFR, which are linked to environmental pollutant exposure and lifestyle exposures such as tobacco smoking (Petrelli et al, 2012; Couraud et al, 2012; Samet et al, 2009; Yano et al, 2012). Although specific details regarding ligand-mediated versus direct oxidative/phosphorylative activation of this receptor are yet to be elucidated, the mechanisms by which this receptor is activated appear to be reflective of its interaction with specific xenobiotic compounds.

A particularly interesting finding in Chapter 3 suggests that there is an inherent link between cellular maintenance of redox status and metabolic pathways (Chapter 3, Section 3.3.2). Observations made as early as 1966 have described the

interplay of ROS with GSH as a molecular basis for metabolic regulation (Jacob and Jandl, 1966). Our findings also indicate a role of energy metabolism in the maintenance of intracellular redox as glucose-deprived cells were sensitized to the effects of O_3-induced increases in E_{GSH} (Figure 3.3.2.1). Concomitantly, NADPH levels were also observed to decrease (Figure 3.3.2.2), and we inferred those decreases to correspond to an impairment of GR activity, inhibiting the reduction of GSSG to GSH, thus sensitizing the cells to a sustained oxidative insult. The major pathway for production of NADPH is the pentose phosphate pathway (PPP). Oxidative stress is believed to indirectly regulate the PPP since the activity of glucose-6-phosphate dehydrogenase (G6PD), the rate limiting enzyme of the PPP, has been demonstrated to increase in response to demand for NADPH in maintenance of cellular redox (Rahman et al, 1999). Moreover, oxidative stress has been observed to increase PPP activity in human epithelial cells, while deficiency in G6PD has been shown to enhance the sensitivity of erythrocytes and fibroblasts to oxidative insult (Wamelink et al., 2008; Ho et al., 2000).

Taken together, reductive maintenance of GSH is dependent on the participation of components within the glutathione system, as well as support from outside metabolic elements such as the PPP. The findings presented in Chapter 4 suggest that the metabolic capacity, and even the nutritional status, of cells exposed to oxidative air pollutants plays a significant role in the ability of cells to prevent oxidative stress. Moreover, considering that GSH is required for maintenance of intracellular redox homeostasis, inhibitory alterations of key metabolic pathways would adversely impact the reductive maintenance of GSH. The implications of

such alteration would ultimately increase cellular susceptibility to oxidative stress. In fact, G6PD deficiency in humans is the most common human enzyme defect (Cappellini and Fiorelli, 2008), and has been recently reported as a factor for increasing oxidative stress in the development of heart failure (Hecker et al, 2012). As evidenced by Hecker and colleagues, G6PD deficiency is not a lethal condition; however, individuals known to have this genetic defect are advised to avoid situations believed to cause overt oxidative stress, as such exposures have been shown to induce hemolysis (Cappellini and Fiorelli, 2008). Hemolysis is a common pathological outcome for individuals with G6PD deficiency since erythrocytes have an enhanced sensitivity to oxidative stress due to their lack of isocitrate dehydrogenase, an enzyme typically found in mitochondria (Wamelink et al., 2008).

Studies examining the effects of air pollution exposure have uncovered the existence of specific genetic polymorphisms that have direct impact on pulmonary defenses against air pollutants. Most notably, polymorphisms yielding deficiencies in the expression of certain GST isozymes, such as GSTM1 and GSTP1, have been linked to increased susceptibility to oxidative injury caused by common air pollutants including ozone and PM (Wu et al, 2011; Ballatori et al, 2009; Cienciwicki et al, 2008). In addition, a simple serine to proline polymorphism in the NADPH:quinone oxidoreductase 1 (NQO1) gene has been observed to make the resulting enzyme resistant to degradation. This resistance to degradation has been shown to contribute to O_3-induced toxicity by enhancing the activity of NQO1, which reduces quinones to hydroquinones, a product that is then oxdized by O_3 to yield secondary ROS (Yang et al, 2008). Furthermore, O_3 exposure studies using human subjects

found individuals with both polymorphisms to have greater decreases in lung function as well as increased markers of oxidative stress, including DNA adducts and lipid peroxides, in comparison to subjects lacking these genotypic changes (Bergamaschi et al, 2001.; Corradi et al, 2002). Also, these same polymorphisms have been associated with the exacerbation or onset of underlying pulmonary diseases such as asthma (Yang et al, 2008). As a whole, these observations provide evidence in support of genetic predisposition being a factor for human susceptibility to the adverse effects of air pollution.

Interestingly, preliminary studies conducted in our lab using primary cells from GSTM1 null and sufficient individuals did not find any significant differences amongst the genotypes in relation to protection or alteration of changes in E_{GSH} as measured by roGFP2 (data not shown). This observation was not necessarily surprising since GSTs directly conjugate GSH to xenobiotic molecules in phase II metabolic reactions, which would ultimately lead to consumption of the GSH pool. While the non-oxidative consumption of GSH could have an impact on the intracellular redox potential, the consumption of GSH would have to be considerable for detectable alteration of the cytosolic E_{GSH} during acute exposures to oxidizing compounds. This is largely due to the presence of high intracellular concentrations of GSH. Thus, this observation reinforces conventional thoughts regarding the protective effects of GSTs being specifically centered on their ability to detoxify and remove xenobiotics as opposed to a direct maintenance of the intracellular redox state. Hence, GSTs are important in detoxifying recognizable reactive species generated

from air pollution exposure in the reduction of oxidative stress once it ensues, as opposed to directly buffering oxidative injury before, or as, it occurs.

In examining the features of oxidant-induced lung injury, perturbation of epithelial integrity is often critical in the toxicological mechanisms of air pollutants. As stated previously, the lung epithelium is the first cellular barrier reached upon entry, often making it a primary target of the deleterious effects of inhaled xenobiotics. All cells are encompassed by a phospholipid bilayer known as the plasma membrane, which differentiates the intra- and extracellular environments. Interaction of oxidants with the plasma membrane has adverse outcomes, with the most common being lipid peroxidation. In general, lipid peroxidation is the oxidative degradation of lipids. It occurs as a series of reactions inducible by a variety of ROS, including H_2O_2 and superoxide, which ultimately results in damage to cellular membranes (Siddique et al, 2012). Additionally, O_3 and PM have been reported to cause lipid peroxidation, with numerous lipid peroxidation products being most frequently characterized as a consequence of O_3 exposure (Mudway and Kelly, 2000; Nemmar et al, 2012). Furthermore, byproducts of lipid peroxidation can themselves be oxidatively active making them capable of inflicting additional oxidative damage (Pulfer and Murphy, 2004; Uhlson et al, 2002).

The epithelial lining fluid (ELF) contains numerous low molecular weight antioxidants, antioxidant proteins, and unsaturated lipids, which generally exist to either aid in the physiological functioning of the lung, or to protect the lung from the outside environment. As a protective barrier, the ELF is there to mitigate the effects

of respired toxicants before they can reach the underlying epithelium. However, the existence of so many oxidizable targets within the ELF likely makes this protective lung component a potentiator of oxidative damage. For example, due to its reactivity, O_3 solubility within the ELF clears rapidly making it unavailable to interact with lung components upon cessation of exposure; but, the adverse effects of O_3 occur long after an acute exposure (Figure 5.2) (Ballinger et al, 2005; Mudway and Kelly, 2000). While these effects are largely attributable to direct cellular damage that occurred during exposure, it is likely that the production of O_3-induced byproducts, resultant from reactions with ELF components, are the latent drivers that potentiate the adverse effects beyond the initial O_3 exposure. This is likely related to the lag time required to detoxify the remaining oxidative byproducts as evidenced by the peak in LOPs (lipid ozonation products) across the initiation and progression periods (Figure 5.2).

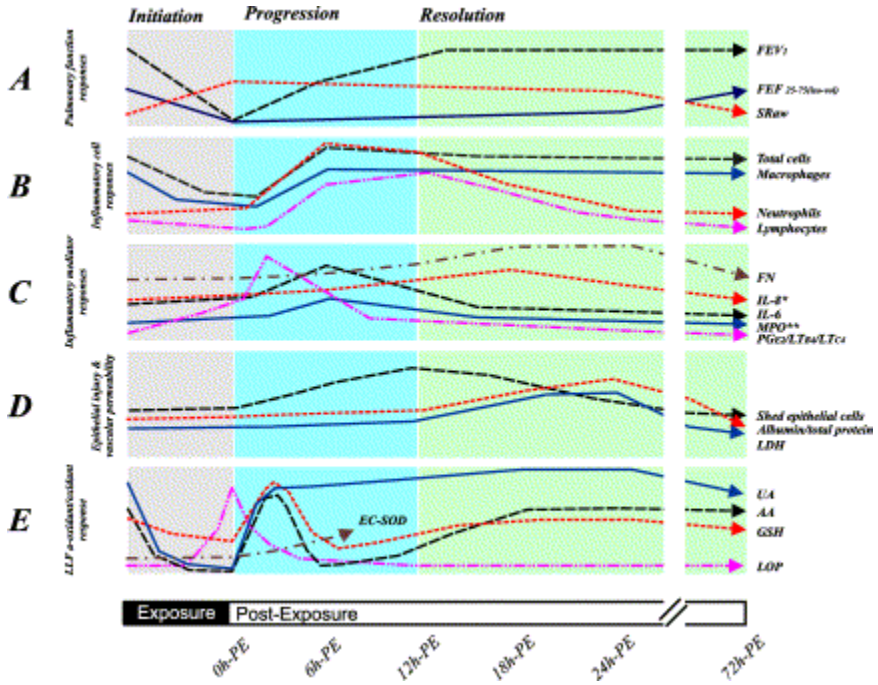

Figure 5.2 Time course of acute human responses to environmentally-relevant O_3 concentrations. (Mudway and Kelly 2000) The temporal profiles of endpoints related to five groups of O_3-induced responses are plotted across time. Each group of profiles is divided into three temporal periods: Initiation (responses observed during the exposure), Progression (the time during which O_3 responses develop after the exposure period), and Resolution (the period of time where acute responses resolve back to pre-exposure levels). The five types of responses are: A) pulmonary function (FEV_1, FEF, SR_{aw}); B) inflammatory cell responses (Total cells, Macrophages, Neutrophils, Lymphocytes); C) inflammatory mediators (FN, IL-8, IL-6, MPO, PG_{E2}); D) epithelial injury (Shed epithelial cells, Albumin/total protein, LDH); and E) extracellular antioxidant responses (UA, AA, GSH, LOP)

Assumably, a plot of PM-induced effects monitoring the same endpoints of the above figure would likely be exaggerated in relation to the exposure effects. Depending on the physiochemical properties of the particulates inhaled, certain particles would likely persist within the lung for longer durations of time beyond the

exposure period. This would be especially true for UFP since the size of these particles causes them to avoid certain pulmonary defenses such as the mucociliary clearance pathway.

Complementary effects of gaseous and particulate air pollutants likely influence the adverse outcomes of air pollution exposure. For example, O_3 has been demonstrated to increase the permeability of epithelial cell membranes (Yang and Omaye, 2009), which could possibly potentiate the ability of particulates to reach intracellular environments. In this situation, cells exposed to O_3 and PM would then face a two-fold oxidative attack. Even if the ELF of pulmonary epithelial cells is capable of fully buffering moderate concentrations of O_3, the generation of secondary ROS, combined with the additional intracellular burden of redox-active particles, could overwhelm antioxidant defenses. Moreover, in the case of DEP exposure, where the organic content of these particles can be relatively high, interaction of O_3 with the organic content could lead to the generation of additional oxidation products that may be capable of transcending injured lipid bilayers for direct oxidative attack. Overall, the proposed conditions would reinforce the progression of an oxidative stress response.

Ultimately, the adverse effects of air pollution exposure leading to oxidative stress are dictated by several factors. Many of these factors are best summarized by the hierarchical model of oxidative stress responses proposed by Andre Nel as depicted in Figure 5.3 (Li et al, 2008).

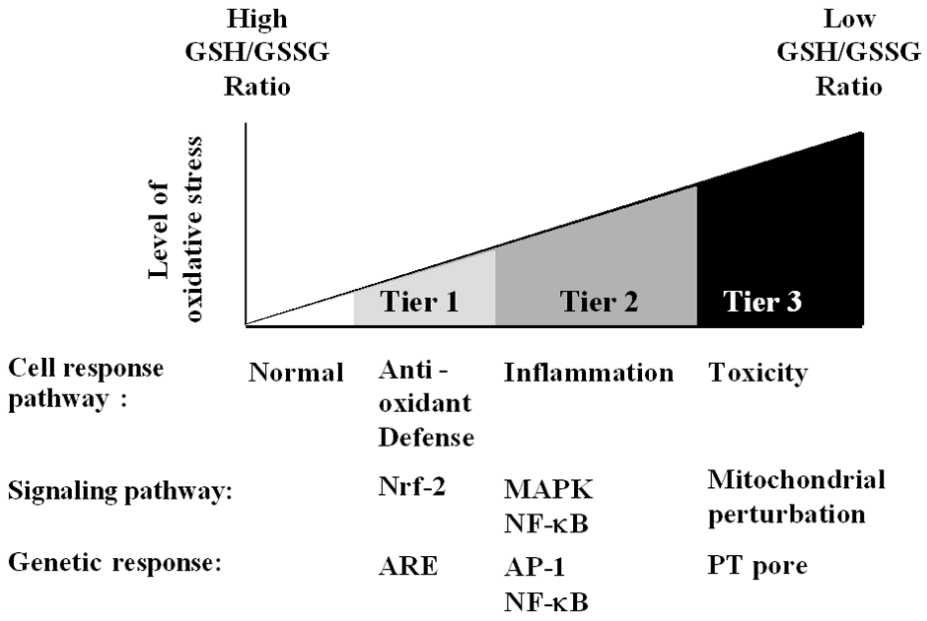

Figure 5.3 Hierarchical model of oxidative stress responses. (Li et al, 2008).

For our purposes, oxidative stress is defined as occurring when an imbalance in the production of reactive species and free radicals exceeds the capacity of cellular mechanisms to avoid or correct oxidative damage. In the hierarchical model by Li and colleagues, the levels of succession for oxidative stress are placed in relation to three tiers of cellular response. Moreover, this particular model places oxidative stress in relation to the GSH/GSSG ratio. In relation to our definition, tier 1 of the hierarchical model is dedicated to mitigating and correcting oxidative damage obtained from a sustained exposure. At this level, the GSH/GSSG ratio is still relatively high, which serves to prevent activation of inflammatory signaling cascades. As the oxidative stress ensues, antioxidant defenses become overwhelmed and the GSH/GSSG ratio drops to a level where redox-sensitive

signaling pathways become activated, possibly due to the loss of protein tyrosine phosphatases that maintain signaling quiescence. This initiates an inflammatory response that attempts to contain and facilitate the repair of damaged tissues. Lastly, total compromise of cellular antioxidant defenses, as reflected by a low GSH/GSSG ratio, in combination with extensive oxidative damage, triggers overt cytotoxicity, resulting in activation of apoptotic or necrotic pathways often directed by mitochondrial cues. In relation to pulmonary oxidative stress, it is important to note that while adequate, this linearized model does not necessarily account for the reversible nature of redox processes. Also, it does not account for adaptive responses mediated via the nervous system such as alteration of breathing patterns. In addition, sustained oxidative stress does not necessarily end with an overt cytotoxicity. As mentioned earlier, the adverse effects of oxidative stress could alter or inactivate critical signaling molecules, such as phosphatases, leading to an aberrant activation of signaling cascades related to cell proliferation and survival (i.e. cancer).

The genetic background and disease burden of exposed individuals must also be taken into account when examining the adverse effects of air pollution. As discussed earlier, the effect of polymorphism of key oxidant-mitigating proteins can certainly affect an individual's level of susceptibility to air pollutant exposure. Similarly, underlying disease burden can also make a relatively unhealthy individual more susceptible to the adverse effects of air pollution exposure. Both cardiovascular and pulmonary diseases, including asthma, COPD, diabetes, hypertension, and atherosclerosis, have been demonstrated to enhance *in vivo*

responses to air pollution in humans and various animal models (American Lung Association, 2012; Bolton et al., 2012; Curtis et al, 2006; Kampa and Castana, 2007; Laumbach, 2010; and Shannahan et al, 2010;). Ultimately, determination of the adverse effects of air pollution exposure is multifactorial.

In moving forward, the future of oxidative stress assessment looks promising. In relation to cellular responses, the redox research community has been making strides to move away from global assessments of oxidative stress in pursuit of assessing changes in specific mechanistic components that impact redox homeostasis. Similarly, toxicologists are always looking for better ways of assessing redox related-endpoints in pursuit of answering mechanistic questions. With improvements upon existing technologies, and development of new tools, our understanding of xenobiotic-induced oxidative stress will progress. While this project has utilized the latest sensors available, new ones emerge continuously. Mutation of GFP continues to drive the development of new fluorescent reporters that improve upon previous versions. For instance, a new version of roGFP2, called roTurbo, was recently reported and is purported to improve upon the current version of the sensor by being a brighter, more readily oxidizable fluorophore (Dooley et al, 2012).

The future of oxidative stress measurement will center on development of probes with enhanced sensitivity, specificity, and targetability to predetermined subcellular locations. Moreover, designers of future probes should seek to diversify their sensors while making them compatible with high throughput technologies.

Currently, many of the available small molecule probes like PG-1 and VSL1, as well as their genetically encoded counterparts, such as roGFP and HyPer, only emit green fluorescence. This makes the process of assessing redox related changes more challenging because observations using different probes must be done independently or through specialized post-acquisitional processing. Of recent, my colleague in the Samet lab, Dr. Wan-Yun Cheng, was able to develop a new imaging technique for resolving closely-emitted fluorophores within the same cells. While this technique is a wonderful contribution to the scientific community, it relies on the use of instruments with spectral detectors, a technology that is not always available in the typical confocal core facility. Ideally, the emitted wavelengths of next-generation fluorophores would be available in blue and red spectra so that combinations of fluorophores can be used simultaneously to characterize different redox endpoints using conventional filter-based optics. Also, improvements upon small molecule sensors should continue in relation to specificity and sensitivity while making them containable within specific subcellular compartments.

In conclusion, the work presented herein use current imaging techniques to advance our understanding of the toxicological implications of exposure of human cells to common air pollutants. Over the course of these studies, we were able to develop and implement approaches for 1) detecting and assessing nanoscaled particle internalization and 2) making real-time assessments of xenobiotic-induced changes in E_{GSH}. These methods became critical for the determination of important endpoints related to the spatiotemporal interaction of air pollutants with cellular environments as well as the direct oxidative consequences of such interactions.

Most importantly, we were able to observe endpoints directly related to air pollutant-induced oxidative stress. Using ozone as a model air pollutant, we have demonstrated perturbation of the intracellular glutathione redox potential, an endpoint specifically attributable to oxidative stress. Moreover, we have generated data that suggest that the observed changes in redox potential are the result of direct O_3 interaction with intracellular components, a phenomenon that was previously thought to be unfeasible. Also, the importance of common extracellular antioxidants in the protection of epithelial cells from O_3-induced increases in E_{GSH} was demonstrated. Using the approach described in our characterization of O_3-induced redox changes, future toxicological studies of various types of xenobiotics can now more directly assess an important endpoint of oxidative stress. Similarly, with growing concerns over the health implications of intentional and unintentional NP exposure, the DF-CLSM methodology should assist in characterizing factors determining particle entry to intracellular environments.

References

Afaq F, Zaid MA, Pelle E, Khan N, Syed DN, Matsui MS, et al. 2009. Aryl hydrocarbon receptor is an ozone sensor in human skin. J Invest Dermatol 129:2396-2403.

American Lung Association. 2012. State of the air. Available: http://www.stateoftheair.org/2012/assets/state-of-the-air2012.pdf [accessed 10/23/12 2012].

Amulic B, Cazalet C, Hayes GL, Metzler KD, Zychlinsky A. 2012. Neutrophil function: From mechanisms to disease. Annual Review of Immunology 30:459-489.

Anathy V, Roberson EC, Guala AS, Godburn KE, Budd RC, Janssen-Heininger YM. 2012. Redox-based regulation of apoptosis: S-glutathionylation as a regulatory mechanism to control cell death. Antioxid Redox Signal 16:496-505.

Anderson ME. 1998. Glutathione: An overview of biosynthesis and modulation. Chemico-Biological Interactions 111-112:1-14.

Arthur JR. 2000. The glutathione peroxidases. Cellular and Molecular Life Sciences 57:1825-1835.

Auerbach A, Hernandez ML. 2012. The effect of environmental oxidative stress on airway inflammation. Current opinion in allergy and clinical immunology 12:133-139.

Ballatori N, Krance SM, Notenboom S, Shi S, Tieu K, Hammond CL. 2009. Glutathione dysregulation and the etiology and progression of human diseases. Biol Chem 390:191-214.

Ballinger CA, Cueto R, Squadrito G, Coffin JF, Velsor LW, Pryor WA, et al. 2005. Antioxidant-mediated augmentation of ozone-induced membrane oxidation. Free Radical Biology and Medicine 38:515-526.

Bandell M, Story GM, Hwang SW, Viswanath V, Eid SR, Petrus MJ, et al. 2004. Noxious cold ion channel trpa1 is activated by pungent compounds and bradykinin. Neuron 41:849-857.

Bargagli E, Olivieri C, Bennett D, Prasse A, Muller-Quernheim J, Rottoli P. 2009. Oxidative stress in the pathogenesis of diffuse lung diseases: A review. Respiratory Medicine 103:1245-1256.

Belousov VV, Fradkov AF, Lukyanov KA, Staroverov DB, Shakhbazov KS, Terskikh AV, et al. 2006. Genetically encoded fluorescent indicator for intracellular hydrogen peroxide. Nat Methods 3:281-286.

Bergamaschi E, De Palma G, Mozzoni P, Vanni S, Vettori MV, Broeckaert F, et al. 2001. Polymorphism of quinone-metabolizing enzymes and susceptibility to ozone-induced acute effects. Am J Respir Crit Care Med 163:1426-1431.

Biswas P, Wu C-Y. 2005. Nanoparticles and the environment. Journal of the Air & Waste Management Association 55:708-746.

Biswas SK, Rahman I. 2009. Environmental toxicity, redox signaling and lung inflammation: The role of glutathione. Molecular Aspects of Medicine 30:60-76.

Bolton JL, Smith SH, Huff NC, Gilmour MI, Foster WM, Auten RL, et al. 2012. Prenatal air pollution exposure induces neuroinflammation and predisposes offspring to weight gain in adulthood in a sex-specific manner. FASEB J.

Bonin K, and Bonissi, D. 2009. Ultra clean microscope slides. Available: http://www.wfu.edu/~bonin/Microscope/UltraCleanSlides.htm 2009].

Brunekreef B, Holgate ST. 2002. Air pollution and health. The Lancet 360:1233-1242.

Burk RF, Hill KE. 2010. 4.13 - glutathione peroxidases. In: Comprehensive toxicology (second edition), (Editor-in-Chief: Charlene AM, ed). Oxford:Elsevier, 229-242.

Cannon MB, Remington SJ. 2006. Re-engineering redox-sensitive green fluorescent protein for improved response rate. Protein Sci 15:45-57.

Cannon MB, Remington SJ. 2008. Redox-sensitive green fluorescent protein: Probes for dynamic intracellular redox responses. A review. Methods Mol Biol 476:51-65.

Cannon MB, James Remington S. 2009. Redox-sensitive green fluorescent protein: Probes for dynamic intracellular redox responses. A review. In: Redox-mediated signal transduction, Vol. 476:Humana Press, 50-64.

Cappellini MD, Fiorelli G. 2008. Glucose-6-phosphate dehydrogenase deficiency. The Lancet 371:64-74.

Chalfant M, Bernd K. 2011. Detecting ozone-induced changes in cellular redox balance via gsh/gssg-glo™ assay [Online February 2012].

Chandler DEaR, R. W. 2009. Bioimaging: Current techniques in light and electron microscopy. Sudbury, MA:Jones and Bartlett Publishers.

Cheng W-Y, Tong H, Miller EW, Chang CJ, Remington J, Zucker RM, et al. 2010. An integrated imaging approach to the study of oxidative stress generation by mitochondrial dysfunction in living cells. Environ Health Perspect 118.

Cheng WY, Currier J, Bromberg PA, Silbajoris R, Simmons SO, Samet JM. 2012. Linking oxidative events to inflammatory and adaptive gene expression induced by exposure to an organic particulate matter component. Environ Health Perspect 120:267-274.

Chiang SM, Schellhorn HE. 2012. Regulators of oxidative stress response genes in escherichia coli and their functional conservation in bacteria. Archives of Biochemistry and Biophysics 525:161-169.

Christman MF, Storz G, Ames BN. 1989. Oxyr, a positive regulator of hydrogen peroxide-inducible genes in escherichia coli and salmonella typhimurium, is homologous to a family of bacterial regulatory proteins. Proc Natl Acad Sci U S A 86:3484-3488.

Chung KF, Marwick JA. 2010. Molecular mechanisms of oxidative stress in airways and lungs with reference to asthma and chronic obstructive pulmonary disease. Annals of the New York Academy of Sciences 1203:85-91.

Churg A, Xie C, Wang X, Vincent R, Wang RD. 2005. Air pollution particles activate nf-kappab on contact with airway epithelial cell surfaces. Toxicol Appl Pharmacol 208:37-45.

Ciencewicki J, Trivedi S, Kleeberger SR. 2008. Oxidants and the pathogenesis of lung diseases. Journal of Allergy and Clinical Immunology 122:456-468.

Circu ML, Aw TY. 2010. Reactive oxygen species, cellular redox systems, and apoptosis. Free Radical Biology and Medicine 48:749-762.

Corradi M, Alinovi R, Goldoni M, Vettori M, Folesani G, Mozzoni P, et al. 2002. Biomarkers of oxidative stress after controlled human exposure to ozone. Toxicol Lett 134:219-225.

Couraud S, Zalcman G, Milleron B, Morin F, Souquet P-J. 2012. Lung cancer in never smokers – a review. European Journal of Cancer 48:1299-1311.

Craig GA, Allen PJ, Mason MD. 2010. Synthesis, characterization, and functionalization of gold nanoparticles for cancer imaging. Methods Mol Biol 624:177-193.

Curtis L, Rea W, Smith-Willis P, Fenyves E, Pan Y. 2006. Adverse health effects of outdoor air pollutants. Environment International 32:815-830.

Dalton TP, Chen Y, Schneider SN, Nebert DW, Shertzer HG. 2004. Genetically altered mice to evaluate glutathione homeostasis in health and disease. Free Radical Biology and Medicine 37:1511-1526.

Devlin RB, McKinnon KP, Noah T, Becker S, Koren HS. 1994. Ozone-induced release of cytokines and fibronectin by alveolar macrophages and airway epithelial cells. American Journal of Physiology - Lung Cellular and Molecular Physiology 266:L612-L619.

Dickinson BC, Chang CJ. 2008. A targetable fluorescent probe for imaging hydrogen peroxide in the mitochondria of living cells. J Am Chem Soc 130:9638-9639.

Dickinson BC, Huynh C, Chang CJ. 2010a. A palette of fluorescent probes with varying emission colors for imaging hydrogen peroxide signaling in living cells. Journal of the American Chemical Society 132:5906-5915.

Dickinson BC, Srikun D, Chang CJ. 2010b. Mitochondrial-targeted fluorescent probes for reactive oxygen species. Current Opinion in Chemical Biology 14:50-56.

Dickinson DA, Forman HJ. 2002. Cellular glutathione and thiols metabolism. Biochemical Pharmacology 64:1019-1026.

Dooley C, Li L, Misler J, Thompson J. 2012. Toxicity of 6-hydroxydopamine: Live cell imaging of cytoplasmic redox flux. Cell Biology and Toxicology 28:89-101.

Dooley CT, Dore TM, Hanson GT, Jackson WC, Remington SJ, Tsien RY. 2004. Imaging dynamic redox changes in mammalian cells with green fluorescent protein indicators. Journal of Biological Chemistry 279:22284-22293.

Dubinina EE, Dadali VA. 2010. Role of 4-hydroxy- trans-2-nonenal in cell functions. Biochemistry (00062979) 75:1069-1087.

Fernandes AP, Holmgren A. 2004. Glutaredoxins: Glutathione-dependent redox enzymes with functions far beyond a simple thioredoxin backup system. Antioxid Redox Signal 6:63-74.

Forman HJ. 2010. Reactive oxygen species and α, β-unsaturated aldehydes as second messengers in signal transduction. Annals of the New York Academy of Sciences 1203:35-44.

Garner AL, St Croix CM, Pitt BR, Leikauf GD, Ando S, Koide K. 2009. Specific fluorogenic probes for ozone in biological and atmospheric samples. Nat Chem 1:316-321.

Geiser M, Rothen-Rutishauser B, Kapp N, Schürch S, Kreyling W, Schulz H, et al. 2005. Ultrafine particles cross cellular membranes by nonphagocytic mechanisms in lungs and in cultured cells. Environmental Health Perspectives 113:1555.

Geiser M, Kreyling W. 2010. Deposition and biokinetics of inhaled nanoparticles. Particle and Fibre Toxicology 7:2.

Gomes A, Fernandes E, Lima JLFC. 2005. Fluorescence probes used for detection of reactive oxygen species. Journal of Biochemical and Biophysical Methods 65:45-80.

Gutscher M, Pauleau A-L, Marty L, Brach T, Wabnitz GH, Samstag Y, et al. 2008. Real-time imaging of the intracellular glutathione redox potential. Nature Methods 5:553(557).

Hallock MF, Greenley P, DiBerardinis L, Kallin D. 2009. Potential risks of nanomaterials and how to safely handle materials of uncertain toxicity. Journal of Chemical Health and Safety 16:16-23.

Hanson GT, Aggeler R, Oglesbee D, Cannon M, Capaldi RA, Tsien RY, et al. 2004. Investigating mitochondrial redox potential with redox-sensitive green fluorescent protein indicators. Journal of Biological Chemistry 279:13044-13053.

Harrison RM, Yin J. 2000. Particulate matter in the atmosphere: Which particle properties are important for its effects on health? Sci Total Environ 249:85-101.

Hecker PA, Lionetti V, Ribeiro RF, Rastogi S, Brown BH, O'Connell KA, et al. 2012. Glucose 6-phosphate dehydrogenase deficiency increases redox stress and moderately accelerates the development of heart failure. Circulation: Heart Failure.

Heidi W, Byron FB-S. 2009. Enhanced dark field microscopy for rapid artifact-free detection of nanoparticle binding to candida albicans cells and hyphae. Biotechnology Journal 4:871-879.

Helfand WH, Lazarus J, Theerman P. 2001. Donora, pennsylvania: An environmental disaster of the 20th century. Am J Public Health 91:553.

Helmy MH, Ismail SS, Fayed H, El-Bassiouni EA. 2000. Effect of selenium supplementation on the activities of glutathione metabolizing enzymes in human hepatoma hep g2 cell line. Toxicology 144:57-61.

Herbst RS. 2004. Review of epidermal growth factor receptor biology. Int J Radiat Oncol Biol Phys 59:21-26.

Hibbs AR. 2004. Confocal microscopy for biologists. New York:Kluwer Academic/Plenum Publishers.

Ho H-y, Cheng M-l, Lu F-j, Chou Y-h, Stern A, Liang C-m, et al. 2000. Enhanced oxidative stress and accelerated cellular senescence in glucose-6-phosphate dehydrogenase (g6pd)-deficient human fibroblasts. Free Radical Biology and Medicine 29:156-169.

Holben DH, Smith AM. 1999. The diverse role of selenium within selenoproteins: A review. Journal of the American Dietetic Association 99:836-843.

Jacob HS, Jandl JH. 1966. Effects of sulfhydryl inhibition on red blood cells. 3. Glutathione in the regulation of the hexose monophosphate pathway. J Biol Chem 241:4243-4250.

Jefferson DA, Tilley EEM. 1999. The structural and physical chemistry of nanoparticles. In: Particulate matter: Properties and effects upon health. Oxford, UK BIOS Scientific Publishers Ltd., 63-84.

Jones CF, Grainger DW. 2009. In vitro assessments of nanomaterial toxicity. Advanced Drug Delivery Reviews 61:438-456.

Jones DP. 2006. Redefining oxidative stress. Antioxid Redox Signal 8:1865-1879.

Jones DP. 2008. Radical-free biology of oxidative stress. American Journal of Physiology - Cell Physiology 295:C849-C868.

Kampa M, Castanas E. 2008. Human health effects of air pollution. Environmental Pollution 151:362-367.

Karin M, Takahashi T, Kapahi P, Delhase M, Chen Y, Makris C, et al. 2001. Oxidative stress and gene expression: The ap-1 and nf-κb connections. Biofactors 15:87.

Katsouyanni K. 2003. Ambient air pollution and health. British Medical Bulletin 68:143-156.

Kelly FJ, Mudway I, Krishna MT, Holgate ST. 1995. The free radical basis of air pullution: Focus on ozone. Respiratory Medicine 89:647-656.

Kelly FJ. 1999. Gluthathione: In defence of the lung. Food Chem Toxicol 37:963-966.

Kelly FJ. 2003. Oxidative stress: Its role in air pollution and adverse health effects. Occupational and Environmental Medicine 60:612-616.

Kensler TW, Wakabayashi N, Biswal S. 2007. Cell survival responses to environmental stresses via the keap1-nrf2-are pathway. Annual review of pharmacology and toxicology 47:89-116.

Kermani S, Ben-Jebria A, Ultman JS. 2006. Kinetics of ozone reaction with uric acid, ascorbic acid, and glutathione at physiologically relevant conditions. Archives of Biochemistry and Biophysics 451:8-16.

Kim CS, Alexis NE, Rappold AG, Kehrl H, Hazucha MJ, Lay JC, et al. 2011. Lung function and inflammatory responses in healthy young adults exposed to 0.06 ppm ozone for 6.6 hours. Am J Respir Crit Care Med 183:1215-1221.

Ko FWS, Hui DSC. 2010. Effects of air pollution on lung health. Clinical pulmonary medicine 17:300-304.

Kohen R, Nyska A. 2002. Invited review: Oxidation of biological systems: Oxidative stress phenomena, antioxidants, redox reactions, and methods for their quantification. Toxicologic Pathology 30:620-650.

Krewski D, Rainham D. 2007. Ambient air pollution and population health: Overview. Journal of Toxicology and Environmental Health, Part A 70:275-283.

Laumbach RJ. 2010. Outdoor air pollutants and patient health. Am Fam Physician 81:175-180.

Leist M, Raab B, Maurer S, Rösick U, Brigelius-Flohé R. 1996. Conventional cell culture media do not adequately supply cells with antioxidants and thus facilitate peroxide-induced genotoxicity. Free Radical Biology and Medicine 21:297-306.

Leung DYM, Nelson HS, Szefler SJ, Busse WW. 2004. Ozone upregulates nasal epidermal growth factor receptors. Journal of Allergy and Clinical Immunology 113:1.

Lewis KN, Mele J, Hayes JD, Buffenstein R. 2010. Nrf2, a guardian of healthspan and gatekeeper of species longevity. Integrative and Comparative Biology 50:829-843.

Li N, Xia T, Nel AE. 2008. The role of oxidative stress in ambient particulate matter-induced lung diseases and its implications in the toxicity of engineered nanoparticles. Free Radical Biology and Medicine 44:1689-1699.

Liu X, Sun J. 2010. Endothelial cells dysfunction induced by silica nanoparticles through oxidative stress via jnk/p53 and nf-[kappa]b pathways. Biomaterials 31:8198-8209.

Lohmann-Matthes M, Steinmuller C, Franke-Ullmann G. 1994. Pulmonary macrophages. European Respiratory Journal 7:1678-1689.

Lu J, Holmgren A. 2009. Selenoproteins. Journal of Biological Chemistry 284:723-727.

Ma Q. 2010. Transcriptional responses to oxidative stress: Pathological and toxicological implications. Pharmacol Ther 125:376-393.

MacNee W. 2001. Oxidative stress and lung inflammation in airways disease. European Journal of Pharmacology 429:195-207.

Madl AK, Pinkerton KE. 2009. Health effects of inhaled engineered and incidental nanoparticles. Crit Rev Toxicol 39:629-658.

Marquis BJ, Love SA, Braun KL, Haynes CL. 2009. Analytical methods to assess nanoparticle toxicity. Analyst 134:425-439.

Mates JM, Sanchez-Jimenez F. 1999. Antioxidant enzymes and their implications in pathophysiologic processes. Front Biosci 4:D339-345.

Maynard RL, Howard CV, eds. 1999. Particulate matter: Properties and effects upon health. Oxford:Bios Scientific in association with the Royal Microscopical Society.

Meister A. 1995. Glutathione metabolism. In: Methods in enzymology, Vol. Volume 251, (Lester P, ed):Academic Press, 3-7.

Meng H, Xia T, George S, Nel AE. 2009. A predictive toxicological paradigm for the safety assessment of nanomaterials. ACS Nano 3:1620-1627.

Meyer AJ. 2008. The integration of glutathione homeostasis and redox signaling. Journal of Plant Physiology 165:1390-1403.

Meyer AJ, Dick TP. 2010. Fluorescent protein-based redox probes. Antioxidants & Redox Signaling 13:621-650.

Miller EW, Tulyathan O, Isacoff EY, Chang CJ. 2007. Molecular imaging of hydrogen peroxide produced for cell signaling. Nat Chem Biol 3:263-267.

Mills LR, Stevens JK, Trogadis JE. 1994. Three-dimensional confocal microscopy : Volume investigation of biological specimens. San Diego:Academic Press.

Morgan B, Sobotta MC, Dick TP. 2011. Measuring Egsh and H_2O_2 with rogfp2-based redox probes. Free Radical Biology and Medicine 51:1943-1951.

Mossman B, Borm P, Castranova V, Costa D, Donaldson K, Kleeberger S. 2007. Mechanisms of action of inhaled fibers, particles and nanoparticles in lung and cardiovascular diseases. Particle and Fibre Toxicology 4:4.

Mudway IS, Housley D, Eccles R, Richards RJ, Datta AK, Tetley TD, et al. 1996. Differential depletion of human respiratory tract antioxidants in response to ozone challenge. Free Radical Research 25:499-513.

Mudway IS, Kelly FJ. 2000. Ozone and the lung: A sensitive issue. Molecular Aspects of Medicine 21:1-48.

Muhlfeld C, Rothen-Rutishauser B, Vanhecke D, Blank F, Gehr P, Ochs M. 2007. Visualization and quantitative analysis of nanoparticles in the respiratory tract by transmission electron microscopy. Particle and Fibre Toxicology 4:11.

Murdock RC, Braydich-Stolle L, Schrand AM, Schlager JJ, Hussain SM. 2008. Characterization of nanomaterial dispersion in solution prior to in vitro exposure using dynamic light scattering technique. Toxicol Sci 101:239-253.

Murphy DB, NetLibrary I. 2001. Fundamentals of light microscopy and electronic imaging [electronic resource]. New York:Wiley-Liss.

Murphy Michael P, Holmgren A, Larsson N-G, Halliwell B, Chang Christopher J, Kalyanaraman B, et al. 2011. Unraveling the biological roles of reactive oxygen species. Cell Metabolism 13:361-366.

Murr LE, Garza KM. 2009. Natural and anthropogenic environmental nanoparticulates: Their microstructural characterization and respiratory health implications. Atmospheric Environment 43:2683-2692.

Nakane H. 2012. Translocation of particles deposited in the respiratory system: A systematic review and statistical analysis. Environmental health and preventive medicine 17:263-274.

Nel AE, Madler L, Velegol D, Xia T, Hoek EMV, Somasundaran P, et al. 2009. Understanding biophysicochemical interactions at the nano-bio interface. Nat Mater 8:543-557.

Nemery B, Hoet PH, Nemmar A. 2001. The meuse valley fog of 1930: An air pollution disaster. Lancet 357:704-708.

Nemmar A, Subramaniyan D, Zia S, Yasin J, Ali BH. 2012. Airway resistance, inflammation and oxidative stress following exposure to diesel exhaust particle in angiotensin ii-induced hypertension in mice. Toxicology 292:162-168.

Newhouse M, Sanchis J, Bienenstock J. 1976. Lung defense mechanisms. New England Journal of Medicine 295:990-998.

Nicod L. 2005. Lung defences: An overview. European Respiratory Review 14:45-50.

Nurkiewicz T, Porter D, Hubbs A, Cumpston J, Chen B, Frazer D, et al. 2008. Nanoparticle inhalation augments particle-dependent systemic microvascular dysfunction. Particle and Fibre Toxicology 5:1.

Oberdorster G, Oberdorster E, Oberdorster J. 2005. Nanotoxicology: An emerging discipline evolving from studies of ultrafine particles. Environ Health Perspect 113:823-839.

Oberdörster G, Ferin J, Lenhert BE. 1994. Correlation between particle size, in vivo particle persistence, and lung injury. Environ Health Perspect 102:173-179.

Oberdörster G, Utell MJ. 2002. Ultrafine particles in the urban air: To the respiratory tract--and beyond? Environmental Health Perspectives 110:A440.

Oberdörster G, Sharp Z, Atudorei V, Elder A, Gelein R, Kreyling W, et al. 2004. Translocation of inhaled ultrafine particles to the brain. Inhalation Toxicology 16:437-445.

Oberdörster G, Maynard A, Donaldson K, Castranova V, Fitzpatrick J, Ausman K, et al. 2005. Principles for characterizing the potential human health effects from exposure to nanomaterials: Elements of a screening strategy. Particle and Fibre Toxicology 2:8.

Ogunseitan O, Robbins JB. Green health: An a-to-z guide. Green health: An a-to-z guide. Sage publications, inc. Thousand Oaks, CA:SAGE Publications, Inc.

Olivieri D, Scoditti E. 2005. Impact of environmental factors on lung defences. European Respiratory Review 14:51-56.

Øvrevik J, Låg M, Holme JA, Schwarze PE, Refsnes M. 2009. Cytokine and chemokine expression patterns in lung epithelial cells exposed to components characteristic of particulate air pollution. Toxicology 259:46-53.

Park E-J, Roh J, Kang M-S, Kim SN, Kim Y, Choi S. 2011. Biological responses to diesel exhaust particles (deps) depend on the physicochemical properties of the deps. PLoS One 6:e26749.

Patton JS. 1996. Mechanisms of macromolecule absorption by the lungs. Advanced Drug Delivery Reviews 19:3-36.

Pedelacq J-D, Cabantous S, Tran T, Terwilliger TC, Waldo GS. 2006. Engineering and characterization of a superfolder green fluorescent protein. Nat Biotech 24:79-88.

Petrelli F, Borgonovo K, Cabiddu M, Barni S. 2012. Efficacy of egfr tyrosine kinase inhibitors in patients with egfr-mutated non–small-cell lung cancer: A meta-analysis of 13 randomized trials. Clinical Lung Cancer 13:107-114.

Pryor WA, Das B, Church DF. 1991. The ozonation of unsaturated fatty acids: Aldehydes and hydrogen peroxide as products and possible mediators of ozone toxicity. Chem Res Toxicol 4:341-348.

Pryor WA. 1992. How far does ozone penetrate into the pulmonary air/tissue boundary before it reacts? Free Radical Biology and Medicine 12:83-88.

Pryor WA, Squadrito GL, Friedman M. 1995. A new mechanism for the toxicity of ozone. Toxicology Letters 82-83:287-293.

Pui DYH, Qi C, Stanley N, Oberdorster G, Maynard A. 2008. Recirculating air filtration significantly reduces exposure to airborne nanoparticles. Environmental Health Prospectives 116:863-866.

Pulfer MK, Murphy RC. 2004. Formation of biologically active oxysterols during ozonolysis of cholesterol present in lung surfactant. J Biol Chem 279:26331-26338.

Rahman Q, Abidi P, Afaq F, Schiffmann D, Mossman BT, Kamp DW, et al. 1999. Glutathione redox system in oxidative lung injury. CRC Critical Reviews in Toxicology 29:543-568.

Reddel RR, Ke Y, Gerwin BI, McMenamin MG, Lechner JF, Su RT, et al. 1988. Transformation of human bronchial epithelial cells by infection with sv40 or adenovirus-12 sv40 hybrid virus, or transfection via strontium phosphate coprecipitation with a plasmid containing sv40 early region genes. Cancer Res 48:1904-1909.

Rothen-Rutishauser B, Mühlfeld C, Blank F, Musso C, Gehr P. 2007. Translocation of particles and inflammatory responses after exposure to fine particles and nanoparticles in an epithelial airway model. Particle and Fibre Toxicology 4:9.

Rubio V, Valverde M, Rojas E. 2010. Effects of atmospheric pollutants on the nrf2 survival pathway. Environmental Science and Pollution Research 17:369-382.

Sadhu SS, Callegari E, Zhao Y, Guan X, Seefeldt T. 2012. Evaluation of a dithiocarbamate derivative as an inhibitor of human glutaredoxin-1. J Enzyme Inhib Med Chem.

Samet JM, Graves LM, Quay J, Dailey LA, Devlin RB, Ghio AJ, et al. 1998. Activation of mapks in human bronchial epithelial cells exposed to metals. Am J Physiol 275:L551-558.

Samet JM, Avila-Tang E, Boffetta P, Hannan LM, Olivo-Marston S, Thun MJ, et al. 2009. Lung cancer in never smokers: Clinical epidemiology and environmental risk factors. Clinical Cancer Research 15:5626-5645.

Samet JM, Tal TL. 2010. Toxicological disruption of signaling homeostasis: Tyrosine phosphatases as targets. Annual review of pharmacology and toxicology 50:215-235.

Sarsour EH, Kumar MG, Chaudhuri L, Kalen AL, Goswami PC. 2009. Redox control of the cell cycle in health and disease. Antioxid Redox Signal 11:2985-3011.

Schwarzlander M, Murphy MP, Duchen MR, Logan DC, Fricker MD, Halestrap AP, et al. 2012. Mitochondrial 'flashes': A radical concept rephined. Trends Cell Biol.

SchwarzlÄNder M, Fricker MD, MÜLler C, Marty L, Brach T, Novak J, et al. 2008. Confocal imaging of glutathione redox potential in living plant cells. Journal of Microscopy 231:299-316.

Scott JA. 1953. Fog and deaths in london, december 1952. Public Health Rep 68:474-479.

Shannahan JH, Schladweiler MC, Richards JH, Ledbetter AD, Ghio AJ, Kodavanti UP. 2010. Pulmonary oxidative stress, inflammation, and dysregulated iron homeostasis in rat models of cardiovascular disease. J Toxicol Environ Health A 73:641-656.

Siddique YH, Ara G, Afzal M. 2012. Estimation of lipid peroxidation induced by hydrogen peroxide in cultured human lymphocytes. Dose-response : a publication of International Hormesis Society 10:1-10.

Simkhovich BZ, Kleinman MT, Kloner RA. 2008. Air pollution and cardiovascular injury: Epidemiology, toxicology, and mechanisms. Journal of the American College of Cardiology 52:719-726.

Skebo JE, Grabinski CM, Schrand AM, Schlager JJ, Hussain SM. 2007. Assessment of metal nanoparticle agglomeration, uptake, and interaction using high-illuminating system. Int J Toxicol 26:135-141.

Slauch JM. 2011. How does the oxidative burst of macrophages kill bacteria? Still an open question. Molecular Microbiology 80:580-583.

Smith CL. 2001. Basic confocal microscopy. Curr Protoc Neurosci Chapter 2:Unit 2 2.

Song H, Tan W, Zhang X. 2010. Ozone induces inflammation in bronchial epithelial cells. Journal of Asthma 48:79-83.

Spencer M. 1982. Fundamentals of light microscopy. Cambridge [Cambridgeshire] ;New York:Cambridge University Press.

Srebot V, Gianicolo EA, Rainaldi G, Trivella MG, Sicari R. 2009. Ozone and cardiovascular injury. Cardiovasc Ultrasound 7:30.

Stanek LW, Brown JS, Stanek J, Gift J, Costa DL. 2011. Air pollution toxicology—a brief review of the role of the science in shaping the current understanding of air pollution health risks. Toxicological Sciences 120:S8-S27.

Taatjes DJ, Mossman BT, Zucker RM. 2006. Evaluation of confocal microscopy system performance. In: Cell imaging techniques, Vol. 319:Humana Press, 77-135.

Tal TL, Bromberg PA, Kim Y, Samet JM. 2008. Epidermal growth factor receptor activation by diesel particles is mediated by tyrosine phosphatase inhibition. Toxicol Appl Pharmacol 233:382-388.

Tal TL, Simmons SO, Silbajoris R, Dailey L, Cho S-H, Ramabhadran R, et al. 2010. Differential transcriptional regulation of il-8 expression by human airway epithelial cells exposed to diesel exhaust particles. Toxicology and Applied Pharmacology 243:46-54.

Taylor-Clark TE, Undem BJ. 2010. Ozone activates airway nerves via the selective stimulation of trpa1 ion channels. The Journal of Physiology 588:423-433.

Terzano C, Di Stefano F, Conti V, Graziani E, Petroianni A. 2010. Air pollution ultrafine particles: Toxicity beyond the lung. Eur Rev Med Pharmacol Sci 14:809-821.

Tetley TD. 2007. Health effects of nanomaterials. Biochemical Society Transactions 35:527-531.

Todokoro M, Mochizuki H, Tokuyama K, Utsugi M, Dobashi K, Mori M, et al. 2004. Effect of ozone exposure on intracellular glutathione redox state in cultured human airway epithelial cells.105-114.

Toppo S, Vanin S, Bosello V, Tosatto SC. 2008. Evolutionary and structural insights into the multifaceted glutathione peroxidase (gpx) superfamily. Antioxid Redox Signal 10:1501-1514.

Uhlson C, Harrison K, Allen CB, Ahmad S, White CW, Murphy RC. 2002. Oxidized phospholipids derived from ozone-treated lung surfactant extract reduce macrophage and epithelial cell viability. Chem Res Toxicol 15:896-906.

United States Environmental Protection Agency. 2012. Our nation's air: Status and trends through 2010. EPA-454/R-12-001.

Vagaggini B, Bartoli ML, Cianchetti S, Costa F, Bacci E, Dente FL, et al. 2010. Increase in markers of airway inflammation after ozone exposure can be observed also in stable treated asthmatics with minimal functional response to ozone. Respir Res 11:5.

Valavanidis A, Fiotakis K, Vlachogianni T. 2008. Airborne particulate matter and human health: Toxicological assessment and importance of size and composition of particles for oxidative damage and carcinogenic mechanisms. Journal of environmental science and health Part C, Environmental carcinogenesis & ecotoxicology reviews 26:339-362.

Van der Vliet A, O'Neil CA, Eiserich JP, Cross CE. 1995. Oxidative damage to extracellular fluids by ozone and possible protective effects of thiols. Arch Biochem Biophys 321:43-50.

Veranth J, Kaser E, Veranth M, Koch M, Yost G. 2007. Cytokine responses of human lung cells (beas-2b) treated with micron-sized and nanoparticles of metal oxides compared to soil dusts. Particle and Fibre Toxicology 4:2.

Wamelink M, Struys E, Jakobs C. 2008. The biochemistry, metabolism and inherited defects of the pentose phosphate pathway: A review. Journal of Inherited Metabolic Disease 31:703-717.

Ward PA. 2010. Oxidative stress: Acute and progressive lung injury. Annals of the New York Academy of Sciences 1203:53-59.

Waterman-Storer CM. 2001. Microtubule/organelle motility assays. Curr Protoc Cell Biol Chapter 13:Unit 13 11.

Wayne R. 2009. Light and video microscopy. Amsterdam; Boston:Academic Press/Elsevier.

World Health Organization. 2003. Health aspects of air pollution with particulate matter, ozone and nitrogen dioxide. (Report on a WHO Working Group). Bonn, Germany:World Health Organization.

World Health Organization. 2006. Who air quality guidelines for particulate matter, ozone, nitrogen dioxide and sulfur dioxide: Global update 2005 (summary of risk assessment). (WHO Air Quality Guidelines). WHO/SDE/PHE/OEH /06.02. World Health Organization, 20 Avenue Appia, 1211 Geneva 27, Switzerland.

Wu W, Doreswamy V, Diaz-Sanchez D, Samet JM, Kesic M, Dailey L, et al. 2011. Gstm1 modulation of il-8 expression in human bronchial epithelial cells exposed to ozone. Free Radical Biology and Medicine 51:522-529.

Xia T, Kovochich M, Liong M, Zink JI, Nel AE. 2007. Cationic polystyrene nanosphere toxicity depends on cell-specific endocytic and mitochondrial injury pathways. ACS Nano 2:85-96.

Xia T, Li N, Nel AE. 2009. Potential health impact of nanoparticles. The Annual Review of Public Health 30:137-150.

Xiao L, Qiao Y, He Y, Yeung ES. 2010. Three dimensional orientational imaging of nanoparticles with darkfield microscopy. Anal Chem.

Yang IA, Fong KM, Zimmerman PV, Holgate ST, Holloway JW. 2008. Genetic susceptibility to the respiratory effects of air pollution. Thorax 63:555-563.

Yang W, Peters JI, Williams III RO. 2008. Inhaled nanoparticles--a current review. International Journal of Pharmaceutics 356:239-247.

Yang W, Omaye ST. 2009. Air pollutants, oxidative stress and human health. Mutation Research/Genetic Toxicology and Environmental Mutagenesis 674:45-54.

Yano T, Haro A, Shikada Y, Maruyama R, Maehara Y. 2011. Non-small cell lung cancer in never smokers as a representative 'non-smoking-associated lung cancer': Epidemiology and clinical features. Int J Clin Oncol 16:287-293.

Zhang J, Campbell RE, Ting AY, Tsien RY. 2002. Creating new fluorescent probes for cell biology. Nature Reviews Molecular Cell Biology 3:906.

Zucker RM. 2006a. Evaluation of confocal microscopy system performance. Methods Mol Biol 319:77-135.

Zucker RM. 2006b. Quality assessment of confocal microscopy slide based systems: Performance. Cytometry A 69:659-676.

Zucker RM. 2006c. Quality assessment of confocal microscopy slide-based systems: Instability. Cytometry A 69:677-690.

Zucker RM, Rigby P, Clements I, Salmon W, Chua M. 2007. Reliability of confocal microscopy spectral imaging systems: Use of multispectral beads. Cytometry A 71:174-189.

Zucker RM, Massaro EJ, Sanders KM, Degn LL, Boyes WK. 2010. Detection of tio2 nanoparticles in cells by flow cytometry. Cytometry A 77:677-685.